UNIVERSITY OF CALIFORNIA, SAN DIEGO

Navigating the Wnt Pathway at the Cilium: Transport Regulation and the Role of Jouberin

A dissertation submitted in partial satisfaction of the requirements for the degree Doctor of Philosophy

in

Biomedical Sciences

by

Madeline Alden Lancaster

Committee in charge:

Professor Joseph G. Gleeson, Chair
Professor M. Geoff Rosenfeld
Professor Karl Willert
Professor Anthony Wynshaw-Boris
Professor Yimin Zou

2010

ProQuest LLC
789 East Eisenhower Parkway
P.O. Box 1346
Ann Arbor, MI 48106-1346

The Dissertation of Madeline Alden Lancaster is approved, and it is acceptable in quality and form for publication on microfilm and electronically:

Chair

University of California, San Diego

2010

TABLE OF CONTENTS

LIST OF FIGURES

LIST OF TABLES

ACKNOWLEDGEMENTS

I would like to thank my thesis advisor, Joseph Gleeson, who has mentored me these past several years and helped enormously in directing my research. Joe has always been available to discuss new findings and their implications and was especially motivating when I was just a bright-eyed beginning student and didn't know what I had in store for me. He has been instrumental in guiding me toward my greatest findings.

I would also like to thank my committee members who have always provided a fresh outlook on the data and have been especially motivating when I sometimes thought my work was in a rut. Without their support, I would probably still be reinventing the wheel.

I would like to acknowledge members of my lab for being supportive and providing an especially fun work environment. Their smiles helped me when my experiments weren't working and they were always there to bounce off ideas.

Finally, I would like to thank my family. My mom and my stepdad, Kevin, have always been supportive and raised me to care about the pursuit of knowledge, and my brothers can be counted on to bring things in perspective and tell me to just "chillax." My dad and my stepmom, Judith, have always been interested in my success, and my dad can be counted on to push me to do my best. And finally I would like to thank my boyfriend, Davide, who has been with me through all of my fickle days after failed experiments and during my greatest successes.

The text of Chapter 1 in part is a reprint of the material as it appears in Current Opinions in Genetics and Development, 2009, Lancaster MA, and Gleeson JG. The dissertation author was the primary author of this paper and the co-author supervised and directed the writing of this publication which forms the basis of this chapter.

The text of Chapter 2 in full is a reprint of the material as it appears in Nature Medicine, 2009, Lancaster MA, Louie CM, Silhavy JL, Sintasath L, DeCambre M, Nigam SK, Willert K & Gleeson JG. The dissertation author was the primary researcher and author of this publication and co-authors preformed experiments, and supervised the research which forms the basis of this chapter.

The text of Chapter 3 in full is being prepared for submission, 2009, Lancaster MA, and Gleeson JG. The dissertation author is the primary researcher and author and the co-author listed directed and supervised the research which forms the basis of this chapter.

The text of Chapter 4 in full is being prepared for submission, 2009, Lancaster MA, Gopal DJ, Silhavy JL, Kim J, Louie CM, and Gleeson, JG. The dissertation author is the primary researcher and author and the co-authors performed experiments and supervised the research which forms the basis of this chapter.

VITA

2004	B.A., Biochemistry, Occidental College, Los Angeles, CA
2010	Ph. D., Biomedical Sciences, UCSD, La Jolla, CA

Publications

Valente EM, Silhavy JL, Brancati F, Barrano G, Krishnaswami SR, Castori M, Lancaster MA, Boltshauser E, Boccone L, Al-Gazali L, Fazzi E, Signorini S, Louie CM, Bellacchio E; International Joubert Syndrome Related Disorders Study Group; Bertini E, Dallapiccola B, Gleeson JG. *Mutations in CEP290, which encodes a centrosomal protein, cause pleiotropic forms of Joubert syndrome.* **Nature Genet.** 2006., 38(6): 623-5.

Lancaster MA, and Gleeson, JG. *The primary cilium as a cellular signaling center: lessons from disease.* **Curr. Opin. Genet. and Develop.** 2009., 19:220-229. Cover article.

Lancaster MA, Louie CM, Silhavy JL, Sintasath L, DeCambre M, Nigam SK, Willert K, Gleeson JG. *Impaired Wnt/β-catenin signaling disrupts adult renal homeostasis and leads to cystic kidney ciliopathy.* **Nature Medicine**. 2009., 15: 1046-1054.

Louie CM, Caridi G, Lopes VS, Rancati F, Kispert A, Lancaster MA et al. *AHI1 is required for outer segment development and is a modifier for retinal degeneration in nephronophthisis.* **Nature Genet.** In Press.

Lancaster MA, Gleeson, JG. *Primary Cilia Regulate Canonical Wnt Signaling through Sequestration of Wnt Components.* Manuscript in preparation.

Lancaster MA, Gopal D, Silhavy JL, Kim J, Louie CM, and Gleeson, JG. *Ahi1 is required for Wnt signaling in early cerebellar midline fusion.* Manuscript in preparation.

ABSTRACT OF THE DISSERTATION

Navigating the Wnt Pathway at the Cilium: Transport Regulation and the Role of Jouberin

by

Madeline Alden Lancaster

Doctor of Philosophy in Biomedical Science

University of California, San Diego 2010

Professor Joseph G. Gleeson

The primary cilium is a unique cellular organelle which in recent years has proven to be a surprisingly multifaceted structure. Primary cilia are ubiquitous; they are present on almost all vertebrate cell types and play important regulatory roles in a growing number of signaling pathways. Recently, these tiny hair-like structures have been recognized for their functions in a variety of disorders termed “ciliopathies.” The

ciliopathies display a broad range of phenotypes that can affect a multitude of organs at varying times in a person's life. We now know that cilia are involved in a growing array of developmental and homeostatic functions which seem to be disrupted in the ciliopathies leading to a variety of phenotypes. Understanding these disorders will require a broader understanding of the vastly diverse biological functions of cilia.

To study the role of primary cilia in two overlapping ciliopathies, Joubert syndrome and nephronophthisis, I have employed a mouse model with a deletion of the Ahi1 gene. AHI1 was the first identified gene mutated in patients with Joubert syndrome, a cerebellar development disorder. Joubert syndrome patients also often display a variety of other ciliopathy phenotypes which can include nephronophthisis, a cystic kidney disorder. Chapter 2 describes the kidney phenotype of Ahi1 mutant mice and the underlying Wnt defect. Ahi1 mutant mice display decreased canonical Wnt signaling which results in abnormal injury repair and a late-onset cyst pathology. Chapter 3 describes a unique signaling role for the primary cilium in regulation of Jouberin, the protein product of Ahi1, and its role in canonical Wnt signaling. The primary cilium seems to inhibit canonical Wnt signaling at multiple steps in the pathway including through sequestration of Jouberin and β-catenin. Finally, Chapter 4 describes the cerebellar phenotype of Ahi1 null mice and the unique role of canonical Wnt signaling in cerebellar midline fusion. Overall, these results suggest that the primary cilium regulates canonical Wnt signaling in a variety of cellular contexts through a unique subcellular mechanism involving Jouberin.

Chapter 1 Introduction

1.1 Primary Cilia and the Ciliopathies

The terms “cilia” and “flagella” often evoke images of microscopic algae gliding through pond water, shifting about with incredible deftness, much as Leeuwenhoek first observed in 1675. Or perhaps instead, images emerge of millions of tiny sperm with lengthy whips projecting them toward their destination: the ovum. But cilia and flagella are not only pistons of unicellular locomotion. From the ciliated epithelium of the oviduct, pushing the ovum towards the uterus, to the epithelial cells of the lung with their millions of tiny bristles brushing fluid and debris along like tiny broom-bearing maids, cilia are ubiquitous. From cleaning up our inside messes to their recently recognized signaling functions, cilia are involved in a myriad of biological processes, and research is beginning to reveal the importance of these tiny hair-like projections in a variety of disorders known as “ciliopathies” (1).

It has been a long road to recognizing the importance of cilia in disease pathogenesis and vertebrate physiology. Until recently, vertebrate cilia were mainly recognized for their roles in clearing mucus from the lungs and generating flow. True, cilia had been described ubiquitously in other organs but they were viewed as “vestigial” organelles, nothing more than a mere oddity. These cilia, known as primary cilia, are unlike their motile cousins which line the trachea. Primary cilia instead are generally nonmotile (with the exception of nodal cilia) and are normally present as a single cilium per cell. The primary cilium is made up of 9 outer microtubule doublets with a modified centrosome at its base, known as the basal body (Figure 1) (2). Primary cilia have been described on a multitude of cell types, from kidney tubules to neurons to the modified

cilium of the retinal photoreceptor. The role of motile epithelial cilia has always been fairly intuitive: to help direct fluid and debris. But what could be the function of the more ubiquitous yet far more mysterious nonmotile cilia? That is precisely the question that has recently captivated the attention of multiple fields of biomedical research.

The list of disorders categorized as ciliopathies is constantly expanding as borders are blurred between what were previously considered distinct disorders. Overlapping phenotypes and genetic causes have revealed a continuum of disorders which all have one crucial thing in common: evidence to suggest a defect of the primary cilium. The primary cilium is at the heart of these disorders and its ubiquity can be blamed for the diversity of phenotypes. The ciliopathies therefore encompass a variety of seemingly distinct disorders depending upon the organs most severely affected (Table 1) (3). For example, nephronophthisis (NPHP) and polycystic kidney disease (PKD) are both ciliopathies defined by cystic kidney pathologies, whereas Leber congenital amaurosis (LCA) is defined by its early onset retinal degeneration phenotype similar to retinitis pigmentosa (RP). Bardet-biedl syndrome (BBS) is a compound phenotype disorder exhibiting obesity, cystic kidneys, and RP while Meckel-Gruber (MKS) and Joubert syndromes (JS) both exhibit brain malformations. These are some of the examples of cilium-associated phenotypes which can be associated with a plethora of other defects in a variety of affected organs. However, genetic and phenotypic overlap between these disorders has revealed that they are not as distinct as was once suspected. CEP290 for example is mutated in several previously distinct disorders: NPHP, LCA, JS and MKS. Additionally, an individual may present with several related disorders such as occurs between JS, NPHP, and RP leading to new classifications (cerebello-oculo-renal syndrome, CORS) and a new appreciation for potential similar molecular mechanisms.

In light of recent genetic findings it is now somewhat puzzling that these disorders have any phenotypic distinctions at all given their mutual underlying causes. Possible explanations for the variable phenotypes seen may be due to genetic background or differences in expression profiles as well as the complexity of the organelle involved: the cilia proteome database at present contains over 2500 genes! Thus, depending on the genetic makeup of an affected individual, some phenotypes may be more prominent, defining a unique syndromic entity. With recent advances we can now focus on understanding the commonalities of the molecular mechanisms of pathogenesis of the ciliopathies and the normal functions of primary cilia in the various organs affected. With that said, this review will focus on the recent advances in our understanding of this perplexing organelle particularly in three major organs affected in the ciliopathies. Recent findings of the functions of ciliopathy proteins will be examined in this context.

1.2 The Retinal Connecting Cilium

The modified cilium of the photoreceptor is not a typical example of a vertebrate primary cilium for it is the only known primary cilium with membrane-enclosed vesicles, perhaps making it seem an odd place to begin our examination. However, the outer segment of the rods and cones of the eye make up a majority of the cell's surface area and consume more energy than any other region of the eye. This modified structure is therefore especially sensitive to disruptions of cilia function particularly in terms of basic architecture and transport. Without an intact connecting cilium, the photoreceptor is prone to apoptosis leading to retinal degeneration. Such degeneration is known as retinitis pigmentosa (RP) (4).

RP can manifest through various mechanisms since it is defined by photoreceptor cell death, a process which may occur because of any number of defects. The congenital form of RP, defined as LCA, currently has 14 known causative genes, 4 of which are localized to the connecting cilium and/or basal body (5). These are TULP1, CEP290, RPGRIP1, and LCA5. Autosomal dominant RP can be caused by mutations in the cilia associated gene RP1 while the majority of X-linked RP cases are caused by mutations in a gene known as RPGR, also localized to the connecting cilium. Thus subtypes of LCA and RP can be considered ciliopathies. Similar RP phenotypes have been identified in several related ciliopathies which include but are not limited to NPHP, Usher syndrome, BBS, and CORS.

Insights into the role of the primary cilium in RP can be gained from understanding the normal functions of the cilium-associated causative genes within the photoreceptor. The strongest findings have come from various protein interaction studies which have identified complexes between several of the proteins involved in RP. RPGR and RPGRIP1 directly interact (6, 7), and this interaction is disrupted with certain disease associated missense mutations suggesting it is relevant to disease pathogenesis (6). Studies from mutant mice indicate a potential scaffolding role for RPGRIP1 at the connecting cilium whereby RPGR localization depends upon the presence of RPGRIP1 (8). In addition, CEP290 has been identified to interact with RPGRIP1 (9) supporting the presence of a multi-protein complex at the connecting cilium. Further interaction studies have revealed a variety of other proteins associated with this complex including NPHP genes 4 (10) and 5 (9) both of which are associated with RP in conjunction with NPHP (known as Senior-Loken syndrome, SLSN). Thus, the “interactome” of the cilium probably consists of large multi-subunit complexes each mainly constituted by proteins clustered based upon the disease they share in common.

So what might be the role of this cilia-associated multi-protein complex? One attractive possibility which is gaining momentum suggests that RP proteins are necessary for transport of photoreceptor components into the outer segment (OS) through the connecting cilium. Transport within the primary cilium, known as intraflagellar transport (IFT), utilizes a specific set of motor proteins to move cargo up and down the cilium (Figure 1). The unicellular flagellate Chlamydomonas reinhardtii has been particularly instrumental in identifying the underlying mechanisms of IFT and the specific proteins involved (2). Many of the IFT components identified in C. reinhardtii have mammalian orthologues which similarly function in IFT, indicating the high level of conservation of this process in general. Disruption of IFT components can perturb cilium architecture, from a complete loss of the cilium or flagellum to defects in length and overall shape. RPGR and CEP290 have both been found to interact with various microtubule transport proteins including IFT88 (11) and the anterograde transport motor Kif3A (9), supporting a trafficking role for RP proteins. In fact, we and others have recently identified a role for CEP290 in cilia localization of Rab8 (12, 13), a protein involved in docking vesicles to the base of cilia. Additionally, evidence from TULP1 mutant mice has revealed abnormal rhodopsin trafficking into the OS (14), and TULP1 has recently been shown to interact with dynamin-1, a GTPase which functions in vesicle trafficking (15). This process is necessary for transport of membrane associated proteins, like rhodopsin, into the OS.

These results are particularly intriguing given the strong support for roles of other ciliopathy proteins in IFT and vesicle transport. Many BBS proteins have been shown to interact as a large multi-protein complex termed the BBsome (16), much like that between RPGR and RPGRIP1, which may serve as a scaffold for IFT components. Moreover, BBS4 mutant mice exhibit defects in vesicle transport along with

mislocalization of rhodopsin (17). These results increasingly point to pathological mechanisms involving disrupted IFT and defective localization of OS components.

1.3 Renal Cilia in NPHP and PKD

NPHP and PKD are related cystic kidney disorders defined as ciliopathies given that nearly all of the known causative genes localize to the primary cilium (1). Importantly, cystic kidney phenotypes have also been identified in several other related ciliopathies including BBS, oral-facial-digital syndrome (OFD) and CORS. NPHP can be caused by mutations in any of the NPHP1-9 genes, while PKD occurs with mutations in PKD1 or 2 (encoding polycystin-1, PC1, or polycystin-2, PC2) or PKHD1 (Table 1). Although the precise mechanisms of cystogenesis are not well understood, cysts seem to arise due to a combination of abnormal proliferation, apoptosis, cell polarity and cell fate disruptions.

Much as described in the retinal connecting cilium, there is some indication that basic cilium architecture or transport may be in part to blame for pathogenesis of cystic kidney disorders. NPHP1 and 4 have both been identified as necessary for precise formation of axoneme architecture in C. elegans (18) and, as described above, NPHP6 (alternatively known as CEP290) is required for Rab8 targeting and ciliogenesis (12, 13). Results from IFT animal mutants, such as IFT88 and Kif3A mouse mutants, underscore the importance of the cilium in pathogenesis of cystic kidney defects (19, 20). Despite this however, none of the intrinsic IFT components have been identified as mutated in the human ciliopathies. This is probably owing to their central roles in overall cilia function and therefore may result in more severe phenotypes than NPHP and PKD.

With this in mind, emphasis has recently been placed on the function of ciliopathy proteins as potential key modulators of specific signaling cascades, which may depend

upon the presence of the primary cilium. In fact, increasing evidence accentuates the role for the primary cilium in at least five different signaling cascades (Figure 2). The primary cilium has been most well characterized in Shh signaling in which Smo translocates into the cilium and activates Gli transcription factors within the cilium (21). PDGFRα similarly translocates into the primary cilium to allow for its activation (22). Additionally, increasing evidence is suggesting that the primary cilium is necessary for noncanonical Wnt signaling (23, 24), while in contrast to this positive regulatory role, it is instead inhibitory to the canonical Wnt pathway (25, 26). In the kidney, calcium signaling, the Shh pathway and both canonical and noncanonical Wnt signaling have been implicated in cystic kidney pathogenesis (Table 1).

The primary cilium is a particularly unique organelle because of its position extending away from the cell body, into the renal tubule lumen. This affords it the distinct ability to sense extracellular molecules as well as mechanostimulation such as fluid flow within the tubule lumen. Bending of the cilium in response to flow has been shown to generate a transient calcium influx (27) which depends upon the formation of a PC1/PC2 cation permeable channel within the primary cilium (28). Disruption of either of these components or the related PKHD1 interrupts calcium signaling (29) potentially leading to a multitude of defects, from apoptosis to proliferation. Thus, a prevailing model has emerged known as the flow hypothesis of cystic kidney disease which suggests that abnormal response to tubular lumen fluid flow leads to pathogenesis of PKD and NPHP.

A similar flow hypothesis has been suggested by Simons et. al. in regards to Wnt signaling in renal cystic disease (30). NPHP2 as well as NPHP3 (31) have been shown to downregulate canonical Wnt signaling and upregulate noncanonical Wnt signaling, potentially in a flow dependent manner. In support of a role for Wnt signaling, several

noncanonical Wnt factors have recently been shown to lead to cystogenesis when mutated in animal models (32, 33), while abnormal activation of the canonical pathway seems to lead to cystogenesis (34, 35). While the data seem to point to abnormal flow response in cystic kidney disease, it is not yet clear whether disrupted mechanosensation is sufficient to lead to cysts.

Recently, adult conditional mutant studies of Kif3a and Pkd1 mutant mice revealed that loss of the cilium or its mechanosensing components does not trigger cyst pathology (36, 37), at least not for several months, suggesting that abnormal flow sensing is not sufficient to cause disease pathology. Additionally, Kottgen et. al. recently identified a necessary component of the mechanosensation machinery, known as TRPV4, which when disrupted abolished flow triggered calcium transients, yet its loss did not lead to cystic kidney pathology (38). These results suggest cilium-mediated flow sensing may not represent the primary pathogenic mechanism of PKD and NPHP.

Wnt signaling in cystic kidney disease likewise seems to be more complex than the initial switch mechanism model proposed by Simons et. al. Although not as well appreciated, cysts have been documented both in mutants associated with reduced canonical Wnt signaling (39) as well as those that lead to hyperactivation of the pathway. Similarly, we have preliminary data suggesting that a gene mutated in JS known as AHI1, encoding Jouberin (Jbn), is required for canonical Wnt signaling, and its loss leads to a cystic phenotype. Finally, BBS10 and BBS12 have recently been shown to be required for GSK3β inhibition and β-catenin cytosolic accumulation in the Wnt pathway (40). Overall, cystic phenotypes seem to occur with disruption of canonical Wnt signaling in either direction or with disrupted noncanonical/PCP signaling.

Although these results at first seem contradictory, there have been several reports of similar canonical Wnt and PCP roles in developing renal tubules (41). Thus,

one possible model is that cystogenesis represents disruption of similar developmental processes. In line with this, Patel et. al. described a particularly key set of experiments in which Kif3a conditional mutant mice were subjected to acute renal injury (42). Although loss of the cilium alone in this model is not sufficient to trigger cystic kidney disease in the adult, cyst pathology was evident with a specific time course following injury. This injury-triggered pathology was also evident in Ahi1 mutant animals in which Wnt activity, although increased in injured wild-type animals, failed to activate. Although not directly tested yet, this supports a model in which cilium-mediated developmental pathways may be reactivated upon injury. Disruption of any cilia signaling components or the cilium itself would be expected to disturb the processes of proliferation and differentiation of new tubules, potentially leading to cystogenesis. According to this model, it is developmental signaling rather than basal flow sensing which is involved in cystogenesis, although one cannot exclude the likely possibility that flow sensing may also occur in the context of these reactivated developmental pathways.

1.4 The Neuronal Primary Cilium

Although cilia were identified throughout mammalian brain as early as the 1970s, their function is only just beginning to be understood. Neuronal cilia are ubiquitous, and are especially abundant in the hippocampus, developing cerebellum, olfactory bulb, and hypothalamus (43). The largely accepted idea of the primary cilium as an antenna acting to bend in response to flow and receive external signals may apply to a subset of neurons in the ventricles, but the larger majority of ciliated neurons lie buried in a sea of dendrites and other cell bodies. In this context, the cilium does not extend nearly as far as other processes such as dendrites and axons. So what might be the function of this relatively tiny neuronal extension?

Several recent findings have begun to pinpoint specific roles for these mysterious organelles in the nervous system. Han et al. and Breunig et al. identified roles for primary cilia in stem cell maintenance of the hippocampus (44, 45) while Spassky et al. and Chizhikov et al. (46, 47) defined a similar role in cerebellar granule neuron proliferation, both in response to Shh. These findings point to a key role in signaling and a model in which the primary cilium may act as a signaling hub capable of concentrating signaling components in order to integrate or amplify specific cascades (Figure 3). Although this model of a concentrator remains to be specifically tested, it may explain the necessity for such an organelle on a cell which otherwise has thousands of longer extensions potentially capable themselves of acting as “antennae.”

The findings by Spassky et al. and Chizhikov et al. that primary cilia of the developing cerebellum are required for CGN proliferation is particularly notable in light of the cerebellar phenotypes associated with MKS and JS, which are reminiscent of potentially similar proliferation defects. Additional insight into the roles of neuronal cilia has also come from Davenport et al. who described a striking obesity in mice with hypothalamic cilia disruption (37) which is particularly applicable to the obesity phenotype seen in BBS. Although increasing evidence from IFT mutants reveal a vital role for the neuronal primary cilium in brain development, the adult neuronal functions of the ciliopathy proteins themselves are less well understood. Perhaps, as in the kidney, ciliopathy genes play more specific roles in neuronal cilium-based signaling. If the past is any judge, there may be many more well established signaling pathways influenced by the primary cilium.

We are still far from understanding the full complexity of the neuronal primary cilium, but these recent findings point to roles for the primary cilium and ciliopathy proteins in processes long thought to depend upon more traditional neuronal cell

architecture. For example, AHI1 has now been identified as associated with both autism and schizophrenia (48, 49), pointing to potential involvement of ciliopathy genes and the cilium itself in behavior. Finally, mental retardation is a fairly common component of several ciliopathies suggesting a role in learning and memory. Thus, cilia in regions of the brain involved in learning and behavior such as the cerebral cortex and hippocampus may play vital roles in neuronal function and these will need to be examined further.

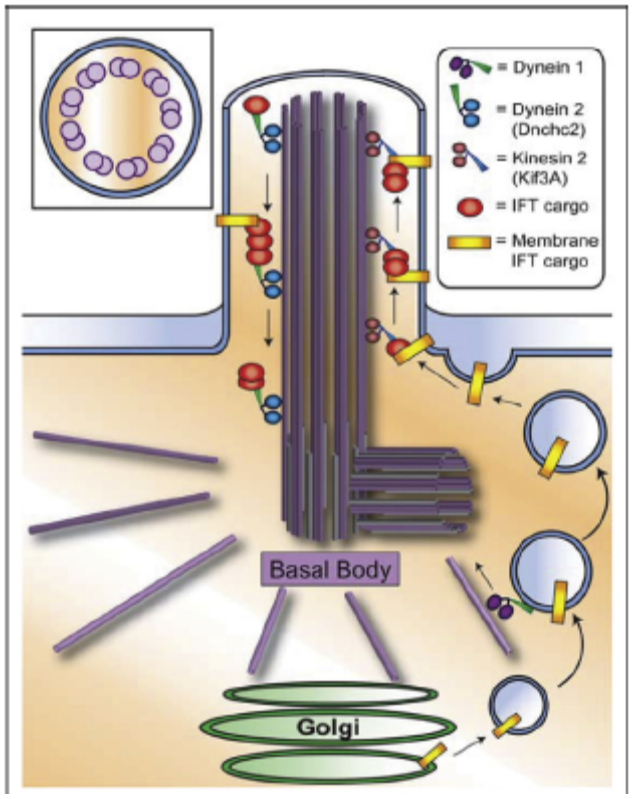

Figure 1.1 Intraflagellar transport within the primary cilium. Kinesin 2 (with its major component Kif3a) transports cargo in an anterograde direction towards the tip of the cilium, while dynein heavy chain 2 (Dnchc2) travels in the retrograde direction towards the base of the cilium. Membrane cargo, like rhodopsin, is first loaded into a vesicle and transported to the basal body from the golgi by dynein 1. Vesicles then fuse with the cilia membrane and membrane bound cargo is transported along the ciliary length by Kif3a and dynein 2. Major components of this process include Rab8 as well as several ciliopathy genes, particularly the BBS proteins. Inset: schematic of a primary cilium cross-section revealing 9+0 architecture.

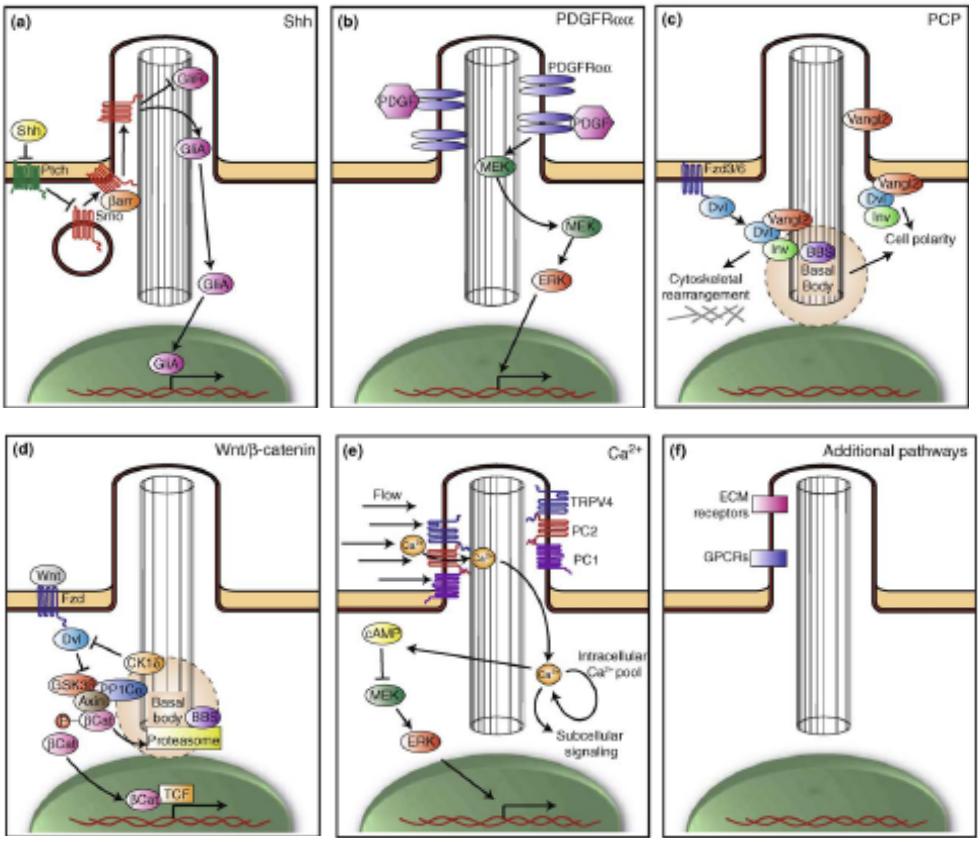

Figure 1.2 Various signaling cascades converge at the cilium. A) Sonic hedgehog (Shh) signaling depends upon translocation of smoothened (Smo) into the primary cilium (a process involving β-arrestins (50)) following binding of Shh to its receptor patched (Ptch) in order to activate Gli transcription factors from the repressor form (GliR) to the activator form (GliA). B) PDGF signaling through PDGFRαα requires localization of the receptor within the primary cilium which activates MEK/ERK signaling. MEK itself is also localized to the primary cilium. C) Although not well understood, noncanonical Wnt signaling (planar cell polarity, PCP) also requires the primary cilium and the basal body. Dishevelled (Dvl) activation through Frizzled 3 or 6 (Fzd3/6) leads to cell polarity determination as well as cytoskeletal rearrangements associated with PCP through interaction with Inversin (Inv, NPHP2) and the PCP component Vangl2. Vangl2 itself has also been localized to the primary cilium. D) Canonical Wnt signaling is inhibited by the primary cilium through regulation of Dvl by CK1δ as well as proteasomal regulation of β-catenin at the basal body. Additional potential regulatory mechanisms are likely to exist as well. E) Calcium signaling is activated by bending of the cilium in response to fluid flow through mechanosensation by polycystin-1 (PC1) and TRPV4 which form a complex with the calcium ion channel polycystin-2 (PC2). Calcium influx leads to further stimulation of calcium release by intracellular pools and activation of downstream signaling including cAMP dependent MEK/ERK signaling(51). F) Additional signaling cascades implicated at the cilium include G-protein coupled receptor (GPCR) signaling(52) and extra-cellular matrix (ECM) receptors(53).

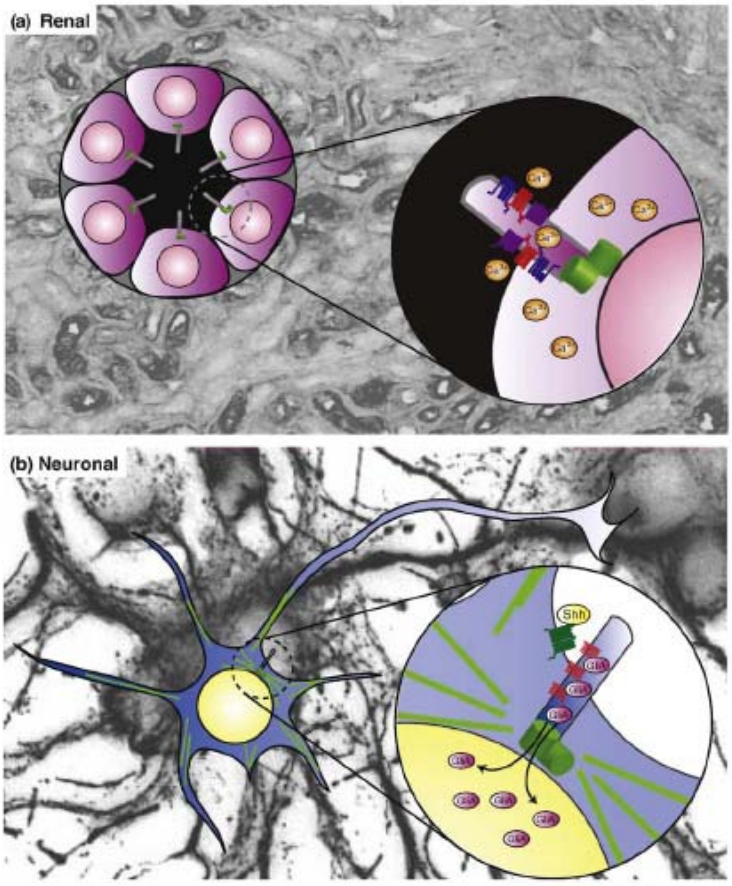

Figure 1.3 The primary cilium as a signaling hub. A) Cilia projecting into fluid-filled luminal spaces are positioned to respond to signals and fluid flow within the tubule lumen in order to activate signaling cascades such as calcium signaling, as shown in the inset. B) The neuronal cilium however appears buried amongst the dendrites and axons of surrounding neurons implicating an alternative rationale for its presence. One model is that the cilium is positioned next to the nucleus such that components of signaling cascades like the Shh pathway (inset) may be concentrated within the cilium in order to faithfully relay messages. Thus, the cilium acts as a concentrator of signaling components, or a signaling hub. Background images are immunostaining within renal tubules or cultured hippocampal neurons.

Table 1. Ciliopathy genes and their subcellular functions. Information available on OMIM (http://www.ncbi.nlm.nih.gov/entrez/query.fcgi?db=OMIM).

Primary phenotypes	Gene/Protein	Localization	Putative subcellular functions
Kartagener's/Primary ciliary diskinesia (PCD)			
situs inversus, chronic sinusitis, bronchiectasis	DNAH5	Outer dynein arms	Cilia motility
	DNAL1	Outer dynein arms	Cilia motility
	DNAH11/LRD	Axonemal	Cilia motility
	KTU	Cytoplasm	Dynein arm preassembly, cilia motility
	DNAI2	Outer dynein arms	Cilia motility
	RSPH9	Radial spokes	Central pair/motility
	RSPH4A	Radial spokes	Central pair/motility
Bardet-Biedl syndrome (BBS)			
obesity, cystic kidneys, retinal degeneration	BBS1	Basal bodies	BBsome, Wnt/PCP, IFT/trafficking
	BBS2	Basal bodies	BBsome, IFT/trafficking
	BBS3; ARL6	Basal bodies	Vesicle trafficking
	BBS4	Basal body, primary cilia	BBsome, Wnt/PCP, IFT/trafficking
	BBS5	Basal bodies	BBsome, IFT/trafficking
	BBS6; MKKS	Basal bodies	IFT/trafficking, Wnt/PCP, cytokinesis, chaperonin
	BBS7	Basal bodies	BBsome, IFT/trafficking
	BBS8; TTC8	Basal body, primary cilia	BBsome, IFT/trafficking
	BBS9; PTHB1	Basal bodies	BBsome
	BBS10	Basal bodies	Ciliogenesis, Wnt, chaperonin
	BBS11; TRIM32	Basal bodies	E3 ubiquitin ligase
	BBS12	Basal bodies	Ciliogenesis, Wnt, chaperonin
Alstrom syndrome			
obesity, retinal degeneration, hearing loss	ALMS1	Basal bodies	Cilia maintenance
Leber Congenital Amaurosis (LCA)			
congenic retinal degeneration	TULP1	Connecting cilia	Rhodopsin trafficking
	LCA5	Connecting cilia	Unknown
	CEP290; NPHP6	Basal bodies	RPGR complex, trafficking
	RPGRIP1	Connecting cilia	RPGR complex
Retinitis Pigmentosa			
retinal degeneration	RPGR	Connecting cilia	IFT/trafficking, Disc morphogenesis
	RP1	Connecting cilia	IFT/trafficking, Disc morphogenesis

Table 1. Ciliopathy genes and their subcellular functions, Continued.

Polycystic kidney disease (PKD)			
cystic kidneys	PKD1/PC1	Primary cilia, cell-cell junction	Mechanosensation, Wnt, cell adhesion
	PKD2/PC2	Primary cilia, cell-cell junction	Calcium channel
	PKHD1/FPC	Primary cilia	PC2 modulation
Nephronophthisis			
cystic kidneys	NPHP1/Nephrocystin	Basal bodies, primary cilia, cell-cell contacts	Cilia structure
	NPHP2; INVS	Basal bodies, primary cilia	Wnt/PCP
	NPHP3	Undetermined	Wnt/PCP
	NPHP4/Nephroretinin	Basal bodies, primary cilia	Cilia structure, IFT
	NPHP5; IQCB1	Primary cilia	RPGR/calmodulin complex
	NPHP6; CEP290	Basal bodies	RPGR complex, trafficking
	NPHP7; GLIS2	Nucleus	Transcription factor, Wnt
	NPHP8; RPGRIP1L	Basal bodies	Shh signaling
	NPHP9; NEK8	Basal bodies, primary cilia	Modulation of PC1 and PC2
Meckel-Gruber syndrome (MKS)			
Brain malformation, cystic kidneys, polydactyly	MKS1	Basal bodies	Ciliogenesis
	MKS3; TMEM67	Primary cilia, membrane	Ciliogenesis
	CEP290; NPHP6	Basal bodies	RPGR complex, trafficking
	CC2D2A	Basal bodies	Unknown
Joubert syndrome (JS)			
Brain malformation	AHI1/Jbn	Basal bodies, primary cilia	Wnt signaling, oncogene
	NPHP1/Nephrocystin	Basal bodies, primary cilia, cell-cell contacts	Cilia structure
	CEP290; NPHP6	Basal bodies	RPGR complex, trafficking
	MKS3; TMEM67	Primary cilia, membrane	Ciliogenesis
	RPGRIP1L	Basal bodies	Shh signaling
	ARL13B	Primary cilia	Cilia structure
	CC2D2A	Basal bodies	Unknown
	INPP5E	Primary cilia	PI signaling, cilia stability
Oral-Facial-Digital syndrome			
Craniofacial abnormalities, polydactyly, cystic kidneys	OFD1	Basal bodies, nucleus	Ciliogenesis, Wnt/PCP

References

1. Fliegauf M, Benzing T, & Omran H (2007) *Nat Rev Mol Cell Biol* **8,** 880-893.

2. Pedersen LB, Veland IR, Schroder JM, & Christensen ST (2008) *Dev Dyn* **237,** 1993-2006.

3. Badano JL, Mitsuma N, Beales PL, & Katsanis N (2006) *Annu Rev Genomics Hum Genet* **7,** 125-148.

4. Adams NA, Awadein A, & Toma HS (2007) *Ophthalmic Genet* **28,** 113-125.

5. den Hollander AI, Roepman R, Koenekoop RK, & Cremers FP (2008) *Prog Retin Eye Res* **27,** 391-419.

6. Roepman R, Bernoud-Hubac N, Schick DE, Maugeri A, Berger W, Ropers HH, Cremers FP, & Ferreira PA (2000) *Hum Mol Genet* **9,** 2095-2105.

7. Boylan JP & Wright AF (2000) *Hum Mol Genet* **9,** 2085-2093.

8. Zhao Y, Hong DH, Pawlyk B, Yue G, Adamian M, Grynberg M, Godzik A, & Li T (2003) *Proc Natl Acad Sci U S A* **100,** 3965-3970.

9. Chang B, Khanna H, Hawes N, Jimeno D, He S, Lillo C, Parapuram SK, Cheng H, Scott A, Hurd RE, Sayer JA, Otto EA, Attanasio M, O'Toole JF, Jin G, Shou C, Hildebrandt F, Williams DS, Heckenlively JR, & Swaroop A (2006) *Hum Mol Genet* **15,** 1847-1857.

10. Roepman R, Letteboer SJ, Arts HH, van Beersum SE, Lu X, Krieger E, Ferreira PA, & Cremers FP (2005) *Proc Natl Acad Sci U S A* **102,** 18520-18525.

11. Khanna H, Hurd TW, Lillo C, Shu X, Parapuram SK, He S, Akimoto M, Wright AF, Margolis B, Williams DS, & Swaroop A (2005) *J Biol Chem* **280,** 33580-33587.

12. Kim J, Krishnaswami SR, & Gleeson JG (2008) *Hum Mol Genet* **17,** 3796-3805.

13. Tsang WY, Bossard C, Khanna H, Peranen J, Swaroop A, Malhotra V, & Dynlacht BD (2008) *Dev Cell* **15,** 187-197.

14. Hagstrom SA, Adamian M, Scimeca M, Pawlyk BS, Yue G, & Li T (2001) *Invest Ophthalmol Vis Sci* **42,** 1955-1962.

15. Xi Q, Pauer GJ, Ball SL, Rayborn M, Hollyfield JG, Peachey NS, Crabb JW, & Hagstrom SA (2007) *Invest Ophthalmol Vis Sci* **48,** 2837-2844.

16. Nachury MV, Loktev AV, Zhang Q, Westlake CJ, Peranen J, Merdes A, Slusarski DC, Scheller RH, Bazan JF, Sheffield VC, & Jackson PK (2007) *Cell* **129,** 1201-1213.

17. Abd-El-Barr MM, Sykoudis K, Andrabi S, Eichers ER, Pennesi ME, Tan PL, Wilson JH, Katsanis N, Lupski JR, & Wu SM (2007) *Vision Res* **47,** 3394-3407.

18. Jauregui AR, Nguyen KC, Hall DH, & Barr MM (2008) *J Cell Biol* **180,** 973-988.

19. Yoder BK, Tousson A, Millican L, Wu JH, Bugg CE, Jr., Schafer JA, & Balkovetz DF (2002) *Am J Physiol Renal Physiol* **282,** F541-552.

20. Lin F, Hiesberger T, Cordes K, Sinclair AM, Goldstein LS, Somlo S, & Igarashi P (2003) *Proc Natl Acad Sci U S A* **100,** 5286-5291.

21. Corbit KC, Aanstad P, Singla V, Norman AR, Stainier DY, & Reiter JF (2005) *Nature* **437,** 1018-1021.

22. Schneider L, Clement CA, Teilmann SC, Pazour GJ, Hoffmann EK, Satir P, & Christensen ST (2005) *Curr Biol* **15,** 1861-1866.

23. Ross AJ, May-Simera H, Eichers ER, Kai M, Hill J, Jagger DJ, Leitch CC, Chapple JP, Munro PM, Fisher S, Tan PL, Phillips HM, Leroux MR, Henderson DJ, Murdoch JN, Copp AJ, Eliot MM, Lupski JR, Kemp DT, Dollfus H, Tada M, Katsanis N, Forge A, & Beales PL (2005) *Nat Genet* **37,** 1135-1140.

24. Jones C, Roper VC, Foucher I, Qian D, Banizs B, Petit C, Yoder BK, & Chen P (2008) *Nat Genet* **40,** 69-77.

25. Corbit KC, Shyer AE, Dowdle WE, Gaulden J, Singla V, Chen MH, Chuang PT, & Reiter JF (2008) *Nat Cell Biol* **10,** 70-76.

26. Gerdes JM, Liu Y, Zaghloul NA, Leitch CC, Lawson SS, Kato M, Beachy PA, Beales PL, DeMartino GN, Fisher S, Badano JL, & Katsanis N (2007) *Nat Genet* **39,** 1350-1360.

27. Praetorius HA & Spring KR (2001) *J Membr Biol* **184,** 71-79.

28. Nauli SM, Alenghat FJ, Luo Y, Williams E, Vassilev P, Li X, Elia AE, Lu W, Brown EM, Quinn SJ, Ingber DE, & Zhou J (2003) *Nat Genet* **33,** 129-137.

29. Wang S, Zhang J, Nauli SM, Li X, Starremans PG, Luo Y, Roberts KA, & Zhou J (2007) *Mol Cell Biol* **27,** 3241-3252.

30. Simons M, Gloy J, Ganner A, Bullerkotte A, Bashkurov M, Kronig C, Schermer B, Benzing T, Cabello OA, Jenny A, Mlodzik M, Polok B, Driever W, Obara T, & Walz G (2005) *Nat Genet* **37,** 537-543.

31. Bergmann C, Fliegauf M, Bruchle NO, Frank V, Olbrich H, Kirschner J, Schermer B, Schmedding I, Kispert A, Kranzlin B, Nurnberg G, Becker C, Grimm T, Girschick G, Lynch SA, Kelehan P, Senderek J, Neuhaus TJ, Stallmach T, Zentgraf H, Nurnberg P, Gretz N, Lo C, Lienkamp S, Schafer T, Walz G, Benzing T, Zerres K, & Omran H (2008) *Am J Hum Genet* **82,** 959-970.

32. Saburi S, Hester I, Fischer E, Pontoglio M, Eremina V, Gessler M, Quaggin SE, Harrison R, Mount R, & McNeill H (2008) *Nat Genet* **40,** 1010-1015.

33. Kishimoto N, Cao Y, Park A, & Sun Z (2008) *Dev Cell* **14,** 954-961.

34. Qian CN, Knol J, Igarashi P, Lin F, Zylstra U, Teh BT, & Williams BO (2005) *J Biol Chem* **280,** 3938-3945.

35. Saadi-Kheddouci S, Berrebi D, Romagnolo B, Cluzeaud F, Peuchmaur M, Kahn A, Vandewalle A, & Perret C (2001) *Oncogene* **20,** 5972-5981.

36. Piontek K, Menezes LF, Garcia-Gonzalez MA, Huso DL, & Germino GG (2007) *Nat Med* **13,** 1490-1495.

37. Davenport JR, Watts AJ, Roper VC, Croyle MJ, van Groen T, Wyss JM, Nagy TR, Kesterson RA, & Yoder BK (2007) *Curr Biol* **17,** 1586-1594.

38. Kottgen M, Buchholz B, Garcia-Gonzalez MA, Kotsis F, Fu X, Doerken M, Boehlke C, Steffl D, Tauber R, Wegierski T, Nitschke R, Suzuki M, Kramer-Zucker A, Germino GG, Watnick T, Prenen J, Nilius B, Kuehn EW, & Walz G (2008) *J Cell Biol* **182,** 437-447.

39. Marose TD, Merkel CE, McMahon AP, & Carroll TJ (2008) *Dev Biol* **314,** 112-126.

40. Marion V, Stoetzel C, Schlicht D, Messaddeq N, Koch M, Flori E, Danse JM, Mandel JL, & Dollfus H (2009) *Proc Natl Acad Sci U S A* **106,** 1820-1825.

41. Schmidt-Ott KM & Barasch J (2008) *Kidney Int* **74,** 1004-1008.

42. Patel V, Li L, Cobo-Stark P, Shao X, Somlo S, Lin F, & Igarashi P (2008) *Hum Mol Genet* **17,** 1578-1590.

43. Bishop GA, Berbari NF, Lewis J, & Mykytyn K (2007) *J Comp Neurol* **505,** 562-571.

44. Breunig JJ, Sarkisian MR, Arellano JI, Morozov YM, Ayoub AE, Sojitra S, Wang B, Flavell RA, Rakic P, & Town T (2008) *Proc Natl Acad Sci U S A* **105,** 13127-13132.

45. Han YG, Spassky N, Romaguera-Ros M, Garcia-Verdugo JM, Aguilar A, Schneider-Maunoury S, & Alvarez-Buylla A (2008) *Nat Neurosci* **11,** 277-284.

46. Spassky N, Han YG, Aguilar A, Strehl L, Besse L, Laclef C, Ros MR, Garcia-Verdugo JM, & Alvarez-Buylla A (2008) *Dev Biol* **317,** 246-259.

47. Chizhikov VV, Davenport J, Zhang Q, Shih EK, Cabello OA, Fuchs JL, Yoder BK, & Millen KJ (2007) *J Neurosci* **27,** 9780-9789.

48. Amann-Zalcenstein D, Avidan N, Kanyas K, Ebstein RP, Kohn Y, Hamdan A, Ben-Asher E, Karni O, Mujaheed M, Segman RH, Maier W, Macciardi F, Beckmann JS, Lancet D, & Lerer B (2006) *Eur J Hum Genet* **14,** 1111-1119.

49. Alvarez Retuerto AI, Cantor RM, Gleeson JG, Ustaszewska A, Schackwitz WS, Pennacchio LA, & Geschwind DH (2008) *Hum Mol Genet* **17,** 3887-3896.

50. Kovacs JJ, Whalen EJ, Liu R, Xiao K, Kim J, Chen M, Wang J, Chen W, & Lefkowitz RJ (2008) *Science* **320,** 1777-1781.

51. Yamaguchi T, Nagao S, Wallace DP, Belibi FA, Cowley BD, Pelling JC, & Grantham JJ (2003) *Kidney Int* **63,** 1983-1994.

52. Berbari NF, Lewis JS, Bishop GA, Askwith CC, & Mykytyn K (2008) *Proc Natl Acad Sci U S A* **105,** 4242-4246.

53. McGlashan SR, Jensen CG, & Poole CA (2006) *J Histochem Cytochem* **54,** 1005-1014.

The text of Chapter 1 in part is a reprint of the material as it appears in Current Opinions in Genetics and Development, 2009, Lancaster MA, and Gleeson JG. The dissertation author was the primary author of this paper and the co-author supervised and directed the writing of this publication which forms the basis of this chapter.

Chapter 2. Impaired Wnt/β-catenin signaling disrupts adult renal homeostasis and leads to cystic kidney ciliopathy

2.1 Abstract

Cystic kidney disease represents a major cause of end-stage renal disease, yet the molecular mechanisms of pathogenesis remain largely unclear. Recent emphasis has been placed on a potential role for canonical Wnt signaling, but investigation of this pathway in adult renal homeostasis is lacking. Here we provide evidence of a previously unidentified canonical Wnt activity in adult mammalian kidney homeostasis, loss of which leads to cystic kidney disease. Loss of the Jouberin (Jbn) protein in mouse leads to the cystic kidney disease, nephronophthisis (NPHP) due to a surprising decrease in endogenous Wnt activity. Jbn interacts with and facilitates β-catenin nuclear accumulation resulting in positive modulation of downstream transcription. Finally, we demonstrate that Jbn is required *in vivo* for a Wnt response to injury and renal tubule repair, absence of which triggers cystogenesis. Our findings implicate a previously unrecognized balance of canonical Wnt regulation in adult kidney homeostasis, disruption of which leads to cystic kidney disease.

2.2 Introduction

Cystic kidney disorders include autosomal recessive and dominant polycystic kidney diseases (ARPKD and ADPKD) as well as nephronophthisis (NPHP)(1, 2). Although the exact causes of these related disorders are not clear, various signaling pathways have been implicated. Specifically, several of the proteins encoded by the NPHP genes have been identified as negative modulators of the canonical Wnt pathway while activating the noncanonical planar cell polarity (PCP) pathway(3, 4), suggesting a

specific link between cystic kidney disease and Wnt signaling. The emerging model is that cystogenesis is at least partly due to overactivation of canonical Wnt signaling. This is supported by work with mutants of negative Wnt regulators which exhibit embryonic kidney cysts(5, 6). However, similar embryonic kidney cysts have also been documented in mutants of *positive* regulators as well(7, 8), pointing to a unique dichotomy which may reflect more complex mechanisms than have previously been recognized. Since none of the cystic disease proteins have been examined for altered Wnt signaling *in vivo* in the mammalian kidney, and Wnt activity has not been examined in the healthy adult kidney, the exact role of canonical Wnt signaling in adult-onset cystic kidney disease is still poorly understood.

2.3 Results

Ahi1$^{-/-}$ mice exhibit pathology consistent with NPHP

Jouberin (Jbn) is the protein product of the *AHI1* gene mutated in Joubert syndrome(9, 10), a disorder associated with cerebellar hypoplasia, retinitis pigmentosa, and NPHP(11). We targeted *Ahi1* using homologous recombination to generate *Ahi1* null mice (manuscript in preparation). Initial examination of *Ahi1*$^{-/-}$ mice revealed a complete loss of the Jbn protein (Supplementary Fig. 1a) but overall normal embryonic development. However, the mice exhibited postnatal runting and the majority (approximately 80%) did not survive to adulthood (manuscript in preparation). We investigated postnatal kidney morphology as a potential cause of mortality. *Ahi1* mutants exhibited no renal abnormalities at any neonatal time points examined from 3–21 days (Supplementary Fig. 1b and data not shown). However, *AHI1* mutations have been reported in some patients with late-onset NPHP(12). Additionally, we identified specific localization of Jbn in mouse kidney inner medullary collecting duct cells

(mIMCDs)(13) at the ciliary basal body (Fig. 1a and Supplementary Fig. 2a, b) and as occasionally distributed puncta along the ciliary axoneme (Fig. 1a and Supplementary Fig. 2a), similar to that recently described(14). *In vivo* examination of endogenous Jbn in adult mouse kidney similarly revealed basal body and axoneme localization in collecting ducts as described by a recent study(14), as well as in proximal and distal tubules (Fig. 1b and Supplementary Fig. 2c) with particular intensity at the cortico-medullary junction (Supplementary Fig. 2d) that was not present in *Ahi1* mutant kidney. Further, western blot for Jbn revealed a steady increase with age from P8 to 5 months (Supplementary Fig. 2e) suggesting a potential role in the adult kidney.

We therefore examined surviving adult *Ahi1*$^{-/-}$ mice for potential late-onset renal phenotypes. By 5 months, null kidneys appeared smaller than littermate controls (Fig. 1c) and exhibited the characteristic histological triad of NPHP(15): tubular basement membrane abnormalities including thickening and disintegration with tubular collapse, interstitial cell infiltrate and fibrosis, and finally, a later appearance (1 year) of multiple microcysts and tubular dilatation (Fig. 1d and Supplementary Fig. 3a, b). Masson's trichrome staining additionally demonstrated these abnormalities (Supplementary Fig. 3c) and antibodies to collagen I and fibronectin revealed increased staining indicating interstitial fibrosis in kidneys of *Ahi1*$^{-/-}$ mice (Fig. 1e), consistent with NPHP pathology. Tubule abnormalities were particularly concentrated in the cortico-medullary region. We therefore examined which tubules were most affected and identified colabeling of cystic tubules with lotus lectin, a proximal tubule marker (Fig. 1f)(16), indicating that, similar to the human disease, proximal tubules of the cortico-medullary region were most affected.

We next quantitatively examined cyst progression by measuring cyst index in littermates at various ages(17). Null mice aged at least 1 year of age exhibited significantly increased average cyst area as a ratio of total kidney area (Supplementary

Fig. 3d). Next, we examined kidney function impairment by testing for proteinuria and urinary concentrating defects. Bradford assay as well as Coomassie stained SDS-PAGE revealed increased urine protein levels in *Ahi1* mutants at 18–21 months of age (Fig. 1g) similar to that described in the related *Glis2* late-onset NPHP mutant(18, 19). *Ahi1* null mice 21 months of age additionally exhibited decreased serum albumin levels (Control littermates average albumin = 4.0g dL^{-1} (n = 3); $Ahi1^{-/-}$ average albumin = 2.9g dL^{-1} (n = 3), P<0.05, Student's t-test). Furthermore, we examined urine specific gravities at various time points to assess the progression of renal impairment. Null mice aged 2.5 months exhibited no impairments while all null mice at 21 months of age exhibited marked defects in urine concentrating ability compared with littermate controls (Fig. 1h and Supplementary Fig. 4a). Since urinary concentrating defects represent a primary diagnostic test in NPHP(20), these findings are further consistent with NPHP. All mice examined at least 1 year of age exhibited cysts (n = 6) and kidney function impairment (n = 8) suggesting a fully penetrant phenotype. Finally, serum creatinine levels revealed two null mice aged 21 months with moderately elevated creatinine (>0.4 mg dL^{-1}; Controls: <0.2 mg dL^{-1}). Interestingly, the late onset of NPHP in the $Ahi1^{-/-}$ mice mimics that seen in NPHP patients with *AHI1* mutations whose symptoms are not evident until their late teens or early 20s(12, 21).

The cystic kidney disorders have now been identified as part of a larger class known as the ciliopathies which all share a common theme: potential abnormal ciliary structure or signaling(22). We therefore hypothesized that loss of Jbn may lead to cilia defects. We examined primary cilia of 5 month affected $Ahi1^{-/-}$ and control littermate kidneys and found that, despite the NPHP phenotype, the same percentage of cells displayed evident primary cilia, and cilia exhibited indistinguishable morphology, at least at this resolution in all kidney regions examined (Supplementary Fig. 4b). Further,

primary mouse embryonic fibroblasts (MEFs) from *Ahi1*$^{-/-}$ mice exhibited indistinguishable primary cilia with comparable length and morphology and in the same percentage of cells as littermate wild-type MEFs (Supplementary Fig. 4c). Finally, electron micrographs from retinal connecting cilia of these mutants revealed grossly normal 9+0 doublet architecture (data not shown). We therefore concluded that Jbn is not necessary for proper ciliogenesis, suggesting alternative mechanisms for the defects in these mice.

Ahi1$^{-/-}$ mice exhibit abrogated adult renal Wnt activity

Several cystic disease proteins have been identified as direct regulators of the Wnt pathway. NPHP2 (Inversin), NPHP3, and Glis2 have all been shown to inhibit canonical Wnt signaling(3, 4, 23). In contrast, polycystin-1 (PC1) has been shown to activate the canonical Wnt pathway(24-26), though recent data suggests its C-terminus may negatively regulate the pathway(27). To test whether Jbn plays a role in canonical Wnt signaling, we crossed *Ahi1* heterozygous mice with TOPGAL (Tg) transgenics, a well documented canonical Wnt transgenic reporter line(28). We first examined time points E13.5, P10 and 2 weeks and did not see a defect in β-galactosidase (β-gal) levels in *Ahi1*$^{-/-}$; Tg^{+} kidneys where strong Wnt activity was present in both control and mutant kidneys (data not shown). We next examined whether Wnt signaling defects were present in adult (5 month) *Ahi1*$^{-/-}$;Tg^{+} mouse kidneys with early signs of NPHP and stained for β-gal using X-Gal. The adult mouse kidney had previously been reported to lack canonical Wnt activity(29). Likewise, we saw almost no staining upon initial examination of control Tg^{+} kidneys with brief X-Gal staining (data not shown). However, we performed extended X-Gal staining, while controlling for endogenous activity by using a pH 7.7–8.0 X-Gal solution(30), with *Ahi1*$^{+/-}$; Tg^{+} control kidneys and identified a

previously unrecognized specific staining pattern in the kidney cortex with particularly high levels in the cortico-medullary region (Fig. 2a). Surprisingly, *Ahi1*$^{-/-}$; Tg^{+} littermate kidney displayed an almost complete absence of activity, even when developed to saturation (Supplementary Fig. 5a).

Due to the existence of endogenous β-gal activity in the adult kidney(31) we confirmed these results by immunostaining using a bacterial β-gal specific antibody which we then quantified (Fig. 2b). This approach revealed absent staining in *Ahi1*$^{-/-}$; Tg^{+} kidney whereas control Tg^{+} littermate kidney exhibited broader staining throughout the kidney cortex compared with X-Gal probably due to the requirement for pentameric β-gal complex formation for enzymatic activity. Overall, antibody staining appeared more specific suggesting this approach is preferable when staining adult kidney for exogenous β-gal reporters. In order to further control for background endogenous β-gal activity, we performed antibody staining in wild-type; Tg^{-} and Tg^{+} kidneys as well as X-Gal staining in Tg^{+} samples alongside Tg^{-} littermates which did not display the specific staining seen in Tg^{+} samples (Supplementary Fig. 5b). Finally, we additionally performed β-gal staining in an alternate Wnt reporter line, BATGAL(32), which exhibited more intense staining in a pattern similar to Tg, supporting the validity of this Wnt activity (Supplementary Fig. 5c). Although the BATGAL reporter exhibited a more robust activity, we were unable to generate either *Ahi1*$^{-/-}$; *Bg*$^{+}$ or *Ahi1*$^{+/+}$; *Bg*$^{-}$ mice, suggesting the two loci are linked.

In order to further test this Wnt effect, we examined an independent and endogenous Wnt reporter, Lef-1(33). In littermate control kidney, tubules positive for β-gal costained for Lef-1; however, *Ahi1*$^{-/-}$ kidney displayed a dramatic reduction in Lef-1 expression concurrent with β-gal reduction (Fig. 2c). Furthermore, examination of two additional Wnt targets, Axin-2(34) and DKK-1(35), both revealed striking reductions in

cortico-medullary protein expression in *Ahi1*$^{-/-}$ kidneys (Fig. 2d). Finally, we examined Lef-1 expression using western blotting from whole kidney lysates as an alternate method of detection. This approach revealed a decrease in expression of the Wnt responsive full-length isoform(36) of Lef-1 in null kidneys compared to littermate controls at 5 months of age and 1 year of age, whereas the smaller isoform was unaffected (Fig. 2e). Thus, these data indicate that loss of Jbn leads to abrogation of basal Wnt activity in the adult mouse kidney.

To determine which specific tubules exhibited Wnt activity, we performed costaining with a variety of lectins and identified co-labeling of β-gal tubules with lotus lectin, Wnt active tubules represent a subset of proximal tubules (Supplementary Fig. 5d), the same tubule type which later exhibits dilatation in *Ahi1* mutants (Fig. 1f). Lotus lectin staining in *Ahi1*$^{-/-}$ 5 month kidneys revealed normal proximal tubule numbers, suggesting the presence of the proximal tubule epithelium was not affected.

In order to further test the specificity of the Wnt defect in these mice and to examine whether the Wnt defect was secondary to early NPHP changes, we performed X-Gal, β-gal and Lef-1 antibody staining prior to the appearance of NPHP pathology. At 2.5 months, *Ahi1*$^{-/-}$ mice exhibited normal kidney morphology yet X-Gal staining and β-gal antibody staining revealed an already noticeable decrease in Wnt activity when compared to littermate controls (Fig. 2f). In addition, *Ahi1*$^{-/-}$ kidneys displayed decreased Lef-1 staining further indicating decreased Wnt activity prior to NPHP onset (Fig. 2g). Finally, we also examined Lef-1 and an alternate Wnt target gene, GAD-1(37), by western blot on whole kidney lysates from age 3 month old mice with no preexisting renal dysfunction (Supplementary Fig. 4a). Both target genes exhibited decreased levels in these mice (Fig. 2h). Overall, all *Ahi1*$^{-/-}$ mutants tested (n = 4 before NPHP onset, n = 5 after disease onset) revealed a reproducible decrease in Wnt activity compared with

control littermates, measured using a variety of assays. Together, these data indicate the loss of Wnt activity precedes the pathological appearance of NPHP.

The timing of Wnt activity abrogation in *Ahi1*$^{-/-}$ mice and the onset of NPHP pathology suggests loss of basal Wnt activity may contribute to NPHP pathogenesis in these mice. To test for a genetic interaction with the Wnt pathway, we generated double heterozygotes for *Ahi1* and *Lrp6* since Lrp6 has previously been identified as a necessary component in the canonical Wnt pathway(8). Although neither *Ahi1*$^{+/-}$ mice nor *Lrp6*$^{+/-}$ control littermates exhibited kidney pathology, the combination of the two genotypes partially phenocopied the *Ahi1*$^{-/-}$ mouse pathology, pointing to nonallelic noncomplementation. *Ahi1*$^{+/-}$*; Lrp6*$^{+/-}$ mice exhibited significantly decreased kidney size (Fig. 3a) and tubular abnormalities consistent with NPHP (Fig. 3b and c). Additionally, later stage cysts and tubule dilatation were evident, similar to that seen in *Ahi1*$^{-/-}$ kidneys, which we quantified by measuring cyst index (Fig. 3d). Finally, we observed a similar decrease in urine specific gravity as that seen in *Ahi1*$^{-/-}$ mice (Fig. 3e). We also measured serum creatinine, and although the majority of *Ahi1*$^{+/-}$*; Lrp6*$^{+/-}$ mice exhibited normal creatinine (<0.2mg dL^{-1}), one double heterozygote did exhibit elevated levels (0.6mg dL^{-1}). These data suggest that Jbn and Lrp6 function in the same pathway, and that the NPHP phenotype in *Ahi1*$^{-/-}$ mice is Wnt-dependent.

Jbn functions downstream of β-catenin stabilization

Although Jbn seems to act as a positive modulator of the canonical Wnt pathway, *Ahi1*$^{-/-}$ mice exhibit a milder phenotype compared with the embryonic lethality and severe defects seen in classical Wnt mutants such as the *Wnt3a* mutant mouse(38). We therefore hypothesized that Jbn may play a modulatory role rather than acting as an intrinsic Wnt pathway component. In order to test this hypothesis, we used an *in vitro*

approach using the Super Topflash Wnt reporter luciferase construct(39, 40). HEK293T cells transfected with this construct and Jbn alone did not exhibit activation of the Wnt pathway, indicating that Jbn is not itself an activator of the pathway (Fig. 4a). However, transfection of Jbn potentiated the response to cotransfected Dvl-1 (Fig. 4a) or treatment with Wnt3a (Supplementary Fig. 6a), suggesting that Jbn positively modulates the canonical Wnt pathway. Additionally, measurement of endogenous levels of the Wnt target gene cyclin D1(41) revealed potentiation of the transcription response similar to that seen in the luciferase assay, whereas Jbn overexpression in the absence of Wnt had no effect on cyclin D1 (Fig. 4b). These results support the hypothesis that Jbn is a canonical Wnt pathway modulator.

Wnt stimulation results in accumulation of cytosolic β-catenin due to disruption of the β-catenin destruction complex as one of the key steps in downstream signaling(42). To elucidate which step in the canonical Wnt pathway Jbn may modulate, we first tested whether Jbn overexpression had an effect on endogenous cytosolic β-catenin protein levels. Treatment of 293T cells with Wnt3A conditioned media resulted in increased cytosolic β-catenin protein levels as expected (Fig. 4c). Overexpression of Jbn, however, did not potentiate this increase suggesting Jbn may function downstream in the pathway. To test this hypothesis, we employed a constitutively active β-catenin lacking the amino terminus (β-catΔN) thus being resistant to degradation(43). We found that cotransfection of wild-type Jbn potentiated the response to β-catΔN (Fig. 4d) implicating modulation downstream of activation of β-catenin.

To further test the hypothesis that Jbn acts downstream of β-catenin stabilization, we utilized siRNA oligonucleotides targeted to mouse Jbn. Out of three siRNAs tested, siRNA 1 and 3 substantially reduced endogenous Jbn in mouse N2A cells (Supplementary Fig. 6b); therefore, these two were used for subsequent analyses. To

test for a requirement for Jbn downstream of β-catenin activation, Jbn siRNAs were cotransfected with β-catΔN. Jbn knockdown with siRNA oligos led to a significant decrease in the response elicited by β-catΔN as compared to control siRNA cotransfection (Fig. 4e). These results support the hypothesis that Jbn modulates and is required for the Wnt signaling response downstream of β-catenin stabilization.

Jbn facilitates β-catenin nuclear translocation

We next tested the possibility that Jbn may interact with β-catenin to modulate its signaling effects using a coimmunoprecipitation approach. 293T cells transfected with GFP-tagged Jbn were subjected to immunoprecipitation using a GFP antibody followed by immunoblotting for endogenous β-catenin. This method revealed an interaction between β-catenin and GFP-Jbn but not GFP empty vector (Fig. 5a). Treatment with Wnt3A led to an increase in the amount of β-catenin pulled down with Jbn, suggesting a specific interaction with the Wnt responsive pool of β-catenin. We next tested this interaction by reciprocal coimmunoprecipitation from wild-type mouse tissue. Endogenous Jbn specifically coimmunoprecipitated with β-catenin but not with GFP negative control mouse IgG_1 antibody, suggesting this interaction occurs reciprocally and *in vivo* (Fig. 5b).

Since Jbn functions downstream of cytosolic β-catenin stabilization and can associate with β-catenin while exhibiting both nuclear and cytosolic localization, we hypothesized that Jbn may function to facilitate translocation and accumulation of β-catenin in the nucleus. To test this possibility, we first examined 293T cells overexpressing GFP-Jbn which displayed a subtle increase in nuclear β-catenin when compared to neighboring untransfected cells (Supplementary Fig. 7a). We next performed nuclear extraction from Cos7 cells transfected with GFP-Jbn followed by

western blot assay of nuclear β-catenin protein levels to better visualize the effect on nuclear β-catenin (Fig. 5c). This assay revealed a potentiation of the Wnt3A dependent nuclear β-catenin increase in the presence of Jbn overexpression. Importantly, Jbn overexpression alone also led to an increase in nuclear β-catenin. Luciferase results however indicate this is not sufficient for triggering a transcription response, likely due to a requirement for other Wnt induced transcription regulators. Notably, although Jbn was primarily present in the cytosolic fraction, it also exhibited nuclear levels which increased in a Wnt dependent manner with β-catenin nuclear accumulation, suggesting it may co-translocate into the nucleus with β-catenin.

We therefore next examined whether Jbn and β-catenin interact in the nucleus by performing coimmunoprecipitation from nuclear extracts of Cos-7 cells, which revealed an interaction between endogenous nuclear β-catenin and GFP-Jbn (Fig. 5d). We then tested whether Jbn is required for β-catenin nuclear localization *in vivo* by examining endogenous β-catenin localization. In control kidneys, in addition to its more recognized basolateral localization, β-catenin was also clearly evident in the nucleus of a subset of cortical tubules adjacent to the medulla (Fig. 5e) which costained for the proximal tubule marker lotus lectin (Supplementary Fig. 7b). A subset of Jbn protein similarly displayed nuclear localization in addition to its primarily cytosolic and basal body staining (Supplementary Fig. 7c). *Ahi1*$^{-/-}$ kidneys, however, showed no evidence of nuclear β-catenin staining while basolateral staining was intact, indicating that *in vivo*, Jbn plays a role in nuclear localization of β-catenin. Given that Jbn potentiates and is required for nuclear β-catenin accumulation, and that Jbn's primary localization appears cytoplasmic with a nuclear subpopulation which is dynamically regulated by Wnt activation, these results suggest a role for Jbn in cytoplasmic-nuclear shuttling of β-catenin.

Since β-catenin does not contain nuclear localization signals (NLS) we hypothesized that Jbn may facilitate translocation of activated β-catenin to the nucleus via three NLSs which we identified within the Jbn protein (PredictNLS(44)). To test this possibility, we inactivated these NLSs by mutating key lysine residues predicted to abolish NLS activity in NLS1 and in the overlapping region of NLS 2 and 3 (Supplementary Fig. 8a). The three mutants (ΔNLS1, ΔNLS2/3, and the combination of both mutations ΔNLS1/2/3) exhibited comparable expression levels to wild type Jbn although NLS1 was somewhat decreased (Supplementary Fig. 8b), but all mutant constructs failed to localize to the nucleus when examined by fluorescence microscopy and exhibited significantly decreased Wnt signaling potentiation compared with wild-type Jbn when cotransfected with Dvl-1 (Supplementary Fig. 8c, d) or β-catΔN (Fig. 5f). We then performed nuclear extraction with cells transfected with the mutant constructs which exhibited decreased nuclear β-catenin levels compared with wild-type Jbn overexpression (Fig. 5g). Although nuclear localization of ΔNLS2/3 was not completely abolished, it failed to potentiate β-catenin nuclear levels, while the mutant lacking all NLS regions (ΔNLS1/2/3) exhibited similar overall expression levels to that of wild type yet failed to enter the nucleus and failed to potentiate β-catenin nuclear accumulation. These data support a mechanism whereby Jbn functions through interaction with cytosolic β-catenin to potentiate nuclear translocation, a function that requires all three NLS regions of Jbn.

Ahi1$^{-/-}$ mice exhibit defective injury repair and Wnt response

We next sought to address how abrogated Wnt signaling might lead to the NPHP phenotype seen in *Ahi1*$^{-/-}$ mice. Wnt activity has previously been reported as upregulated in mouse renal injury lasting as long as 28 d post-injury(45) suggesting it

may be involved in adult renal homeostatic injury repair. We therefore performed injury experiments using established protocols for either cisplatin or ischemia-reperfusion injury (IRI). Control and *Ahi1* null littermates (4 months old) were subjected to intraperitoneal injection of cisplatin or saline or unilateral IRI. At this age, mutant kidneys do not yet display cysts as indicated in mock treated kidneys (Fig. 6a). However, 2.5 to 4 weeks post-injury, microcysts were evident in mutant kidneys, which was reminiscent of the pathology normally observed at one year suggesting acceleration of the phenotype. Control kidneys in contrast displayed signs of injury recovery without evidence of cysts. These findings were quantified by measuring cyst index (Fig. 6b).

To test for the possibility that null mice were more susceptible to the injury itself we also performed a representative renal IRI in a pair of littermate control and *Ahi1* null mice and examined pathology as well as serum chemistry 2 h following injury. Histology revealed comparable signs of injury (vacuolization and epithelial cell sloughing) in mice of both genotypes (Supplementary Fig. 9a), and serum chemistry revealed similarly elevated creatinine (Control: 0.6 mg dL^{-1}, *Ahi1*$^{-/-}$: 0.5 mg dL^{-1}) suggesting the renal insult was not more severe in *Ahi1* null mice. These results support the hypothesis that renal injury repair is abnormal in *Ahi1*$^{-/-}$ mice leading to cystogenesis rather than a more severe injury.

In order to investigate Wnt signaling in this repair process, we performed IRI on *Ahi1*$^{+/+}$*; Tg*$^{+}$ and *Ahi1*$^{-/-}$*; Tg*$^{+}$ kidneys and compared β-gal Wnt reporter activity 5 to 7 d post-injury. In the uninjured right kidney, morphology and Wnt activity appeared similar to that described above for mutant and control though there were mild defects in the wild-type contralateral kidney possibly a result of indirect injury(46). However, the wild-type injured left kidney exhibited clear morphological indications of injury 7 d post-IRI (Fig. 6c) along with a striking upregulation of Wnt activity, as measured by X-Gal and β-

gal antibody staining (Fig. 6d). High magnification revealed a subpopulation of highly Wnt responsive cells which exhibited nonpolarized morphology (Fig. 6e). Histological examination of *Ahi1*$^{-/-}$ injured kidney in contrast revealed tubular dilatation and glomerulosclerosis already present at 7 d post-injury (Fig. 6c) that lacked comparable Wnt reporter upregulation (Fig. 6d). We then performed quantification of Wnt activity using a β-gal luminescence assay on whole kidney lysates of an independent set of injured littermates aged 3 months with no prior renal impairment (Supplementary Fig. 4a). This assay revealed upregulation of Wnt activity in the control injured kidney 5 d post-IRI compared with the uninjured kidney (Supplementary Fig. 9b), whereas both *Ahi1*$^{-/-}$ kidneys exhibited decreased Wnt activity which was especially evident in the injured kidney lysate. These results suggest a role for canonical Wnt signaling in recovery from injury, a function which is abrogated in *Ahi1* mutant kidneys leading to renal cyst pathology.

2.4 Discussion

Our findings provide the first indication that the canonical Wnt pathway is necessary for adult kidney homeostasis, and that abrogation of this signaling can lead to cystic kidney pathogenesis. Despite the ciliopathy nomenclature, the NPHP phenotype which arises with loss of Jbn seems not to relate to structural ciliary defects. Instead, Jbn acts as a direct positive modulator of canonical Wnt signaling. Some ciliopathy proteins have been found to regulate the structure of the cilium itself (NPHP1 and 4)(47) yet several others (i.e. Inversin, Glis2) appear to play primarily signaling roles(3, 23). With recent evidence pointing to a negative regulatory role for the primary cilium itself in canonical Wnt signaling, we hypothesize that the renal pathology associated with ciliopathies is at least partly due to disruption of downstream signaling. This may occur

either through an indirect effect of the cilium on these pathways, or through direct regulation of the pathway itself. While indirect regulation through disruption of the cilium might be expected to result in an *increase* in canonical Wnt activity, Jbn instead directly potentiates the pathway as indicated by a lack of effect on the presence of the primary cilium and *reduced* endogenous Wnt signaling.

Like Jbn, several other ciliopathy proteins are modulators of canonical Wnt signaling, but to date, the data suggests that they mainly function as negative regulators of the pathway. These seemingly contradictory results suggest a unique balance of Wnt/β-catenin regulation modulating renal development and homeostasis. Parallels can be discerned from renal tubule development in which disruption of canonical Wnt signaling in either direction leads to inhibition of terminal epithelial differentiation, suggesting a similar delicate balance of regulation(48-50). Likewise, noncanonical Wnt (planar cell polarity, PCP) disruption similarly leads to defects in formation of the polarized epithelium(51), and abnormal PCP has also been implicated in cystic kidney disease pathogenesis(52, 53). Thus, differentiation of the renal tubular epithelium exhibits sensitivity to precise Wnt regulation similar to that seen in adult cystogenesis with loss of Jbn, suggesting similar mechanisms.

Given the parallels between renal tubular development and cystogenesis, the question arises: how might these *developmental* processes be involved in pathogenesis of an *adult-onset* disease? One model suggests developmental processes can be reactivated in adult renal epithelial cells during basal cell turnover or in response to injuries in order to regenerate renal tubules(54). Differentiated epithelial cells may in fact be capable of dedifferentiating in order to proliferate and repopulate damaged tubules with new epithelium(31, 55). Our findings suggest that precise Wnt signaling regulation,

similar to that seen in developing tubules, may be vital to tubular epithelial cell renewal in the adult kidney, and that this signaling is particularly active following injury.

Similar to *Ahi1*$^{-/-}$ mice, acute injury has been shown to trigger cystogenesis in other cystic kidney mouse models whereas conditional ablation leads to a slow accumulation of cysts in the absence of acute injury(17, 56, 57). These late-onset phenotypes may reflect a gradual accumulation of mild damage leading to vulnerability to cystogenesis when tubular regeneration is initiated. Thus, the homeostatic balance of Wnt activity in adult tissues may regulate the regenerative response to subtle injuries and basal cell turnover, a function whose loss leads to a mammalian ciliopathy(58). These findings may reflect a general requirement for reactivation of developmental pathways in injury repair, which, given the vital developmental signaling role for the primary cilium, may be abnormally regulated in adult-onset ciliopathy pathogenesis.

Acknowledgements

We are grateful to members of the Gleeson lab for technical expertise and feedback and the Nigam lab for helpful kidney related discussions and reagents, as well as B. Brinkman and the UCSD Neuroscience Microscopy Core. We also thank the M. G. Rosenfeld, K. Kaushansky, M. Karin, and P.L. Mellon labs as well as E. L. Stone for reagents and technical expertise. We are grateful to S. Piccolo at the Departments of Histology, Microbiology and Medical Biotechnologies, University of Padua, Italy for the BATgal mice. We thank S. Pleasure at the Department of Neurology, University of California, San Francisco for *Lrp6* mutant mice. We also thank M.G. Rosenfeld at the School of Medicine, University of California, San Diego for the β-catΔN construct, and R.T. Moon at the Department of Pharmacology, University of Washington for the Super Topflash construct. M.A.L. and C.M.L received support from NIH/NIGMS funded UCSD

Genetics Training Program (T32 GM08666). This work was supported by the US National Institutes of Health, and the Burroughs Wellcome Fund in Translational Research (J.G.G.). J.G.G. is an investigator with Howard Hughes Medical Institute.

Author contributions

M.A.L. designed the experimental approach, conducted the experiments, and wrote the manuscript. J.G.G. supervised the project and experimental approach, interpreted data, and contributed to manuscript preparation. C.M.L. designed and generated the *Ahi1*$^{-/-}$ mouse mutant and provided feedback. J.L.S. generated mutant constructs and assisted in microscopy. L.S. contributed to *in vitro* localization. M.D. contributed to IRI experiments. S.K.N. provided feedback regarding renal characterization and manuscript preparation. K.W. provided feedback and reagents for *in vitro* Wnt assays.

2.5 Methods

Plasmid constructs and materials.

We generated the GFP tagged Jbn construct by amplification of full-length Jbn (1196 amino acid variant) from human fetal cDNA and cloned into pCR-BluntII-TOPO vector (Invitrogen) then subcloned into pEGFP-C3 (Clontech). We generated NLS mutants by using the QuikChange Site-Directed Mutagenesis Kit (Stratagene). Highlighted lysines (Supplementary Fig. 8a) were mutated to glutamic acid (NLS1) or glutamine (NLS2/3). Jbn siRNA oligonucleotides were from Invitrogen (Stealth RNAi) while negative control siRNA was a scrambled oligo with no genomic homology (Invitrogen).

Kidney histology and functional assessment.

Mouse lines are described in detail in the Supplementary Methods. We stained kidney sections for hematoxylin and eosin (Richard Allen Scientific) or Masson's Trichrome (Sigma) or for X-Gal for approx. 2 h (for neonatal), 12 h (for adult, short staining) or 48 h (for adult, maximal staining). We used ImageJ software (NIH) to measure cyst index by taking the sum of areas of cysts >60 μm in diameter from H&E stained kidney sections as a ratio of total kidney area from at least three medial sections per kidney. We examined renal function from equal volumes of collected urine samples using the Bradford protein assay (Biorad) or coommassie stained SDS-PAGE for proteinuria studies, and using a veterinary refractometer (UCSD mouse diagnostic core) for specific gravity measurements. We obtained urine before and after dehydration for 16 h (for *Ahi1* mutants) or towards the end of the sleep cycle (late afternoon) to mimic dehydration similar to clinical diagnostic testing (for *Ahi1/Lrp6* mutants). We measured serum albumin and creatinine using the VetScan comprehensive diagnostic profile (Abaxis). We performed β-gal luminescence as described below for luciferase assays and values were normalized for total protein content using the Bradford method (Biorad protein assay). Kidney injury is described in detail in Supplementary Methods.

Immunofluorescence.

We fixed mIMCD and HEK293T cells (ATCC) with 4% PFA for 15 min at room temperature, washed in PBS, blocked in 4% donkey serum in 0.1% TritonX, and stained with primary antibody. We obtained kidney sections by perfusion fixation followed by embedding in 10%/7.5% gelatin/sucrose and cryosectioning at 10 μm (for histology), 20 μm (for immunostaining) or 60 μm (for X-Gal staining) thicknesses. We generated an affinity purified rabbit polyclonal Jbn (generated to amino acids

VKIHVVDEHTGQYVKKDDS, Quality Controlled Biochemicals). For Jbn staining, we performed antigen retrieval by heating samples in 100 mM Tris, 5% urea, pH9.5 at 95 ºC for 10 min. Primary antibodies were: acetylated tubulin (Zymed 32-2700, 1:500 dilution), pericentrin (Covance PRB-432C, 1:200), fibronectin (Chemicon AB2033, 1:80), Collagen I (Abcam AB6308, 1:100), anti β-galactosidase (Zymed 32100, 1:200), anti Lef-1 (Genetex GTX12034, 1:100), rabbit β-catenin (Cell Signaling 95825, 1:100), Lotus lectin (Vector labs FL-1321, 1:100), mouse Conductin (Santa Cruz sc-25302) and goat anti DKK1 (Santa Cruz sc-14949). Samples were washed and incubated in secondary antibodies (AlexaFluor donkey anti-mouse 594, donkey anti-rabbit 594, donkey anti-rabbit 488, donkey anti-mouse 488, donkey anti-goat 594, Molecular Probes, 1:500). Hoechst was the nuclear stain (Molecular Probes, H3570). We acquired and quantified images using a DeltaVision Spectris deconvolution or a FV1000 Spectral Deconvolution Confocal microscope (UCSD Neuroscience Microscopy Core).

Immunoprecipitation and western blotting.

We perfomed western blotting on lysates prepared in modified RIPA buffer using the following antibodies: rabbit Jbn (Quality Controlled Biochemicals), mouse α-tubulin (Sigma, T-6074), rabbit Cyclin D1 (Santa Cruz Biotech, SC-718), anti Lef-1 (Genetex GTX12034), SC-40), mouse β-catenin (BD Transduction Labs, 610153), goat GAPDH (Santa Cruz Biotech, SC-20357), mouse GFP (Covance, B34) and rabbit TFIIH (Santa Cruz Biotech., SC-293). We used all antibodies at 1:1000 dilution. Rabbit antibody to GFP (Genetex, Gtx26556, 1µg), mouse IgG_1 antibody to β-catenin (BD Transduction Labs, 610153), or mouse IgG_1 GFP as a negative control were used for immunoprecipitations from modified RIPA lysates using protein A sepharose beads for rabbit antibody or protein G beads for mouse IgG_1. We perfomed i*n vivo*

immunoprecipitation on brain tissue lysates because both Jbn and β-catenin are well-expressed. We performed cytosolic preparations using a 0.1% saponin solution in 25 mM HEPES and 75 mM potassium acetate which we added directly to wells of confluent 293T cells followed by clearance by centrifugation at 3000 rpm for 5 min. Luciferase assays and nuclear fractionation are described in detail in Supplementary Methods.

2.6 Supplementary Methods

Mouse line generation.

We generated *Ahi1*$^{+/-}$ mice using homologous recombination to generate a floxed allele containing exons 6 and 7 followed by germline transmission using EIIa-Cre transgenics. *Ahi1*$^{+/-}$ were then crossed to TOPGAL^{+} mice(28) (JAX) to generate *Ahi1*$^{+/-}$; TOPGAL^{+} mice. F1 generation was then crossed to *Ahi1*$^{+/-}$ mice to generate *Ahi1*$^{-/-}$; TOPGAL^{+} and *Ahi1*$^{+/-}$; TOPGAL^{+} mice. We genotyped mice using primers for *Ahi1* and *LacZ* on tail DNA. We performed X-Gal staining using a previously published protocol(59) and maintaining a pH 7.7–8.0 to minimize endogenous activity(30, 31). Mouse work was carried out in compliance with Institutional Animal Care and Use Committee approved protocols.

Kidney injury.

We performed kidney injury by either intraperitoneal injection of 20mg kg^{-1} body weight of cisplatin(60) or an equal volume/weight ratio of saline or by unilateral IRI similar to previously described(61). Briefly, mice were anesthetized and the left kidney was exposed and subjected to vascular clamping for 30 min followed by removal of the clamp. The right kidney was left uninjured and animals were then sutured and allowed to recover.

Nuclear fractionation.

We performed nuclear fractionation according to a previously published protocol(62), and nuclear coimmunoprecipitation was performed using rabbit antibody to GFP (Genetex) from nuclear extracts similarly prepared.

Transfection and luciferase assay.

For transient transfections of 293T, mIMCD, Cos7, and N2A cells, we used Lipofectamine 2000 (Invitrogen) according to the manufacturer's protocol. For luciferase assays, we grew 293T cells and N2A cells in 12-well plates and transfected with 600 ng Topflash, 120 ng βGal, and 650 ng of Jbn-GFP expression plasmid or empty vector (GFP was mutated at Y66G to disrupt fluorescence using QuikChange mutagenesis). We co-transfected cells with 650 ng Dvl-1 expression plasmid, 650 ng β-CateninΔN, or treated with Wnt3a conditioned media (WCM) to stimulate the Wnt pathway. We obtained Wnt3A conditioned media from stably transfected L cells with Wnt3A expression vector and used as described(63). Control media was from untransfected L cells. For experiments involving siRNA, we cotransfected 2.5pmol siRNA with half the above DNA amounts using Lipofectamine 2000 according to the manufacturer allowing for >80% transfection efficiency. 48 h following transfection, cells were serum starved for 16 h or treated with WCM diluted 3:1 in serum free media. We performed the luciferase assay according to a previously published protocol(64) and β-galactosidase activity was measured using the Tropix Galacto-light Plus kit (Applied Biosystems, T1007).

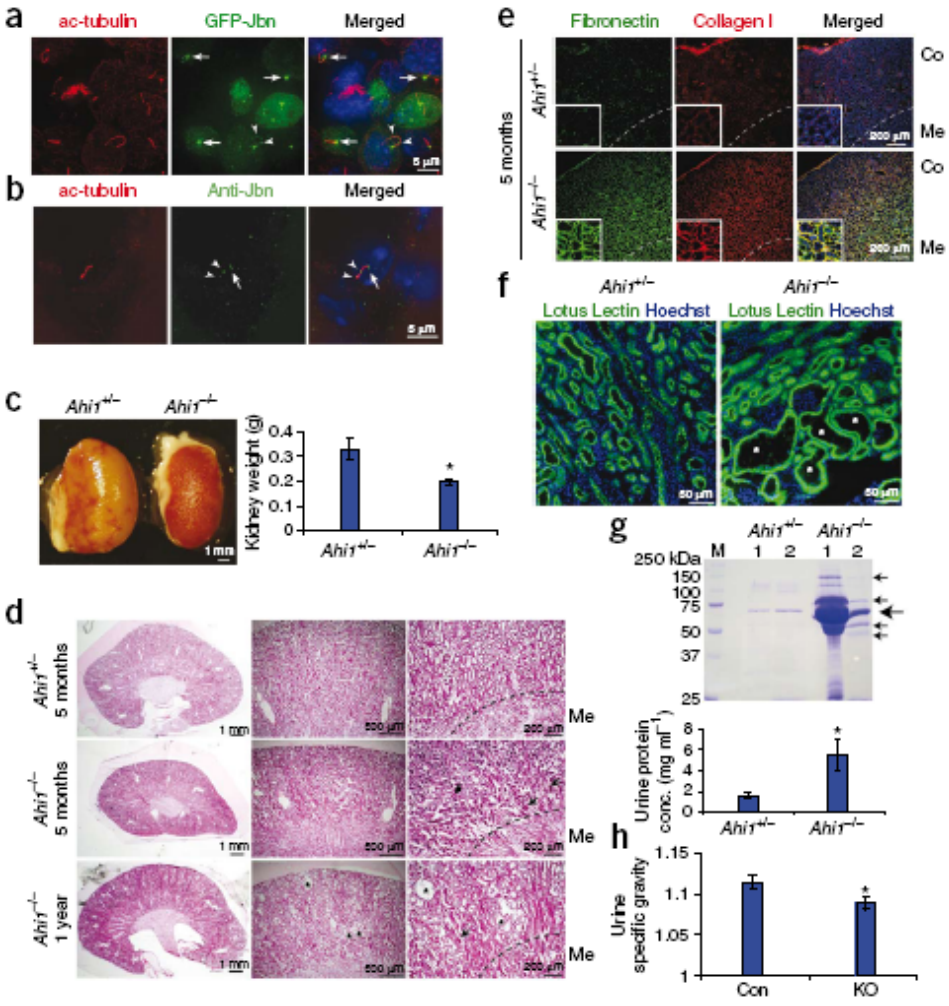

Figure 2.1 Loss of Jbn leads to NPHP pathology. (a) mIMCDs transfected with GFP-Jbn (green) and stained for acetylated tubulin (red) to visualize cilia. Hoechst (blue) labels nuclei. (b) Endogenous Jbn antibody staining (α-Jbn, green) in vivo in tubular epithelial cells of mouse kidney with acetylated tubulin costaining (red). Note basal body localization (arrows), and punctate axonemal staining (arrowheads). (c) Kidneys from Ahi1$^{+/-}$ and Ahi1$^{-/-}$ littermates and average kidney weight measurement at 5 months of age (Student's t-test, *P<0.05, n = 3). (d) H&E staining of 5 month Ahi1$^{-/-}$ kidney sections compared to littermate Ahi1$^{+/-}$. Tubular collapse (arrows) and mononuclear cell infiltrate (#) are evident with tubule dilatation (*) at 1 year. Dashed line indicates medullary (Me) boundary. (e) Antibody staining of 5 month littermate kidneys for fibronectin (green) and collagen I (red). (f) Lotus lectin staining (green) in 1 year littermate kidneys revealing cysts (*) within proximal tubules of Ahi1$^{-/-}$ kidney. (g) Coommassie stained SDS-PAGE on equal volumes of urine from two 18 month old littermates of each of Ahi1$^{+/-}$ and Ahi1$^{-/-}$. Predicted size of albumin is shown (large arrow) as well as additional bands present in Ahi1$^{-/-}$ samples (small arrows). Histogram of average urine protein concentration (n = 5, *P<0.05, Student's t-test). (h) Average urine specific gravity following 16 hour dehydration in control (Ahi1$^{+/+}$ or Ahi1$^{+/-}$, Con) or Ahi1 knock-out (KO) littermates 21 months of age (*P<0.05, Student's t-test, n = 5). Error bars are s.e.m.

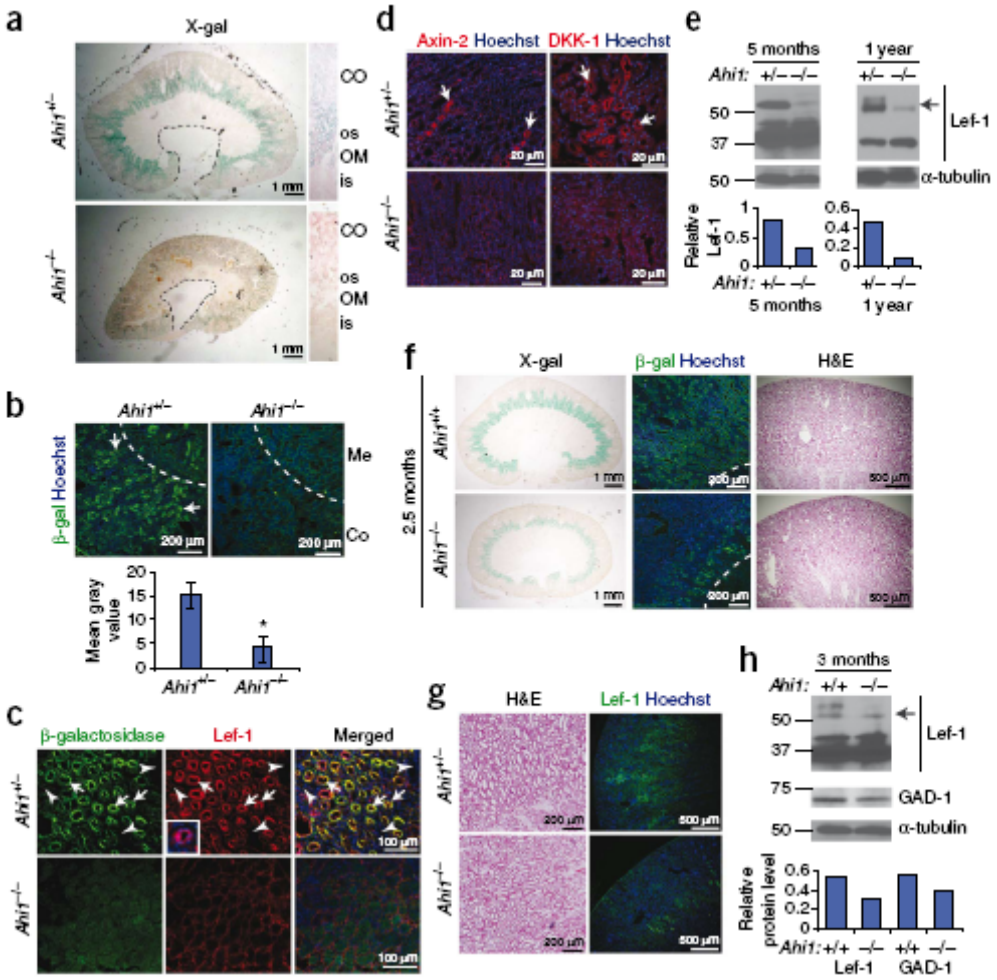

Figure 2.2 Jbn is required for Wnt activity in adult mouse kidney. (a) X-Gal staining in 5 month littermate kidneys. Cross-section reveals outer stripe (os) staining. OM = outer medulla, CO = cortex, is = inner stripe. Dashed line = calyx boundary. (b) Antibody staining for β-gal (green) in 5 month Ahi1$^{+/-}$; Tg^{+} or Ahi1$^{-/-}$; Tg^{+} kidneys. Hoechst labels nuclei (blue). Quantification of β-gal fluorescence (mean gray value, ImageJ). *P<0.05, Student's t-test, n = 3 images. Error bars represent s.e.m. (c) β-gal (green) and Lef-1 (red) costaining (arrows) which is absent in Ahi1$^{-/-}$ kidney. Inset provides higher magnification of Lef-1 staining. Arrowheads indicate negative tubules for reference. (d) Axin-2 and DKK-1 staining (red, arrows) in the corticomedullary region of littermate kidneys. (e) Lef-1 western blot from whole kidney lysates of littermates at 5 months and 1 year of age revealing decreased expression of full length isoform (55–57kDa, arrow). Lef-1 (pixel measurement, ImageJ) was quantified relative to α-tubulin (loading control). (f) X-Gal and β-gal antibody staining in littermate kidneys at 2.5 months of age, before the onset of pathology (H&E at right). Dashed line demarcates medullary boundary (g) Lef-1 target gene staining (green) prior to NPHP pathology (H&E at left). (h) Lef-1 and GAD-1 western blots from whole kidney lysates of Ahi1$^{+/+}$ and Ahi1$^{-/-}$ littermates at 3 months of age. Lef-1 and GAD-1 (pixel measurement, ImageJ) were quantified relative to α-tubulin.

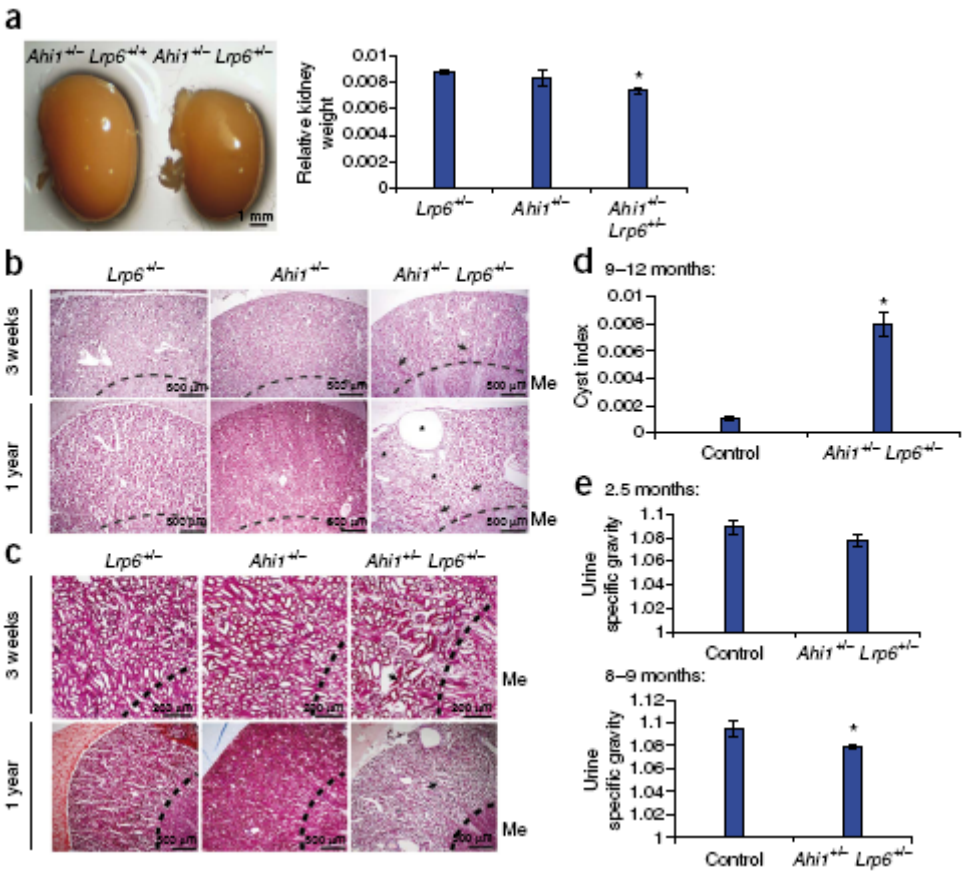

Figure 2.3 Ahi1 exhibits nonallelic noncomplementation with Lrp6. (a) Whole mount image of Ahi1$^{+/-}$ kidney compared with Ahi1$^{+/-}$; Lrp6$^{+/-}$. Average kidney weight relative to total body weight (kidney/body weight ratio, arbitrary units) is shown at right. *P<0.05, n = 3, Students's t-test. (b) H&E and (c) Masson's trichrome staining in Lrp6 and Ahi1 single heterozygotes compared with double heterozygotes. Arrows point to collapsed dysmorphic tubules within the cortex at 3 weeks with a worsening of the phenotype at 1 year in which a large cyst as well as tubule dilatation (*) are evident. (d) Average of cyst index measurements from three sections of each kidney of single heterozygote control littermates (Ahi1$^{+/-}$ or Lrp6$^{+/-}$, Con) and double heterozygote mutants (Ahi1$^{+/-}$; Lrp6$^{+/-}$, Mut) at 9–12 months of age (Student's t-test, *P<0.05, n = 3). (e) Average urine specific gravity at 2.5 months and 8–9 months of age. Both ages exhibit decreased levels in Ahi1$^{+/-}$; Lrp6$^{+/-}$ mutants compared to single heterozygote littermates (Ahi1$^{+/-}$ or Lrp6$^{+/-}$) with significance at 8–9 months (*P<0.05, Student's t-test, n = 3). Error bars in all histograms represent s.e.m.

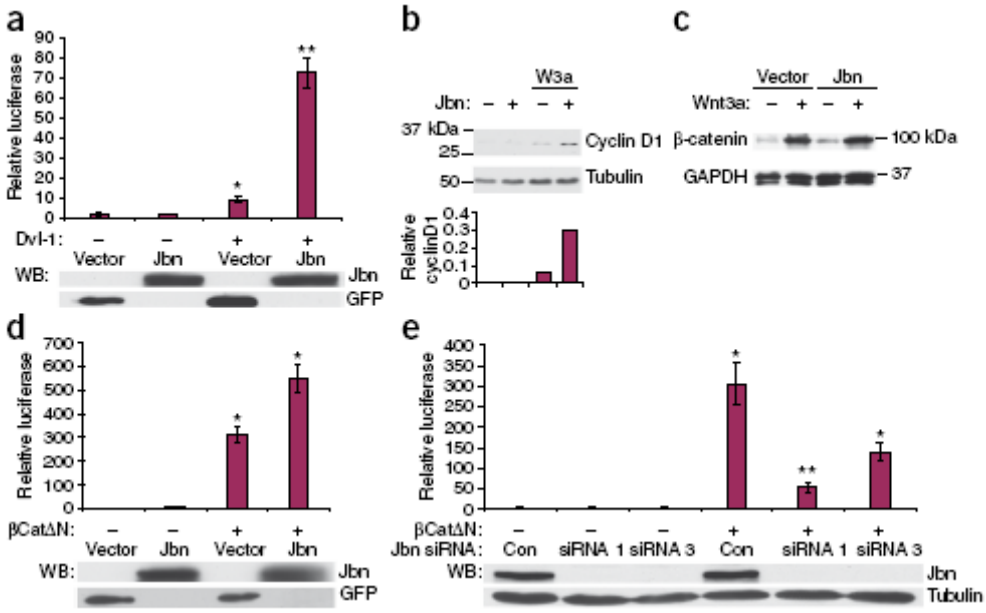

Figure 2.4 Jbn is a positive modulator of Wnt signaling downstream of β-catenin stabilization. (a) Induction of TCF/Lef luciferase reporter with Dvl-1 transfection is potentiated by 7-fold with cotransfection of Jbn. *P<0.001, **P<5E-07, n = 10 from four experiments, Student's t-test. Values are relative to control untreated condition and were normalized for co-transfected β-Gal. Western blot for construct expression from a representative luciferase is shown below each histogram. (b) Western blot for Cyclin D1 with Wnt3A conditioned media treatment (W3A) and overexpression of Jbn. Quantification of cyclin D1 relative to α-tubulin (loading control) shown below. (c) Western blot of cytosolic extracts from 293T cells treated with Wnt3A conditioned media and expressing Jbn or empty vector. GAPDH is the loading control. (d) Luciferase activity relative to vector transfected alone reveals potentiation of Wnt response from 311-fold with βCatΔN expression in the absence of Jbn (vector) to 548-fold increase with Jbn overexpression in 293T cells. *P<0.0005, Student's t-test, n = 24 from nine experiments. (e) Luciferase reporter activity in N2A cells transfected with Jbn siRNA constructs and βCatΔN. *P<0.05, **P<0.001 Student's t-test, n = 7 from four experiments. Values were normalized for total protein concentration and expressed as relative to control untreated condition. Error bars in all experiments represent s.e.m.

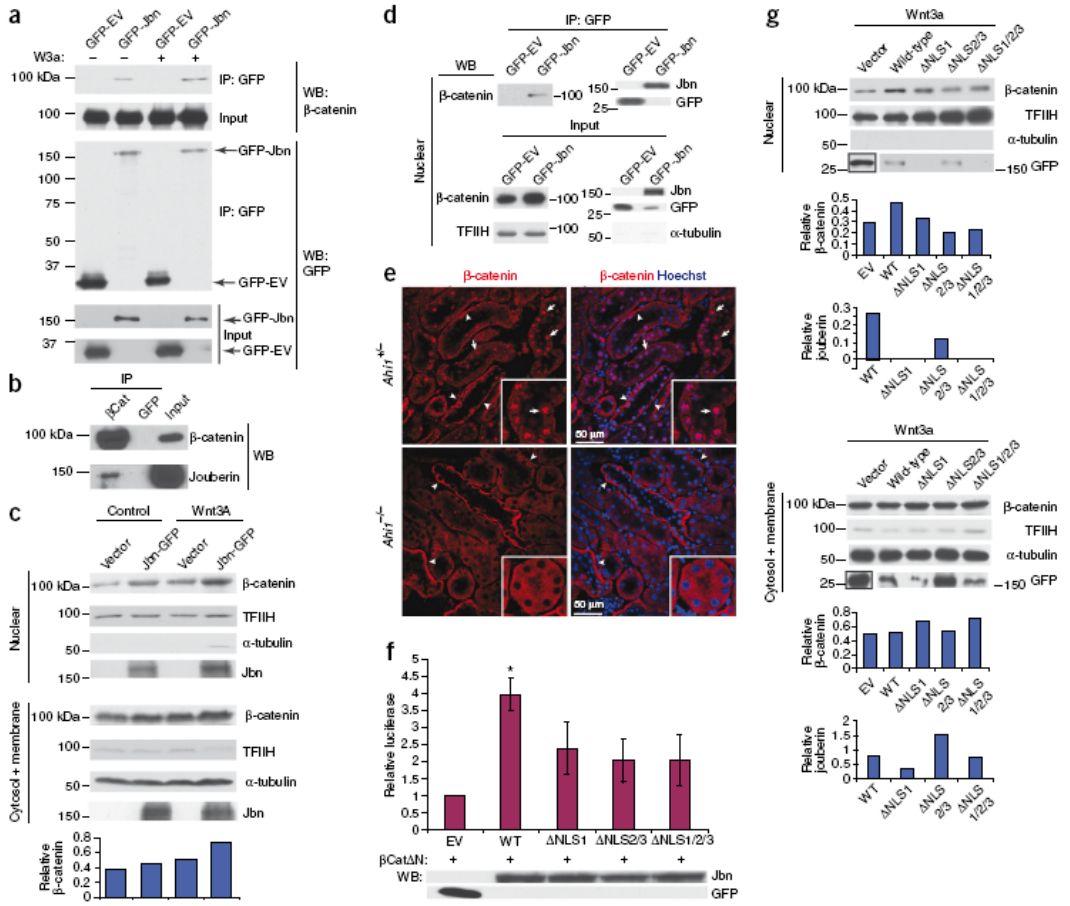

Figure 2.5 Jbn facilitates β-catenin nuclear accumulation. (a) Western blot for β-catenin following GFP-Jbn immunoprecipitation (IP) compared with vector control (GFP-EV) with and without Wnt3a treatment (W3A). Input is total cell lysate before IP. (b) IP for endogenous β-catenin from P5 mouse whole brain lysates with western blot for endogenous Jbn. (c) Western analysis of nuclear extraction from cells transfected with Jbn or vector, with and without Wnt3A treatment. TFIIH and tubulin are nuclear and cytosolic fractionation controls. Quantification of two repeats of this experiment is shown below (β-catenin relative to TFIIH and controlling for cytosolic contamination by subtraction of tubulin, ImageJ). (d) IP from cos-7 nuclear extracts for GFP-Jbn with GFP antibody and western blotting for endogenous nuclear β-catenin. Input is nuclear lysate before the addition of GFP antibody. (e) β-catenin staining (red) of littermate 1 year kidneys revealing nuclear (Hoechst, blue) localization of β-catenin (arrows) that is absent in Ahi1 null kidney. Arrowheads denote basolateral localization. (f) Luciferase activity in 293T cells transfected with βCatΔN and NLS mutants compared to wild-type Jbn. *P<0.05, n = 4 from four separate experiments, Student's t-test. Values are relative to vector control and normalized for co-transfected β-Gal. Error bars represent s.e.m. Western blot is from a representative luciferase. (g) Nuclear extraction and β-catenin western blot from Cos7 cells with overexpression of wild-type Jbn or NLS mutants. TFIIH and α-tubulin are controls for the nuclear extraction. Jbn and β-catenin levels were quantified relative to TFIIH levels for nuclear fraction or α-tubulin for cytosolic fraction (ImageJ).

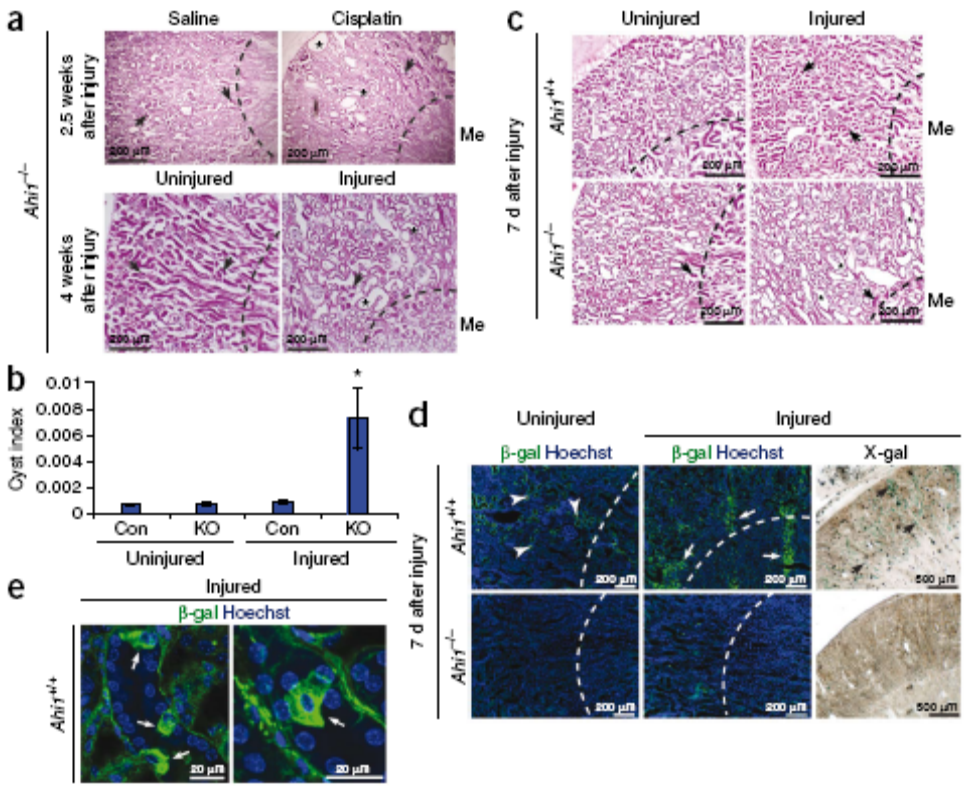

Figure 2.6 Ahi1$^{-/-}$ mice exhibit defective recovery from renal injury. (a) H&E histology in 4 month old injured Ahi1$^{-/-}$ kidneys (cisplatin administration or renal IRI on the left kidney) compared with uninjured kidneys. Cisplatin or mock saline treatment or unilateral IRI were performed on Ahi1$^{-/-}$ mice with early signs of NPHP (arrows) though cysts were not present. 2.5 weeks following cisplatin injection or 4 weeks following IRI of the left kidney, cysts and tubule dilatation are evident (*). Dashed line indicates medullary (Me) boundary. (b) Average cyst index measurement from littermate control (Con) and Ahi1$^{-/-}$ (KO) uninjured and injured kidneys at 2.5 to 4 weeks post injury with either cisplatin or IRI (n = 3 kidneys each, *P<0.05, Student's t-test). (c) H&E histology of injured left kidney of littermate wild-type 7 d after IRI showing tubular obstruction and collapse (arrows). Ahi1$^{-/-}$ injured kidney instead exhibits tubular dilatation and microcysts (*) with evident glomerulosclerosis. Dashed line indicates medullary (Me) boundary. Overall, tubular dilatation was evident in all mutants post-injury (n = 3) but none of the control animals (n = 4). (d) β-gal antibody (green) and X-Gal staining in control littermate uninjured right kidney and injured left kidney revealing increased Wnt activity which is absent in mutant kidney. Hoechst (blue) labels nuclei and the dashed line indicates the medullary boundary. (e) Higher magnification of β-gal positive kidney tubules in control injured sections revealing Wnt responsive cells with fibroblast-like morphology.

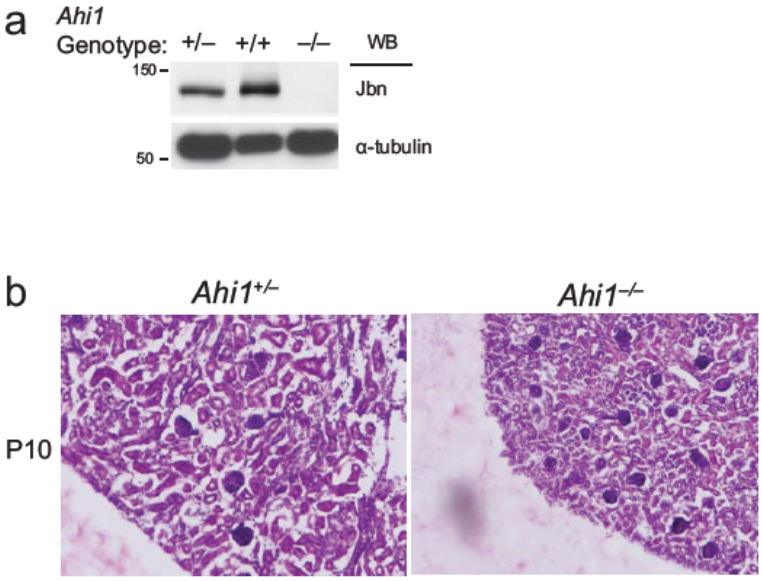

Supplementary Figure 2.1 Ahi1–/– analysis for the presence of Jbn protein. (a) Western blotting performed on brain lysates from littermates show complete lack of Jbn protein (exhibiting an approxim ate molecular weight of 125kDa) in Ahi1–/– sam ples and decreased levels in Ahi1+/– samples indicating complete loss of Jbn in the knockout and the specificity of the Jbn antibody. α-tubulin is shown as a loading control. (b) H&E staining of postnatal day 10 (P10) kidney sections from Ahi1+/– and Ahi1–/– littermates showing no clear differences in morphology.

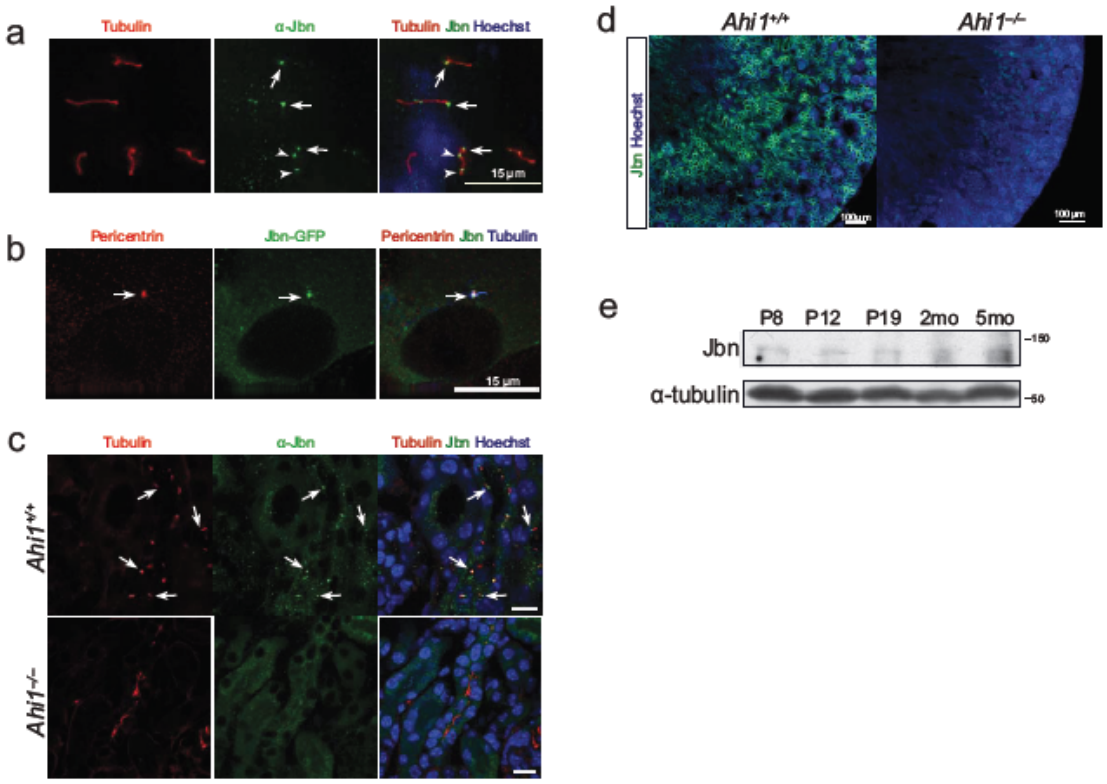

Supplementary Figure 2.2 Jouberin localizes primarily to the basal body in vitro and in vivo. (a) S taining for endogenous Jbn (green) in mIMCDs using the Jbn antibody reveals basal body (arrows) and ciliary punctate (arrowheads) staining. Acetylated tubulin (red) labels the cilium while Hoechst stains the nucleus. (b) GFP-tagged Jbn (green) co-localizes with pericentrin staining (red), a basal body m arker. Acetylated tubulin staining is shown in blue. (c) Jbn antibody staining (green) in Ahi1+/+ kidney tubules at 2 weeks of age reveals basal body localization (arrows) absent in the littermate Ahi1–/– kidney. (d) Low m agnification image of Jbn antibody staining (green) in 2 week old kidney revealing high levels of expression in the cortex particularly adjacent to the m edulla which is largely absent in Ahi1–/– littermate kidney. Hoechst stains the nuclei (blue). (e) Western blot analysis of Jbn expression in murine kidney which demonstrates increasing protein levels w ith age. α -tubulin is shown as a loading control.

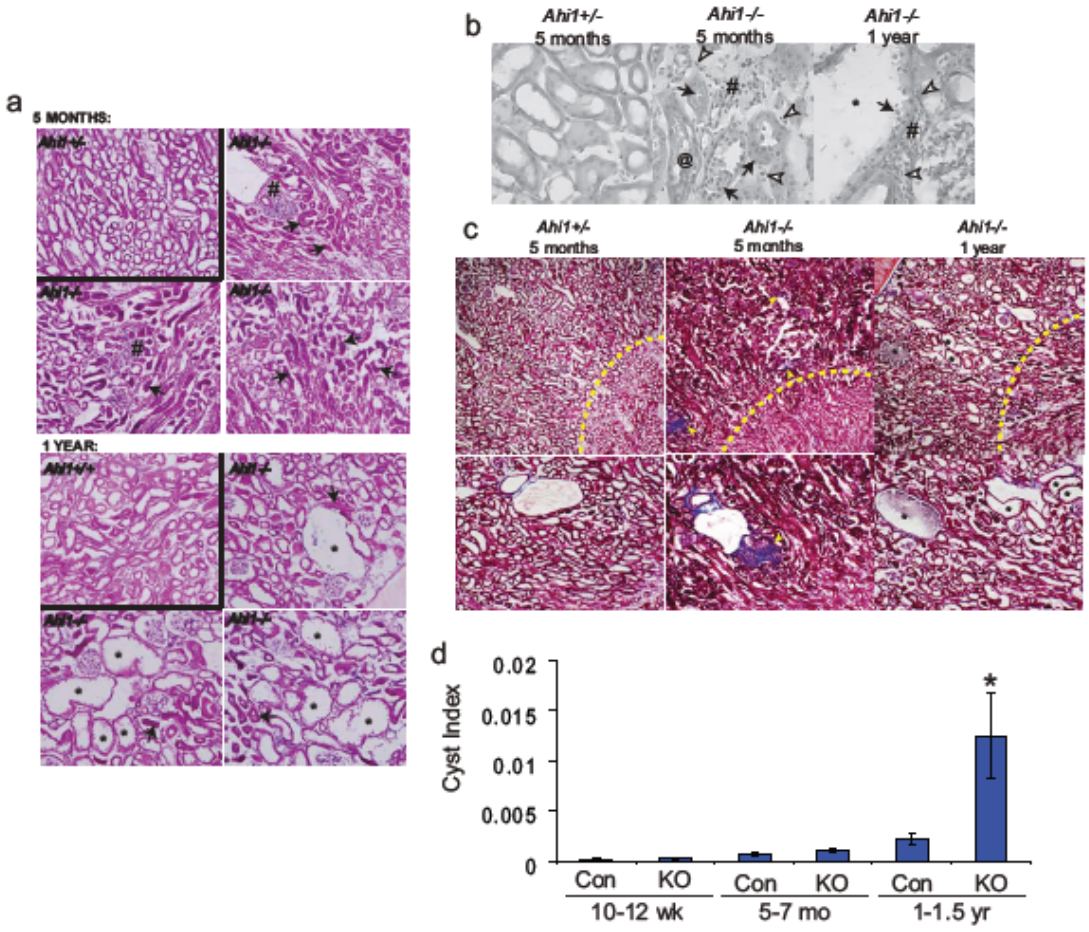

Supplementary Figure 2.3 *Ahi1*$^{-/-}$ kidneys display characteristic features of NPHP. (**a**) H&E staining reveals early NPHP pathology in 5 m onth old *Ahi1–/–* kidney compared to A*hi1+/–* littermate. Interstitial cell infiltrate (#) and fibrosis are present, as well as basement membrane abnormalities and tubular collapse (arrows). At one year, multiple microcysts and tubular dilatation become noticeable (*), and tubular basement membrane disintegration and atrophy are still present as well as tubular collapse (arrows) which are not evident in *Ahi1+/+* littermate control. (**b**) H&E staining at higher m agnification which reveals properties of interstitial tissue. Again, tubule abnormalities are present (arrows) with collapsed tubules and thickened epithelial cell wall as well as deposits within the tubule lumen (@). O pen arrowheads point to individual interstitial cells, which are part of a cluste r of cell infiltrate (#). (**c**) Masson's trichrome further reveals tubular abnormalities including cystic dilation at 1 ye ar (*) and aniline blue positive fibrosis (arrowheads). The large open structure visible in control and m utant 5 month sections is a blood vessel with nearby fibrosis. Dashed line represents the medullary boundary. (**d**) Average cyst index from three H&E stained sections of each kidney and both kidneys of at least 3 mice at each age. Control (Con, *Ahi1+/–* or *Ahi1+/+*) littermates compared with *Ahi1* knockouts (KO). *P<0.05, Student's *t*-test.

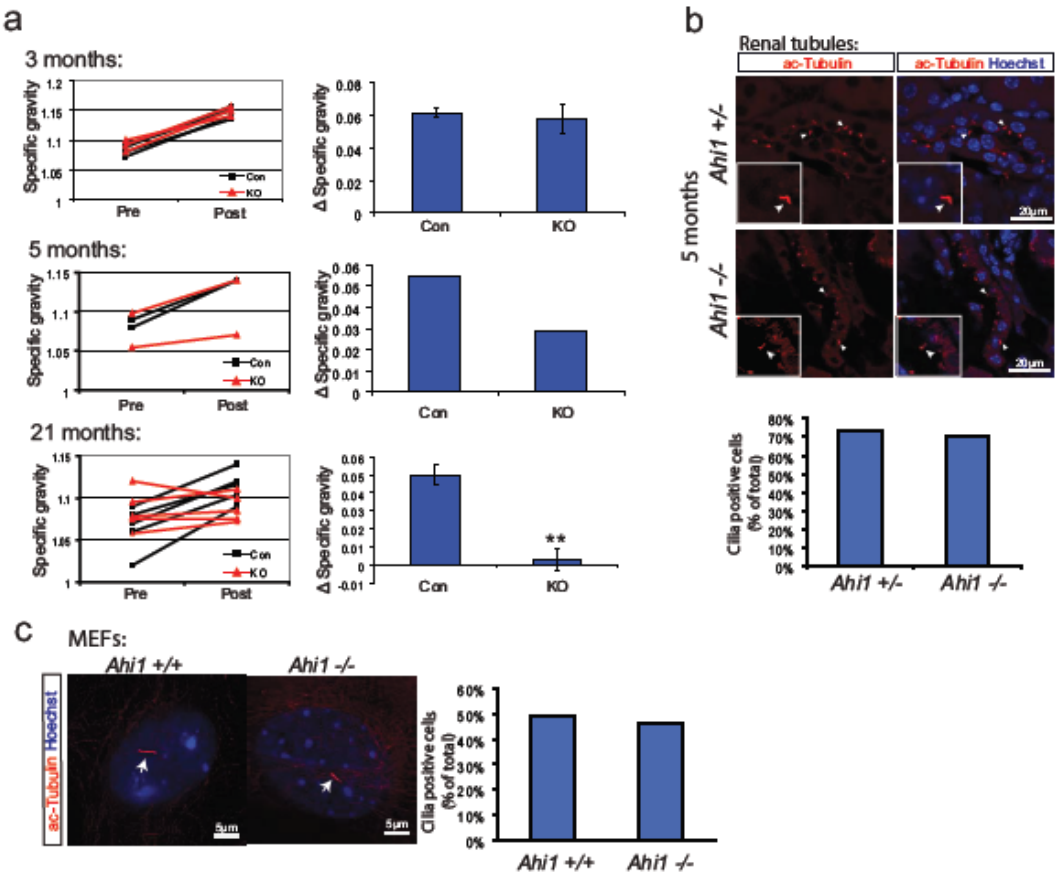

Supplementary Figure 2.4 *Ahi1–/–* display urine concentrating defects but normal percent ciliated MEFs and renal tubule cells. (**a**) Urine specific gravity measurements in *Ahi1–/–* and control littermates at 3 months, 5 m onths, and 2 years of age. Raw m easurements before (Pre) and after (Post) dehydration are graphed at left while the average difference in specific gravity is graphed at right. ***P*<0.001, S tudent's *t*-test, n=5 m ice at 21 m onths of age. (**b**) Staining for acetylated tubulin (red) reveals normal cilia number and morphology in *Ahi1–/–* kidneys compared with littermate control. Quantification of at least 100 cells from various tubule regions per sample reveals no significant difference in number of ciliated cells as determined by chisquared test. (**c**) Mouse em bryonic fibroblasts (MEFs) from *Ahi1+/+* and *Ahi1–/–* reveal normal cilia num ber and morphology. Quantitation of 100 MEF cells reveals no significant difference (chi-squared) in number of ciliated cells. Hoechst (blue) stains nuclei.

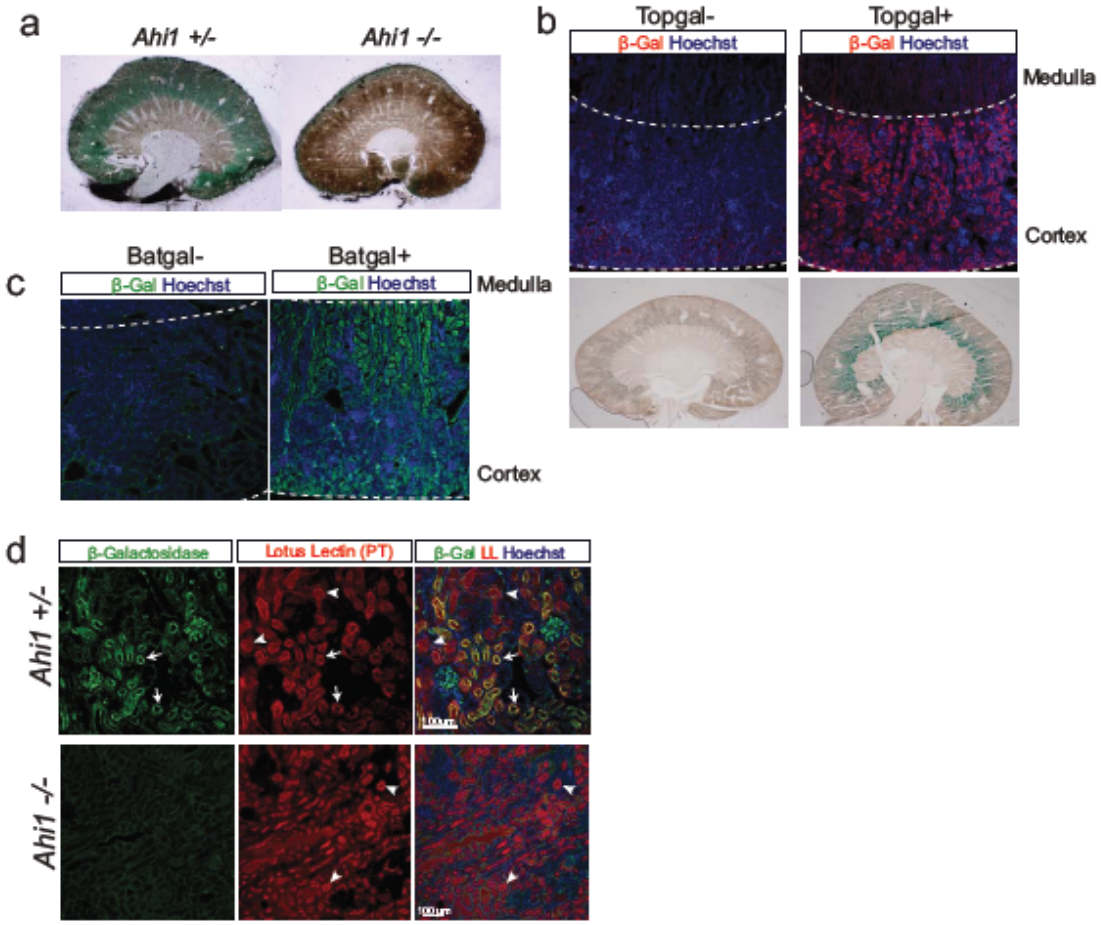

Supplementary Figure 2.5 *Ahi1–/–* kidneys display decreased Wnt activity. (**a**) X-Gal staining of *Ahi1+/–; Tg+* and *Ahi1–/–;Tg+* kidneys to saturation reveals a dramatic decrease in basal Wnt activity with loss of Jbn. (**b**) β-gal antibody staining (red) in wild-type Topgal negative kidney compared with Topgal positive kidney dem onstrating the specificity of the Topgal reporter line. Dashed lines outline the cortex and Hoechst stains nuclei. Additionally, X-gal staining (at pH 7.7) was done in littermates revealing similar specificity of the reporter. (**c**) β-gal antibody staining (green) in an independent Wnt reporter line, B atgal, reveals similar cortical staining with highest activity proximal to the m edulla. (**d**) β -gal (green) positive tubules colabel for lotus lectin (LL, red) which is a proximal tubule (PT) marker in *Ahi1+/–* kidney compared with *Ahi1–/–* littermate. A rrows point to the subset of proximal tubules which are co -positive for β -gal while arrowheads point to those which do not express β -gal. Despite the loss of β -gal expression in *Ahi1–/–*, proximal tubules are still abundant. Hoechst (blue) marks nuclei.

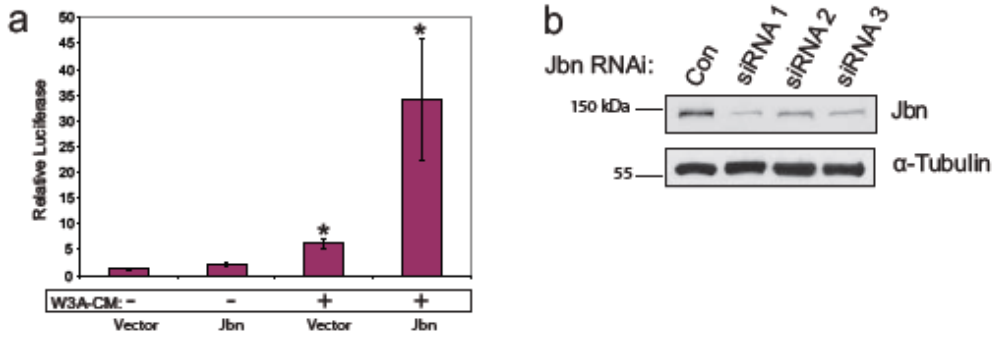

Supplementary Figure 2.6 Jbn overexpression potentiates the response to Wnt conditioned media. (**a**) 293T cells treated with Wnt3A conditioned m edia (W3A-CM) exhibit a 4.6-fold induction of luciferase response using the Topflash Wnt reporter. This response was potentiated by approximately 5.5-fold with Jbn overexpression. **P*<0.05, Student's *t*-test, n=12 from four experiments. V alues were normalized for protein concentration and expressed as a ratio to the untreated vector condition. (**b**) N2A cells transfected with 3 different siRNA oligonucleotides exhibit decreased Jbn protein levels compared with negative control siRNA transfected. siRNA 1 and siRNA 3 show the most robust decreases.

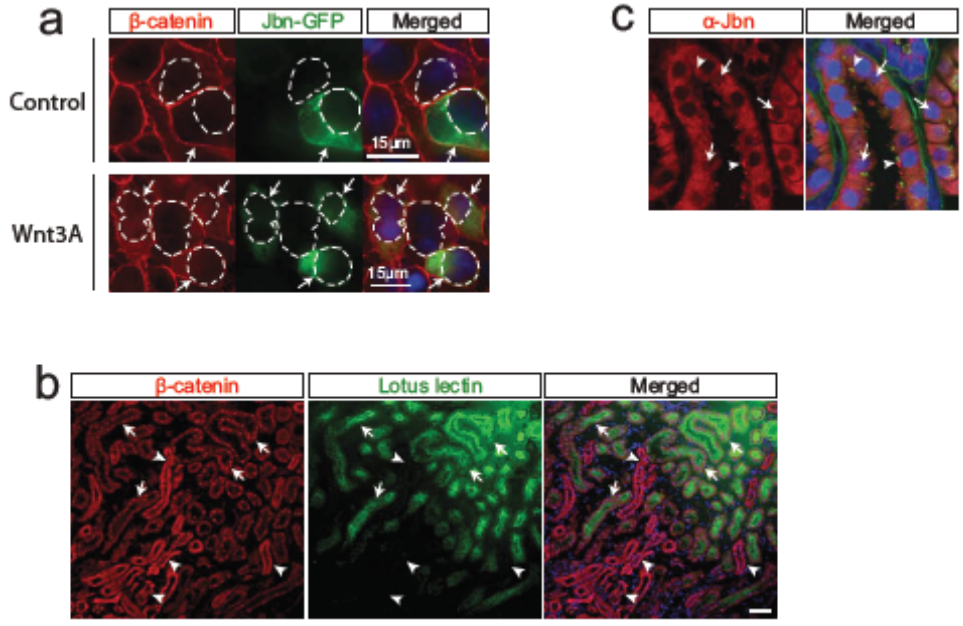

Supplementary Figure 2.7 Jouberin facilitates nuclear translocation of β-catenin (**a**) β -catenin localization in a single z-section through the plane of the nucleus in 293T cells reveals a subtle increase in nuclear levels of β –catenin (red) in cells overexpressing Jbn-GFP (green, arrows). Nuclei are labeled with Hoechst (blue) and are outlined by a dashed line. Jbn –GFP is not visible at the centrosome since it is out of the plane of focus. (**b**) β –catenin (red) and lotus lectin (green) costaining reveals nuclear localization of β –catenin in a subset of lotus lectin positive proximal tubules (arrows). Arrowheads point to tubules negative for lotus lectin which exhibit cytosolic and membrane β –catenin localization. © Immunostaining for Jbn (red) in kidney epithelium which demonstrates primarily cytosolic and basal body (arrowheads) localization at the base of acetyl-tubulin (green) positive cilia. Some nuclear □unctuate staining is visible as w ell (arrows). Hoechst (blue) labels nuclei.

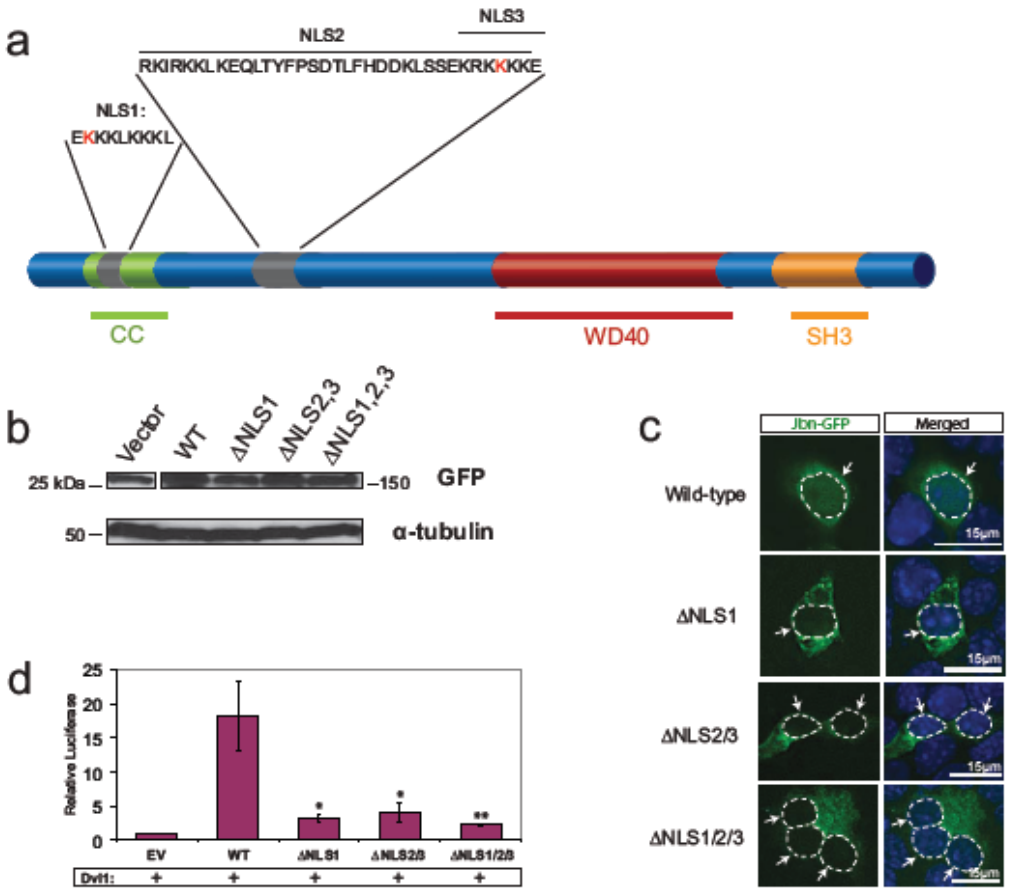

Supplementary Figure 2.8 NLS regions of Jbn are required for its Wnt function.
(**a**)Schematic representation of Jbn with NLS sequences outlined. Mutated lysine residues are highlighted in red in NLS regions. CC = coiled-coil, WD40 = seven WD40 repeat region, and SH3 = SH3 binding dom ain. (**b**) 293T whole cell lysates transfected with NLS mutant constructs display comparable expression levels to wild -type as assayed by western blotting for GFP. α-tubulin is shown as a loading control. (**c**) Localization of NLS m utant EGFP constructs (green) in m IMCD cells. Nucleus (Hoechst, blue) is outlined by a dashe d line. (**d**) Luciferase reporter activity in 293T cells transfected with Dvl-1 reveals a decrease in potentiation by NLS mutants compared to wild-type Jbn. **P*<0.05, ***P*<0.01, n=3 from three separate experiments, Student's *t*-test. Values are relative to empty vector control and were normalized for co- transfected β -Gal.

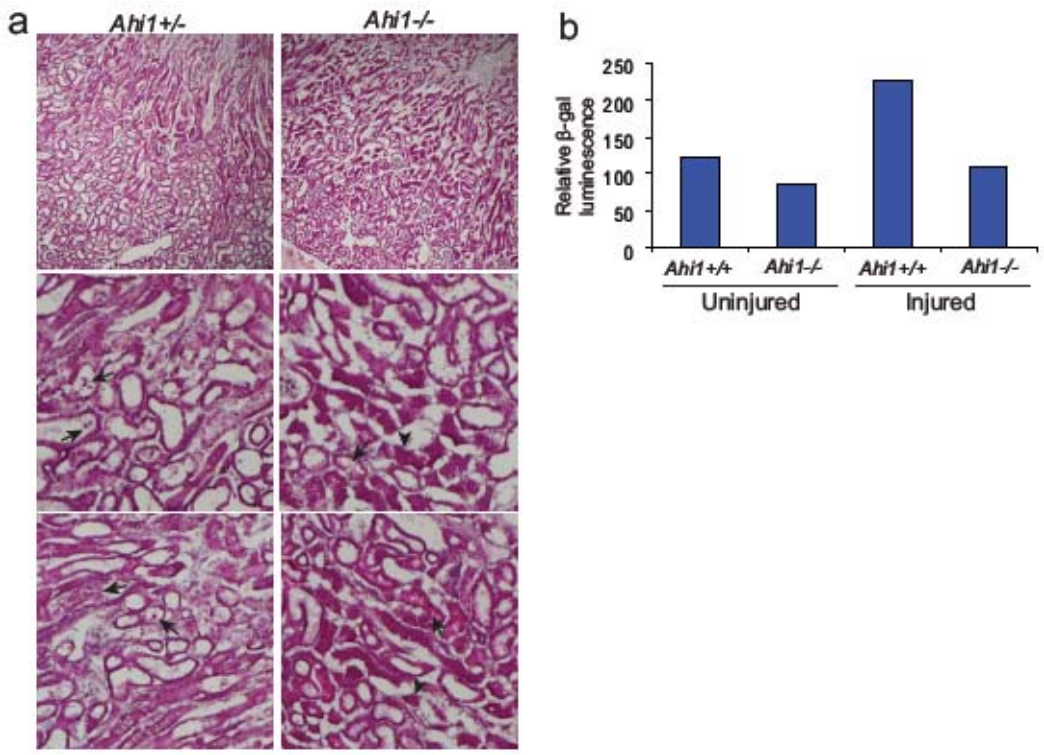

Supplementary Figure 2.9 Pathology immediately following injury in *Ahi1-/-* and *Ahi1+/-* kidney. (**a**) H&E staining of injured kidneys following unilateral IRI in *Ahi1–/–* and *Ahi1+/–* littermates aged 5 m onths. Signs of injury such as vacuolization and cell sloughing (arrows) are visible in both control and m utant injured kidneys. The *Ahi1–/–* kidney additionally exhibits the typical early m anifestations of NPHP with som e tubular abnormalities (arrowheads). (**b**) β -galactosidase luminescence relative to total protein concentration from whole kidney lysates of a pair of *Ahi1+/+* and *Ahi1–/–* littermates aged 3 m onths subjected to IRI revealing overall decreased Wnt activity even in the uninjured *Ahi1–/–* kidney at this early age prior to NPHP disease onset, and abrogated Wnt upregulation following injury com pared with *Ahi1+/+* kidney lysate.

References

1. Harris PC (2002) *Curr Opin Nephrol Hypertens* **11,** 309-314.

2. Hildebrandt F & Zhou W (2007) *J Am Soc Nephrol* **18,** 1855-1871.

3. Simons M, Gloy J, Ganner A, Bullerkotte A, Bashkurov M, Kronig C, Schermer B, Benzing T, Cabello OA, Jenny A, Mlodzik M, Polok B, Driever W, Obara T, & Walz G (2005) *Nat Genet* **37,** 537-543.

4. Bergmann C, Fliegauf M, Bruchle NO, Frank V, Olbrich H, Kirschner J, Schermer B, Schmedding I, Kispert A, Kranzlin B, Nurnberg G, Becker C, Grimm T, Girschick G, Lynch SA, Kelehan P, Senderek J, Neuhaus TJ, Stallmach T, Zentgraf H, Nurnberg P, Gretz N, Lo C, Lienkamp S, Schafer T, Walz G, Benzing T, Zerres K, & Omran H (2008) *Am J Hum Genet* **82,** 959-970.

5. Saadi-Kheddouci S, Berrebi D, Romagnolo B, Cluzeaud F, Peuchmaur M, Kahn A, Vandewalle A, & Perret C (2001) *Oncogene* **20,** 5972-5981.

6. Qian CN, Knol J, Igarashi P, Lin F, Zylstra U, Teh BT, & Williams BO (2005) *J Biol Chem* **280,** 3938-3945.

7. Marose TD, Merkel CE, McMahon AP, & Carroll TJ (2008) *Dev Biol* **314,** 112-126.

8. Pinson KI, Brennan J, Monkley S, Avery BJ, & Skarnes WC (2000) *Nature* **407,** 535-538.

9. Ferland RJ, Eyaid W, Collura RV, Tully LD, Hill RS, Al-Nouri D, Al-Rumayyan A, Topcu M, Gascon G, Bodell A, Shugart YY, Ruvolo M, & Walsh CA (2004) *Nat Genet* **36,** 1008-1013.

10. Dixon-Salazar T, Silhavy JL, Marsh SE, Louie CM, Scott LC, Gururaj A, Al-Gazali L, Al-Tawari AA, Kayserili H, Sztriha L, & Gleeson JG (2004) *Am J Hum Genet* **75,** 979-987.

11. Louie CM & Gleeson JG (2005) *Hum Mol Genet* **14 Spec No. 2,** R235-242.

12. Utsch B, Sayer JA, Attanasio M, Pereira RR, Eccles M, Hennies HC, Otto EA, & Hildebrandt F (2006) *Pediatr Nephrol* **21,** 32-35.

13. Rauchman MI, Nigam SK, Delpire E, & Gullans SR (1993) *Am J Physiol* **265,** F416-424.

14. Eley L, Gabrielides C, Adams M, Johnson CA, Hildebrandt F, & Sayer JA (2008) *Kidney Int*.

15. Davison AM, Cameron, J.S., Grunfeld, J-P., Ponticelli, C., Ritz, E., Winearls, C.G., Van Ypersele, C. (2005) *Oxford Textbook of Clinical Nephrology* (Oxford University Press, Oxford, England).

16. Faraggiana T, Malchiodi F, Prado A, & Churg J (1982) *J Histochem Cytochem* **30,** 451-458.

17. Patel V, Li L, Cobo-Stark P, Shao X, Somlo S, Lin F, & Igarashi P (2008) *Hum Mol Genet* **17,** 1578-1590.

18. Attanasio M, Uhlenhaut NH, Sousa VH, O'Toole JF, Otto E, Anlag K, Klugmann C, Treier AC, Helou J, Sayer JA, Seelow D, Nurnberg G, Becker C, Chudley AE, Nurnberg P, Hildebrandt F, & Treier M (2007) *Nat Genet* **39,** 1018-1024.

19. Kim YS, Kang HS, Herbert R, Beak JY, Collins JB, Grissom SF, & Jetten AM (2008) *Mol Cell Biol* **28,** 2358-2367.

20. Krishnan R, Eley L, & Sayer JA (2008) *Kidney Blood Press Res* **31,** 152-162.

21. Parisi MA, Doherty D, Eckert ML, Shaw DW, Ozyurek H, Aysun S, Giray O, Al Swaid A, Al Shahwan S, Dohayan N, Bakhsh E, Indridason OS, Dobyns WB, Bennett CL, Chance PF, & Glass IA (2006) *J Med Genet* **43,** 334-339.

22. Badano JL, Mitsuma N, Beales PL, & Katsanis N (2006) *Annu Rev Genomics Hum Genet* **7,** 125-148.

23. Kim YS, Kang HS, & Jetten AM (2007) *FEBS Lett* **581,** 858-864.

24. Zhang K, Ye C, Zhou Q, Zheng R, Lv X, Chen Y, Hu Z, Guo H, Zhang Z, Wang Y, Tan R, & Liu Y (2007) *Cell Biochem Funct* **25,** 767-774.

25. Kim E, Arnould T, Sellin LK, Benzing T, Fan MJ, Gruning W, Sokol SY, Drummond I, & Walz G (1999) *J Biol Chem* **274,** 4947-4953.

26. Zheng R, Zhang Z, Lv X, Fan J, Chen Y, Wang Y, Tan R, Liu Y, & Zhou Q (2008) *Cell Biol Int* **32,** 427-435.

27. Lal M, Song X, Pluznick JL, Di Giovanni V, Merrick DM, Rosenblum ND, Chauvet V, Gottardi CJ, Pei Y, & Caplan MJ (2008) *Hum Mol Genet*.

28. DasGupta R & Fuchs E (1999) *Development* **126,** 4557-4568.

29. Iglesias DM, Hueber PA, Chu L, Campbell R, Patenaude AM, Dziarmaga AJ, Quinlan J, Mohamed O, Dufort D, & Goodyer PR (2007) *Am J Physiol Renal Physiol* **293,** F494-500.

30. Weiss DJ, Liggitt D, & Clark JG (1999) *Histochem J* **31,** 231-236.

31. Duffield JS, Park KM, Hsiao LL, Kelley VR, Scadden DT, Ichimura T, & Bonventre JV (2005) *J Clin Invest* **115,** 1743-1755.

32. Maretto S, Cordenonsi M, Dupont S, Braghetta P, Broccoli V, Hassan AB, Volpin D, Bressan GM, & Piccolo S (2003) *Proc Natl Acad Sci U S A* **100,** 3299-3304.

33. Filali M, Cheng N, Abbott D, Leontiev V, & Engelhardt JF (2002) *J Biol Chem* **277,** 33398-33410.

34. Jho EH, Zhang T, Domon C, Joo CK, Freund JN, & Costantini F (2002) *Mol Cell Biol* **22,** 1172-1183.

35. Niida A, Hiroko T, Kasai M, Furukawa Y, Nakamura Y, Suzuki Y, Sugano S, & Akiyama T (2004) *Oncogene* **23,** 8520-8526.

36. Hovanes K, Li TW, Munguia JE, Truong T, Milovanovic T, Lawrence Marsh J, Holcombe RF, & Waterman ML (2001) *Nat Genet* **28,** 53-57.

37. Li CM, Kim CE, Margolin AA, Guo M, Zhu J, Mason JM, Hensle TW, Murty VV, Grundy PE, Fearon ER, D'Agati V, Licht JD, & Tycko B (2004) *Am J Pathol* **165,** 1943-1953.

38. Takada S, Stark KL, Shea MJ, Vassileva G, McMahon JA, & McMahon AP (1994) *Genes Dev* **8,** 174-189.

39. Korinek V, Barker N, Morin PJ, van Wichen D, de Weger R, Kinzler KW, Vogelstein B, & Clevers H (1997) *Science* **275,** 1784-1787.

40. Kaykas A, Yang-Snyder J, Heroux M, Shah KV, Bouvier M, & Moon RT (2004) *Nat Cell Biol* **6,** 52-58.

41. Tetsu O & McCormick F (1999) *Nature* **398,** 422-426.

42. Willert K & Nusse R (1998) *Curr Opin Genet Dev* **8,** 95-102.

43. van Noort M, Meeldijk J, van der Zee R, Destree O, & Clevers H (2002) *J Biol Chem* **277,** 17901-17905.

44. Cokol M, Nair R, & Rost B (2000) *EMBO Rep* **1,** 411-415.

45. Surendran K, Schiavi S, & Hruska KA (2005) *J Am Soc Nephrol* **16,** 2373-2384.

46. Meldrum KK, Meldrum DR, Meng X, Ao L, & Harken AH (2002) *Am J Physiol Heart Circ Physiol* **282,** H540-546.

47. Jauregui AR, Nguyen KC, Hall DH, & Barr MM (2008) *J Cell Biol* **180,** 973-988.

48. Schmidt-Ott KM & Barasch J (2008) *Kidney Int*.

49. Kuure S, Popsueva A, Jakobson M, Sainio K, & Sariola H (2007) *J Am Soc Nephrol* **18,** 1130-1139.

50. Park JS, Valerius MT, & McMahon AP (2007) *Development* **134,** 2533-2539.

51. Osafune K, Takasato M, Kispert A, Asashima M, & Nishinakamura R (2006) *Development* **133,** 151-161.

52. Saburi S, Hester I, Fischer E, Pontoglio M, Eremina V, Gessler M, Quaggin SE, Harrison R, Mount R, & McNeill H (2008) *Nat Genet* **40,** 1010-1015.

53. Kishimoto N, Cao Y, Park A, & Sun Z (2008) *Dev Cell* **14,** 954-961.

54. Bonventre JV & Zuk A (2004) *Kidney Int* **66,** 480-485.

55. Bonventre JV (2003) *J Am Soc Nephrol* **14 Suppl 1,** S55-61.

56. Davenport JR, Watts AJ, Roper VC, Croyle MJ, van Groen T, Wyss JM, Nagy TR, Kesterson RA, & Yoder BK (2007) *Curr Biol* **17,** 1586-1594.

57. Piontek K, Menezes LF, Garcia-Gonzalez MA, Huso DL, & Germino GG (2007) *Nat Med* **13,** 1490-1495.

58. Calvet JP (1994) *Curr Opin Nephrol Hypertens* **3,** 340-348.

59. Yee SP & Rigby PW (1993) *Genes Dev* **7,** 1277-1289.

60. Megyesi J, Safirstein RL, & Price PM (1998) *J Clin Invest* **101,** 777-782.

61. Rabb H, Ramirez G, Saba SR, Reynolds D, Xu J, Flavell R, & Antonia S (1996) *Am J Physiol* **271,** F408-413.

62. Zambrano N, Minopoli G, de Candia P, & Russo T (1998) *J Biol Chem* **273,** 20128-20133.

63. Willert K, Brown JD, Danenberg E, Duncan AW, Weissman IL, Reya T, Yates JR, 3rd, & Nusse R (2003) *Nature* **423,** 448-452.

64. Nelson SB, Lawson MA, Kelley CG, & Mellon PL (2000) *Mol Endocrinol* **14,** 1509-1522.

The text of Chapter 2 in full is a reprint of the material as it appears in Nature Medicine, 2009, Lancaster MA, Louie CM, Silhavy JL, Sintasath L, DeCambre M, Nigam SK, Willert K & Gleeson JG. The dissertation author was the primary researcher and author of this publication and co-authors preformed experiments, and supervised the

research which forms the basis of this chapter. The dissertation author designed the experimental approach with the advisor, conducted the experiments, and co-wrote the manuscript.

Chapter 3 Primary Cilia Regulate Canonical Wnt Signaling Through Sequestration of Wnt Components

3.1 Abstract

Mechanisms of canonical Wnt pathway regulation remain a fundamental question in cancer and developmental biology. Here, we investigate the mechanisms of cilia regulation of Wnt signaling and the role of the ciliopathy protein Jouberin (Jbn) through specific cilia knock-down and knock-out approaches. We found that Jbn is capable of being transported into the cilium and it can be sequestered within the cilium by knock-down of retrograde transport (Dnchc2). This sequestration inhibits Jbn's role in canonical Wnt signaling whereas complete loss of the primary cilium through knock-down of Kif3A instead facilitates Jbn's role in canonical Wnt signaling. This effect thus leads to overactivation of canonical Wnt signaling downstream of β-catenin, a previously unidentified regulatory point in the pathway. Furthermore, we identified a mechanism whereby the primary cilium sequesters both Jbn and β-catenin and prevents translocation to the nucleus. These findings suggest a model in which the cilium acts as a regulatory gateway to the nucleus in the canonical Wnt pathway.

3.2 Introduction

The Wnt signaling pathway functions in a variety of cellular processes, and mutations in this pathway have been identified in a broad array of disorders, from developmental disease to certain cancers(1, 2). Thus, understanding the regulation of this pathway is vital in treating these disorders. Recently, primary cilia, which are themselves connected with a variety of disorders known as ciliopathies(3, 4), have been implicated in negative regulation of the canonical Wnt pathway(5, 6). Similarly, we have

shown that Jouberin, mutated in the ciliopathy Joubert syndrome(7-9), is a positive regulator of the pathway through facilitation of β-catenin nuclear translocation(10). Though these findings suggest cilia may play an instrumental role in regulation of this conserved pathway, the mechanism of how such an organelle regulates this pathway is not known.

3.3 Results

To examine this issue directly, we have assayed canonical Wnt signaling activity with systematic manipulation of the primary cilium itself. First, we examined the precise role of Jbn within the primary cilium since Jbn is a positive regulator of the pathway and is cilia-localized. To this end, we examined whether Jbn is capable of interacting with the microtubule structure of the cilium by performing a microtubule association assay, which revealed a clear association preference with microtubules (Fig. S1a).

The punctate staining of Jbn along the ciliary length reported previously suggests Jbn may be transiently transported by the intraflagellar transport (IFT) machinery associated with the axoneme. In order to test this possibility, we performed a ciliary redistribution assay involving inhibition of the retrograde transport motor dynein cytoplasmic heavy chain 2 (Dnchc2)(11). In this assay, inhibition of Dnchc2 leads to inadequate retrograde transport resulting in a redistribution of IFT transported components due to their inability to return to the basal body. This assay allows for identification of novel IFT transported proteins which require retrograde transport for their proper localization. Inhibition of Dnchc2 was performed using siRNA knockdown which resulted in a substantial decrease in Dnchc2 protein levels with two siRNAs tested (Fig. S1b). As predicted, knockdown of Dnchc2 led to a redistribution of Jbn along the length of the primary cilium, which we then quantified (Fig. 1a). These data indicate that

although Jbn localizes primarily to the basal body with only a few puncta along the axoneme(10), Jbn is most likely transported along the cilium. Jbn ciliary localization seems to be best visualized with inhibition of Dnchc2, suggesting that this transport may occur transiently or perhaps continuously but in minute quantities which may not be visible by light microscopy.

We next tested whether this ciliary sequestration by Dnchc2 knock-down affected Jbn's role in Wnt signaling. We performed luciferase experiments in 293T cells which have been shown to display primary cilia in culture(5) and, similar to other cell types tested, Jbn localizes specifically to these primary cilia (Fig. S1c). For this assay we cotransfected Super Topflash and Dvl-1 to activate canonical Wnt signaling upstream of Jbn as well as cotransfected Jbn and Dnchc2 siRNAs to block retrograde transport. Under these conditions, Jbn's potentiation was reduced by approximately ½ with inhibition of Dnchc2 (Fig. 1b), indicating that sequestration of Jbn within the primary cilium is inhibitory to its Wnt function.

These findings suggest that intraflagellar transport within the primary cilium regulates Jbn in the Wnt pathway. The primary cilium has recently been described to inhibit the canonical Wnt pathway potentially at multiple points in the pathway(5, 6) though exact mechanisms of how an organelle like the cilium can regulate protein components of the pathway are not clear. Since sequestration of Jbn within the cilium is inhibitory to its role in Wnt signaling, one hypothesis is that the primary cilium regulates canonical Wnt signaling through Jbn.

In order to test this possibility, we performed experiments similar to Gerdes et al.(5) in which we employed Kif3A siRNA to inhibit anterograde IFT and effectively remove the primary cilium. We performed siRNA transfections in 293Ts and identified an siRNA which specifically knocked down endogenous Kif3A levels (Fig. S1d). We next

performed luciferase assays utilizing this Kif3A siRNA in 293Ts (Fig. 1c) and ciliated mouse embryonic fibroblasts (MEFs, Fig. 1d). Interestingly, we found that Jbn exhibited enhanced potentiation of canonical Wnt signaling in the absence of the cilium. These findings were further verified using an alternate knock-out approach which does not rely on efficient siRNA knock-down. We used Dnchc2 nonsense mutant MEFs which display no cilia (Fig. S2a) and a much increased Wnt response compared with control MEFs (Fig. S2b) as is expected for a non-ciliated cell type(6). Luciferase results using this approach validated our findings that Jbn's function in the canonical Wnt pathway was enhanced in the absence of cilia (Fig. 1e) indicating that the primary cilium is not necessary for Jbn function but rather is inhibitory to Jbn's role in Wnt signaling.

Components of the Wnt pathway have been described to be inhibited by the primary cilium. Our data indicate that Jbn is likewise inhibited by the primary cilium. Therefore, since Jbn functions downstream of β-catenin stabilization, we hypothesized that the primary cilium may be inhibitory downstream of β-catenin stabilization. Notably, our luciferase assays were performed with Wnt3a conditioned media, Dvl-1 or β-catΔN overexpression to activate the pathway. In all cases, loss of the cilium led to an additional increase in canonical Wnt response (Fig. 1c-e) indicating that the primary cilium is, at least in part, inhibitory downstream of both Dvl-1 and β-catenin activation. We further tested this hypothesis directly by performing luciferase in the cilia-absent Dnchc2 nonsense MEFs which revealed potentiation of the Wnt response in the absence of the primary cilium with activation using either LiCl (Fig. 2a) or β-catΔN (Fig. 2b). This was also the case when wild-type MEFs were transfected with Kif3A siRNA to remove the primary cilium (Fig. 2c). These results suggest that the primary cilium inhibits canonical Wnt signaling downstream of β-catenin stabilization with inhibition of Jbn.

Since Jbn and β-catenin have been shown to interact and Jbn is transported within the cilium, we hypothesized that perhaps the cilium inhibits β-catenin and Jbn through spatial regulation of these components. We therefore examined localization of Jbn and β-catenin in the cilia mutant Dnchc2 nonsense MEFs. Without Wnt stimulation in wild-type ciliated MEFs, endogenous Jbn can be seen at the basal body with some nuclear staining as well (Fig. 2d). Under these conditions, β-catenin primarily localized to the cell membrane as expected. With Wnt3A treatment, β-catenin can be seen at higher levels in the nucleus indicating a response to Wnt. Interestingly, β-catenin can also be observed at the basal body colocalized with Jbn, suggesting that cytosolic β-catenin may accumulate at the base of the cilium upon Wnt stimulation. Next we examined Dnchc2 mutant MEFs which do not exhibit primary cilia. Even in the absence of treatment, Jbn can already be seen in the nucleus while β-catenin is primarily at the cell membrane. However, upon Wnt treatment, a dramatic increase in nuclear β-catenin, as well as Jbn, is clearly evident, without accumulation at the centrosome. These data indicate that under nonciliated conditions in which Wnt response is high, both Jbn and β-catenin are more abundant in the nucleus. However, when cilia are present and both components are inhibited, Jbn and β-catenin are instead present at the basal body suggesting this localization may in fact be inhibitory.

3.4 Discussion

Our findings suggest a unique mechanism for inhibition of a signaling pathway through sequestration at a discrete subcellular location: the primary cilium. These results suggest a model whereby Jouberin is transported along the cilium in order to regulate its role in facilitating nuclear translocation of β-catenin (Fig. 2e). Thus, the primary cilium acts as a gateway to the nucleus for both Jbn and its associated β-catenin, and in the

absence of the primary cilium, both components are free to enter the nucleus without first passing through this ciliary “turnpike.” This model at least partly explains why many cancer cells exhibit a loss of the primary cilium(12) since this would be expected to lead to hyperactivation of the oncogenic Wnt pathway.

3.5 Methods

Plasmid constructs and materials

GFP tagged Jbn was used as described previously(10). β-catΔN expression construct was obtained from M.G. Rosenfeld and Super Topflash construct was provided by R.T. Moon. Wnt3A conditioned media was obtained from stably transfected L cells with Wnt3A expression vector (provided by K Willert) and used as described(13). Control media was obtained from untransfected L cells. Dnchc2 siRNA oligonucleotides were purchased from Invitrogen (Stealth RNAi). Dnchc2 siRNA 1: GGGCGGAUAUUUGUUGGGUUGGUAA. Dnchc2 siRNA 2: GAGCAGUGUUCUCACUGAUUGAUUA. Dnchc2 siRNA 3: ACUGCUGUGUCAGUUUGCAU GGUUU. Low GC content siRNA control oligo was used as a negative control (Invitrogen).

Immunofluorescence

3T3, HEK293T cells (ATCC) or Dnchc2 MEFs (obtained from A. S. Peterson) were fixed with 4% PFA for 15 min at room temperature, washed in PBS, blocked in 4% donkey serum/0.1% TritonX, and stained with primary antibody: mouse anti-acetylated tubulin (Zymed 32-2700, 1:500 dilution), mouse anti-β-catenin (BD Transduction Labs, 610153, 1:200), goat anti-γ-tubulin (Santa Cruz Biotech. Sc7396, 1:100) and rabbit anti-Jbn(10) (Quality Controlled Biochemicals). Samples were washed and incubated in

secondary antibodies (AlexaFluor donkey anti-mouse 594, donkey anti-rabbit 488, and donkey anti-goat 647, Molecular Probes, 1:500). Hoechst was used as a nuclear stain (Molecular Probes, H3570). Images were acquired using a DeltaVision Spectris deconvolution microscope (UCSD Neuroscience Microscopy Core).

Cell culture and luciferase assays

293Ts and 3T3s were grown in DMEM with 10% fetal bovine serum (FBS), and MEFs were grown in 15% FBS. For transient transfections of 293Ts, 3T3s or MEFs, Lipofectamine 2000 (Invitrogen) was used according to manufacturer's protocol. For luciferase assays, 293T cells and MEFs were grown in 24-well plates and transfected with 300ng Topflash, 60ng βGal, and 325ng of Jbn-GFP expression plasmid or empty vector (GFP was mutated at Y66G to disrupt fluorescence using QuikChange mutagenesis). Cells were co-transfected with 325ng Dvl-1 expression plasmid, 325ng β-CateninΔN, or treated with Wnt3a conditioned media (WCM) to stimulate the Wnt pathway. For experiments involving siRNA, 1.25pmol siRNA was cotransfected with half the above DNA amounts according to the manufacturer. Twenty-four hrs following transfection, cells were serum starved for 16hrs or treated with WCM diluted 3:1 in serum free media. The luciferase assay was performed according to a previously published protocol(14) and β-galactosidase activity was measured using the Tropix Galacto-light Plus kit (Applied Biosystems, T1007).

Western blot and microtubule association assay

For the microtubule association assay, five P5 mice were dissected and the cerebellum was removed and homogenized in MES buffer followed by centrifugation at 25,000 rpm for 15 min. Supernatant was subsequently centrifuged at 75,000 rpm for 90

minutes and samples were then treated with 100mM GTP and 1mM Taxol for 30 min at 37ºC. Samples were centrifuged through a 10% sucrose cushion and the pellet was resuspended in MES buffer and loaded on a 12% SDS-PAGE. Western blotting was performed on lysates prepared in modified RIPA buffer using the following antibodies: rabbit anti-Jbn (Quality Controlled Biochemicals), goat anti-DCX (Santa Cruz Biotech., SC-8067), mouse anti-α-tubulin (Sigma, T-6074), rabbit anti-total ERK (Upstate, 06-182), rabbit anti-Dhc1 and rabbit anti-Dhc2 antibodies (both kindly provided by R. B. Vallee), anti-Kif3a (Covance, MMS-198P, 1:100). All antibodies were used at 1:1000 dilution.

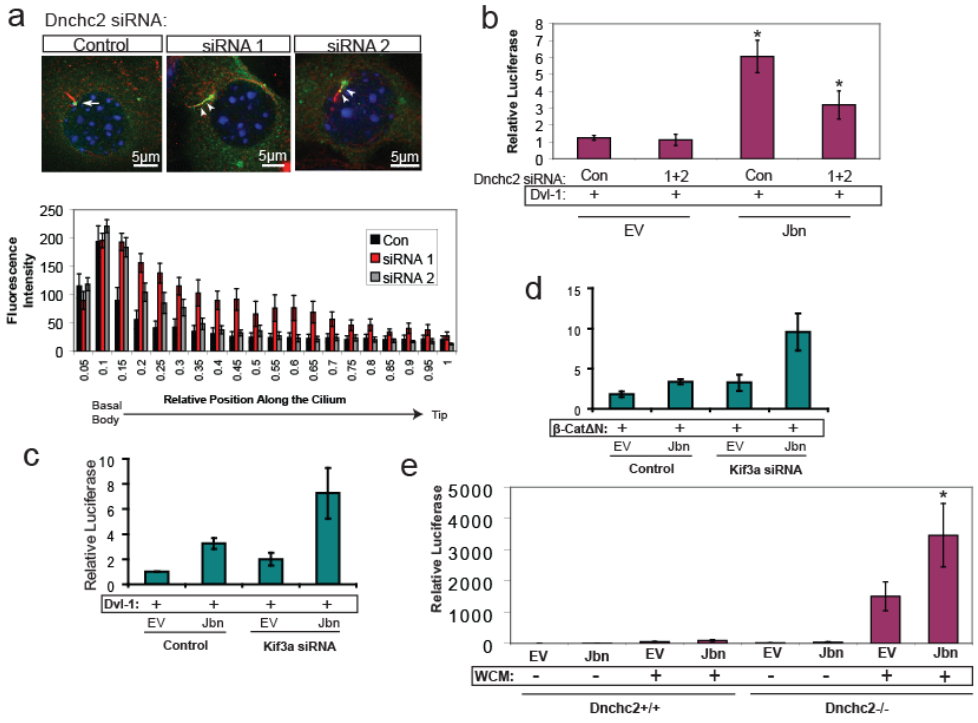

Figure 3.1 Jouberin is regulated by the primary cilium. **a.** 3T3s transfected with two siRNAs to Dnchc2 exhibit accumulation of Jbn-GFP (green) along the length of the cilium (labeled with antibody to acetylated tubulin, red). The nucleus is labeled with Hoechst (blue). Quantification of the green fluorescence along the length of the cilium and at the basal body reveals a shifted localization along the length away from the basal body in siRNA transfected cells especially with siRNA 1. Average fluorescence intensities along the length of the cilium of cells transfected with negative control siRNA (n=7), dnchc2 siRNA 1 (n=10), or dnchc2 siRNA 2 (n=11) were normalized and displayed in arbitrary units. Position along the cilium was normalized for total cilia length and results were binned into 20 equal segments. **b.** Luciferase reporter activity in 293T cells with overexpression of wild-type Jbn or empty vector(EV) and cotransfection of negative control siRNA or pooled dnchc2 siRNAs 1 and 2. *P<0.05, n=6 from three experiments, Student's *t*-test. Cells were cotransfected with Dvl-1 to activate the Wnt pathway and values are represented as relative to control empty vector condition and normalized for co-transfected β-Gal. **c**. Luciferase activity in 293T cells transfected with Kif3a siRNA and overexpressed Jbn or EV with activation of the pathway with cotransfected Dvl-1. *P<0.05, n=3 experiments, Student's *t*-test. **d**. Luciferase activity in MEFs transfected with Kif3a siRNA and overexpressed Jbn or EV with activation of the pathway with cotransfected β-catΔN. *P<0.05, n=3 experiments, Student's *t*-test. **e**. Luciferase activity in Dnchc2 MEFs transfected with Jbn or EV with activation of the pathway with cotransfected β-catΔN. *P<0.05, n=3 experiments, Student's *t*-test.

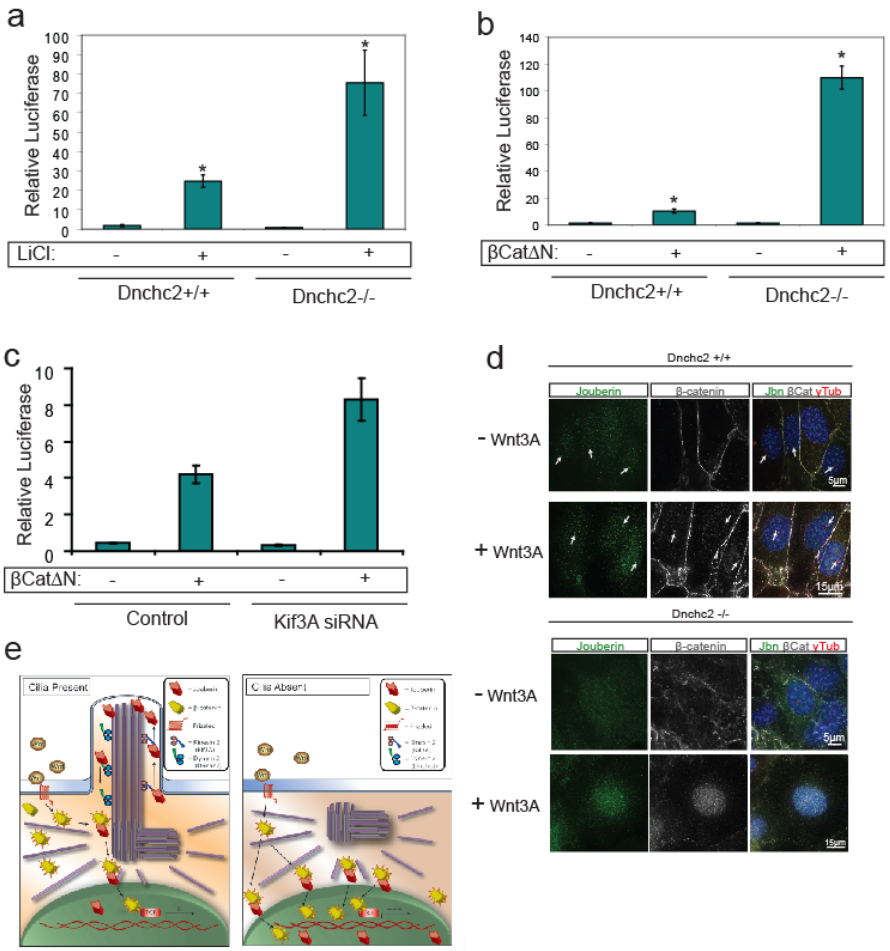

Figure 3.2 The primary cilium sequesters Jbn and β-catenin. **a**. Luciferase activity in Dnchc2 MEFs with activation of the pathway with lithium (LiCl). **P*<0.05, n=3 experiments, Student's *t*-test. **b**. Luciferase activity in Dnchc2 MEFs with activation of the pathway with transfected β-catΔN. **P*<0.05, n=3 experiments, Student's *t*-test. **c**. Luciferase activity in MEFs transfected with Kif3a siRNA and activation of the pathway with cotransfected β-catΔN. **P*<0.05, n=3 experiments, Student's *t*-test. **d**. Localization of endogenous β-catenin (grey) and Jbn (green) in Dnchc2 MEFs. Control MEFs (top) exhibit basal body localization (γ-tubulin, red) of β-catenin and Jbn when treated with Wnt3A conditioned media, whereas Dnchc2-/- MEFs exhibit increased nuclear staining (Hoechst, blue) of β-catenin and Jbn. **e**. Model of the proposed mechanism of Jbn potentiation of canonical Wnt signaling at the primary cilium. Jbn is proposed to interact with β-catenin upon Wnt activation and facilitate its translocation into the nucleus. This process is dependent upon intact retrograde IFT of Jbn down the cilium to the basal body where it can then interact with β-catenin and facilitate its nuclear accumulation. In the absence of the cilium, Jbn and β-catenin directly enter the nucleus leading to an increased transcriptional response.

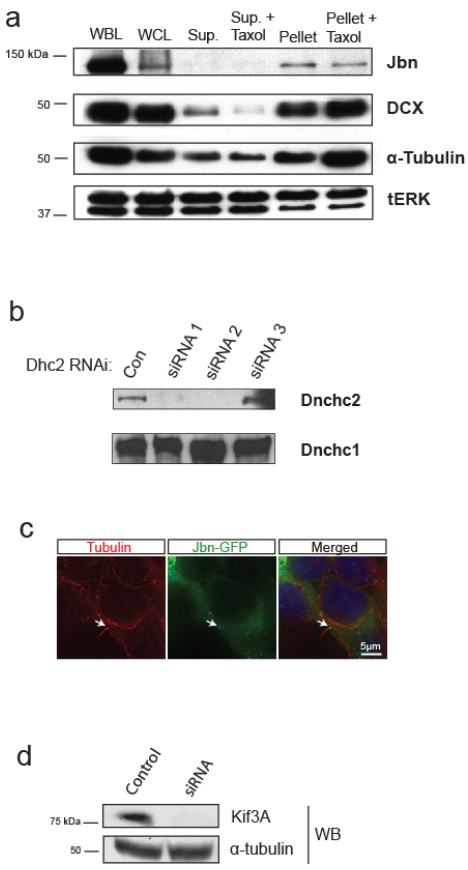

Supplementary Figure 3.1 Jbn is a microtubule associated protein. **a**. Lysates from P5 mouse cerebellum were exposed to microtubule repolymerization conditions and samples at each step were analyzed by SDS-PAGE. Western blotting reveals endogenous Jbn associates with repolymerized microtubules in the Pellet and Pellet + Taxol fractions. Blots were probed for Doublecortin (DCX) as a positive control, and total ERK as a negative control. α-tubulin is enriched in pellet fractions. **b**. Western blot analysis of whole cell lysates from 3T3s transfected with Dnchc2 siRNA constructs. Dnchc2 levels are specifically decreased in siRNA 1 and siRNA 2 transfected cells without an effect on dynein heavy chain 1 (Dnchc1) which is shown as a loading control. **c**. 293T cells stained for cilia with antibody to acetylated tubulin (red) display clear cilia with Jbn-GFP (green) localized to the basal body. Hoechst is used to stain the nucleus (blue). **d**. Western blot analysis of whole cell lysates from 293Ts transfected with Kif3A siRNA. Tubulin is shown as a loading control.

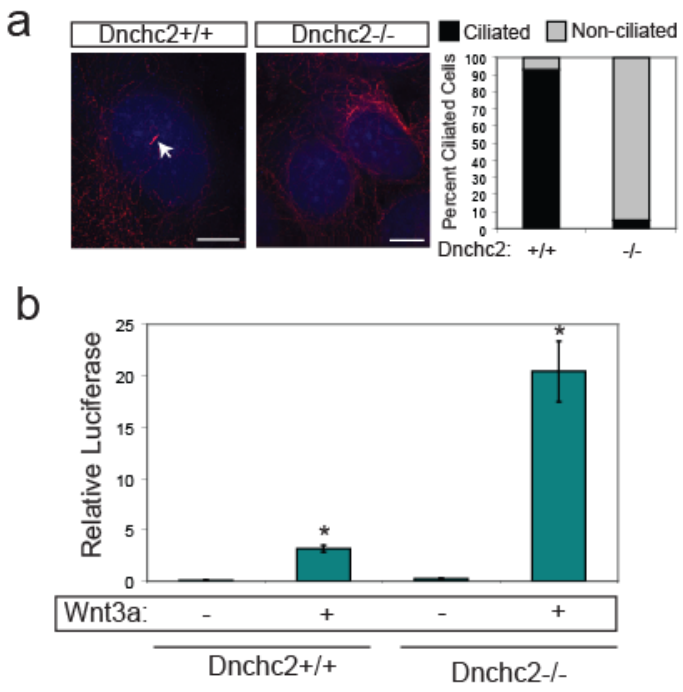

Supplementary Figure 3.2 Dnchc2 MEFs do not exhibit cilia. **a**. Staining for the primary cilium (acetylated tubulin, red) in Dnchc2 MEFs reveals loss of cilia in *Dnchc2-/-* MEFs. These results are quantified in the panel on the right. Nuclei are labeled with Hoechst (blue). **b**. Luciferase assay in Dnchc2 MEFs reveales increased Wnt response to Wnt3a in *Dnchc2-/-* cilium mutant MEFs. **P*<0.05, n=3 from three separate experiments, Student's *t*-test. Values were normalized for co-transfected β-Gal.

References

1. Klaus A & Birchmeier W (2008) *Nature reviews* **8,** 387-398.

2. Nusse R (2005) *Cell Res* **15,** 28-32.

3. Lancaster MA & Gleeson JG (2009) *Curr Opin Genet Dev* **19,** 220-229.

4. Fliegauf M, Benzing T, & Omran H (2007) *Nat Rev Mol Cell Biol* **8,** 880-893.

5. Gerdes JM, Liu Y, Zaghloul NA, Leitch CC, Lawson SS, Kato M, Beachy PA, Beales PL, DeMartino GN, Fisher S, Badano JL, & Katsanis N (2007) *Nat Genet* **39,** 1350-1360.

6. Corbit KC, Shyer AE, Dowdle WE, Gaulden J, Singla V, Chen MH, Chuang PT, & Reiter JF (2008) *Nat Cell Biol* **10,** 70-76.

7. Louie CM & Gleeson JG (2005) *Hum Mol Genet* **14 Spec No. 2,** R235-242.

8. Dixon-Salazar T, Silhavy JL, Marsh SE, Louie CM, Scott LC, Gururaj A, Al-Gazali L, Al-Tawari AA, Kayserili H, Sztriha L, & Gleeson JG (2004) *Am J Hum Genet* **75,** 979-987.

9. Ferland RJ, Eyaid W, Collura RV, Tully LD, Hill RS, Al-Nouri D, Al-Rumayyan A, Topcu M, Gascon G, Bodell A, Shugart YY, Ruvolo M, & Walsh CA (2004) *Nat Genet* **36,** 1008-1013.

10. Lancaster MA, Louie CM, Silhavy JL, Sintasath L, Decambre M, Nigam SK, Willert K, & Gleeson JG (2009) *Nat Med* **15,** 1046-1054.

11. Signor D, Wedaman KP, Orozco JT, Dwyer ND, Bargmann CI, Rose LS, & Scholey JM (1999) *The Journal of cell biology* **147,** 519-530.

12. Plotnikova OV, Golemis EA, & Pugacheva EN (2008) *Cancer research* **68,** 2058-2061.

13. Willert K, Brown JD, Danenberg E, Duncan AW, Weissman IL, Reya T, Yates JR, 3rd, & Nusse R (2003) *Nature* **423,** 448-452.

14. Nelson SB, Lawson MA, Kelley CG, & Mellon PL (2000) *Mol Endocrinol* **14,** 1509-1522.

The text of Chapter 3 in full is being prepared for submission, 2009, Lancaster MA, and Gleeson JG. The dissertation author is the primary researcher and author and the co-author listed directed and supervised the research which forms the basis of this chapter.

Chapter 4 Ahi1 is Required for Canonical Wnt Signaling During Early Cerebellar Midline Fusion

4.1 Abstract

Joubert syndrome (JS), a member of the ciliopathies, is marked by a unique cerebellar vermis hypoplasia, the pathogenic mechanism of which is completely unknown. In order to examine mechanisms of JS pathogenesis and the role of primary cilia in cerebellar development, we have examined Jouberin (Jbn) mutant mice as a model of JS. These mice exhibit a smaller cerebellum marked by a striking vermis/midline fusion defect early in development. This defect is concomitant with expansion of the roof plate and is also evident in another JS model: Cep290 mutant mice. Further, fetal MRIs from JS patients reveal a similar midline fusion defect suggesting parallel pathogenic mechanisms. Previous evidence has suggested a role for Jbn in canonical Wnt signaling. We therefore examined canonical Wnt signaling in developing cerebellum of Jbn mutant mice and identified a prominent decrease in activity at the site of hemisphere fusion. As support for a role for canonical Wnt signaling in JS pathogenesis, patient mutation constructs failed to function in canonical Wnt signaling in contrast to previously shown for wild-type Jbn. Our findings implicate a unique Wnt regulatory role for the primary cilium and the ciliopathy protein Jbn in cerebellar development and JS pathogenesis.

4.2 Introduction

Ciliopathies are a relatively recent classification for a broad spectrum of disorders which all share a common theme: abnormalities in ciliary structure and/or function(1-4).

Several of these include Alstrom syndrome, Oral-Facial-Digital type I, Bardet-Biedl syndrome (BBS), primary ciliary dyskinesia, autosomal dominant and recessive polycystic kidney disease (PKD), nephronophthisis (NPHP), retinitis pigmentosa (RP), Meckel-Gruber syndrome (MKS) and Joubert syndrome (JS)(5-7). JS is marked by cerebellar vermis hypoplasia as a primary phenotype(8, 9) though there is quite a lot of overlap with other ciliopathies such as NPHP and RP(10, 11). Although the primary cilium seems to be the underlying player in pathogenesis of these disorders, its function within this context is not clear.

While normal structure and movement of motile cilia is known to be vital for left-right asymmetry(12, 13) as well as several homeostatic functions such as mucus clearing in the lungs(14), the molecular function of the more ubiquitous primary nonmotile cilium is not as apparent. Recent evidence has identified several key signaling pathways which rely on or are regulated by the primary nonmotile cilium(15, 16). These include calcium signaling(17, 18), PDGF receptor signaling(19), canonical and noncanonical Wnt signaling(20-23) and the hedgehog pathway(24, 25). In many of these pathways, the primary cilium may influence signaling components by modulating their spatial localization. For example, hedgehog signaling requires ciliary translocation of smoothened leading to activation of Gli transcription factors within the cilium(26, 27), suggesting the cilium may act as a site for enrichment of hedgehog signaling machinery. In contrast, the canonical Wnt signaling pathway appears to be inhibited by the presence of the primary cilium potentially through multiple mechanisms. These include impairment of the proteasome in the absence of the cilium allowing for increased β-catenin(28) as well as enhanced CK1 phosphorylation of Dvl(29). The exact mechanisms of cilium inhibition of canonical Wnt are not clear but may involve spatial regulation of several components similar to that seen in Shh.

Due to increasing evidence that the primary cilium influences multiple signaling pathways, the phenotypes associated with ciliopathies are likely caused by abnormal downstream signaling events. Specifically, Sonic hedgehog (Shh) and Wnt signaling pathways have both been implicated in BBS, NPHP, PKD, OFD and MKS(30-33). In particular, Shh signaling defects may underlie the polydactyly seen in many ciliopathies(34, 35), and Wnt signaling seems to be an important pathway in cystic kidney ciliopathies(36, 37). However, the mechanisms of brain malformations such as those seen in JS are not as evident. Some hints have come from cilia mouse mutants which have revealed a vital role for the cerebellar primary cilium in Shh-dependent proliferation of cerebellar granule neurons(38, 39). However, the resulting phenotypes seem to affect the cerebellum overall and appear more severe than that seen in JS. Since examination of mouse mutants for those genes which exhibit null mutations in JS have not been examined for cerebellar phenotypes, the mechanisms of JS pathogenesis and ciliary functioning in cerebellar vermis formation are not clear.

Here, we report that Jbn, encoded by *AHI1* and mutated in JS, is required for early cerebellar vermis formation in a Wnt dependent manner. We provide evidence that Jbn functions in early Wnt signaling at the site of hemisphere fusion, and that this role affects proliferation and later cerebellum size. Our findings provide the first evidence of the mechanism of JS pathogenesis, and the role of the primary cilium in Wnt signaling within the developing cerebellum.

4.3 Results

Cerebellum size defect in *Ahi1* mutants

In order to study the role of Jbn in development of the cerebellum as well as mechanisms of JS pathogenesis, we examined a mouse model of loss of function of

Jbn(37), encoded by the *Ahi1* gene mutated in patients with JS(40, 41). Adult *Ahi1-/-* mice exhibited overall smaller body size as reported previously (manuscript submitted) with a slightly reduced brain size visible on whole mount imaging compared with *Ahi1+/-* or *Ahi1+/+* mice, which were indistinguishable from each other. Overall brain morphology of *Ahi1-/-* mice appeared normal except for a smaller cerebellum and underdeveloped vermis with a mildly defective foliation pattern. Cerebellar vermis lobes VI and VII appeared fused while lobe V appeared smaller and underdeveloped at 3 weeks of age. Additionally, midbrain inferior colliculus and superior colliculus both appeared slightly enlarged which may be due to the decreased vermis size, thus revealing more of the underlying midbrain tissue. Overall, the cerebellum appeared slightly underdeveloped suggesting a developmental defect.

In order to quantify this size defect we examined cresyl-violet stained midline sagittal sections which revealed that although the overall brain size was reduced (80% of control) the cerebellar vermis appeared more severely affected with a reduction in size of 40% at three weeks of age. Furthermore, foliation defects in lobes V, VI and VII were also clearly visible on sagittal sections similar to that seen on whole mount. Additionally, these size and foliation defects persisted beyond three weeks throughout adulthood suggesting an inability to recover from a developmental defect. However, despite the evident defect in overall vermis formation, the cellular organization within lobes appeared normal.

To test the developmental basis of this phenotype, we examined histological sections from postnatal day 4 (P4) and embryonic day 18.5 (E18.5) mice. At P4, *Ahi1-/-* mice exhibited smaller cerebellar vermis size and underdeveloped foliation with lobes V, VI and VII most affected, similar to that described above at P21. At E18.5, a very subtle size defect was evident, but the early foliation pattern appeared normal. Overall, these

findings suggest Jbn is required for proper development of the cerebellum, and *Ahi1* mutants may represent a model of the cerebellar vermis hypoplasia seen in JS.

Early proliferation defect and normal Shh in *Ahi1* mutants

Since both foliation and size are dependent upon expansion of cerebellar neurons, this phenotype could be due to defects in proliferation. We therefore tested for possible proliferation defects within the vermis of *Ahi1* mutants compared with littermate controls. Since cerebellar granule neurons (CGNs) are the major cell type of the cerebellum and undergo the most proliferation, and Jbn has previously been described to be expressed in this cell type(41), we tested BrdU staining in CGNs. We examined several stages from E16.5 to P5 and detected a significant decrease in CGN BrdU staining within the vermis at E16.5 which recovered by E18.5. This suggests a relatively early defect in proliferation of CGN precursors which appears to recover postnatally.

The major regulatory pathway in CGN proliferation is Shh signaling; however, this pathway is most active at post-natal timepoints rather than during early CGN precursor proliferation when the defect is evident in *Ahi1-/-* mice. However, since cilia have been shown to be required for Shh signaling within CGNs, and JS is a ciliopathy, we tested for a Shh defect in these mice. We stained sections from P5 *Ahi1-/-* and *Ahi1+/-* littermates for N-myc, a proliferative gene target of Shh signaling. N-myc staining appeared strongest in CGNs, as reported previously, and was not decreased in *Ahi1-/-* cerebella suggesting normal Shh signaling. Furthermore, western blot analysis of N-myc protein levels from whole cerebellum lysates revealed equal levels in *Ahi1-/-* mouse cerebellum compared with littermate control. These findings suggest that Shh signaling does not appear defective in *Ahi1-/-* cerebella. However, given the inconsistent timing of

the *Ahi1-/-* defect and Shh activity, these findings are not surprising and suggest an alternate mechanism.

Midline fusion defect and roof plate expansion in *Ahi1* mutants

Given the early proliferation defect, we next examined morphology of the developing cerebellum at earlier embryonic stages. Transverse sections from *Ahi1-/-* embryos stained with cresyl-violet revealed a striking midline fusion defect at the cerebellar vermis primordium compared with control littermates. This defect was most striking at E16.5 when control vermis had nearly completely fused whereas *Ahi1-/-* vermis was thinner and malformed. At E14.5, the defect was also clearly visible with a separation of cerebellar hemispheres visible in *Ahi1* mutant brain compared with littermate control. Whole mount images of embryos at E12.5 also revealed a size decrease in the cerebellar anlage with a separation of the two hemispheres at the midline and a striking expansion of the rhombic roof plate, the structure directly posterior to the developing cerebellum.

To further examine this roof plate abnormality, we sagittally sectioned an independent set of E12.5 embryonic brains and stained with cresyl-violet. Serial midline and medial sections revealed a lengthened roof plate in *Ahi1-/-* brain compared with littermate control reflecting the results seen on whole mount imaging. As a further verification of this phenotype, we examined transverse sections at E13.5 and identified an overall widened roof plate in the *Ahi1* mutant that became wider much more abruptly through a series of anterior to posterior transverse sections. Anterior sections at the site of cerebellar hemisphere fusion in controls revealed defective fusion in *Ahi1* mutant brain.

To test whether early midline fusion is a precursor to the vermal defect in JS patients, we examined fetal MRI images from verified JS patients and identified defective cerebellar hemisphere fusion in a 25 week gestation patient. This defect is most severe on inferior axial images where the lack of fusion leads to an apparent connection between the fourth ventricle and the cisterna magna. Similarly, midline fusion appears most defective on inferior horizontal sections from Ahi1-/- mice further suggesting this is a valid model of the early defects leading to JS. Although examination of roof plate on fetal MRIs was not possible since this structure is only visible very early in gestation (8-12 weeks), we were able to identify an enlarged fourth ventricle roof, a structure which is derived from the earlier roof plate. These findings suggest that the cerebellar vermal hypoplasia of JS is due to an early midline fusion defect and roof plate expansion similar to that seen in the JS Ahi1-/- mouse model.

Early Wnt signaling defect in Ahi1 mutants

To examine the mechanism of these early defects in Ahi1-/- mice, we next tested for signaling defects during early midline fusion. Jbn, the protein product of the Ahi1 gene, has recently been identified as a positive modulator of canonical Wnt signaling(37). Since canonical Wnt mouse mutants such as the swaying(42, 43) and β-catenin conditional mutant mice(44) exhibit similar roof plate expansion(45) and vermal defects, we tested whether Ahi1 mice exhibited defective canonical Wnt signaling. We crossed Ahi1+/- mice to BATgal transgenic mice(46). BATgal mice express a transgenic reporter of canonical Wnt signaling which consists of the β-galactosidase gene under the control of a series of TCF/Lef binding sites. We previously reported that Ahi1 and the BATgal transgene are linked. Therefore, in order to generate these mice, we backcrossed Ahi1+/-; BATgal+ mice to Ahi1+/- mice and recovered approximately 1 in 9

Ahi1+/+; BATgal- mice indicating a linkage of approximately 11.1 centimorgans. In order to obtain BATgal linkage to the Ahi1 null allele, and since Ahi1-/- mice are infertile, we then backcrossed at least 9 Ahi1+/-; BATgal+ males from this cross to Ahi1+/- mice to test for linkage in the father. Fathers that exhibited linkage between Ahi1 null and BATgal alleles were then used for subsequent timed matings.

Since midline fusion begins as early as E13.5(47, 48), we examined E13.5 Ahi1-/-; BATgal+ embryos for Wnt defects compared with Ahi1+/-; BATgal+ littermate controls. Whole mount imaging revealed a decrease in Wnt signaling specifically at the cerebellar midline anlage where the fusion defect is clearly visible compared with control embryos. Horizontal sectioning revealed a similar defect with a specific decrease in Wnt activity in cerebellar cells surrounding the midline. These results suggest defective Wnt signaling may underlie the midline fusion defect in JS.

Patient Mutations Exhibit Defective Wnt Signaling and Cilia Localization

Since we have previously reported that Jbn is a positive modulator of canonical Wnt signaling(37), we next tested if previously described JS patient mutations disrupt Jbn's function in the canonical Wnt pathway. We used a luciferase approach similar to previously described in which fibroblasts were cotransfected with a Super Topflash Wnt reporter construct and a Jbn expression plasmid. Cells were then treated with Wnt3A conditioned media and tested for Wnt activity by measuring luciferase activity. We generated three missense mutants of Jbn corresponding to three patient missense mutations: R723Q and H896R, in the WD40 domain, and V443D, adjacent to a putative PKC phosphorylation site(40, 49, 50). These patient mutations all exhibited comparable protein expression levels to wild-type Jbn as visualized by western blot analysis. Overexpression of wild-type Jbn in Wnt3A-stimulated cells resulted in a 1.6-fold increase

in reporter activity over empty vector control. In contrast, none of the patient mutants exhibited significantly increased Wnt activity compared with vector control cells. These findings suggest patient mutations disrupt Jbn's role in canonical Wnt signaling and support a role for Wnt signaling in JS pathogenesis.

Since we previously reported that Jbn interacts with β-catenin(37), we tested the ability of patient mutations to co-immunoprecipitate with β-catenin. Using 293T cells transfected with GFP-tagged Jbn constructs, we performed immunoprecipitation with a GFP antibody followed by western blot for endogenous β-catenin. This approach revealed an interaction between Jbn and β-catenin as previously described as well as interaction with the R723Q and H896R mutations. Patient mutation V443D however exhibited a considerable decrease in pulldown of endogenous β-catenin. Although soluble protein levels varied between mutant and wild-type Jbn constructs, immunoprecipitation efficiencies were indistinguishable among patient mutations indicating a specific reduction in interaction between β-catenin and patient mutation V443D. These data suggest a role for the interaction between Jbn and β-catenin in the pathogenesis of JS.

In order to further characterize these patient mutation constructs, we examined subcellular localization in ciliated IMCD cells. Jbn has previously been described to localize to the primary cilium in renal cell types including IMCDs. Patient mutant proteins however failed to localize to the primary cilium in IMCD cells and instead displayed diffuse localization throughout the cytosol. Quantification revealed cilia localization of wild-type Jbn in 90% of cells while patient mutations exhibited cilia localization in only 2% to 7% of cells. These results implicate cilia localization in JS pathogenesis and suggest the WD40 and the putative PKC site are necessary for localization of Jbn to the cilium.

These findings point to a possible role for the primary cilium in Jbn's Wnt modulatory role since both Jbn and β-catenin colocalize to the primary cilium of CGNs. We therefore tested whether primary cilia were disrupted in Ahi1-/- CGNs. CGNs isolated from Ahi1 null and control littermates exhibited indistinguishable number and morphology similar to that recently described in kidney of Ahi1-/- mice. These results suggest that Jbn does not play a role in ciliogenesis during cerebellar development and instead functions specifically in early Wnt signaling in the developing vermis.

Since the patient missense mutations, which exhibit abnormal localization, lead to the striking cerebellar defect seen in JS, we tested whether Jbn exhibits similar cilia localization in cerebellar granule neurons (CGNs). Granule neurons isolated from P5 wild-type mouse cerebella exhibited cilia during the first 24 hours following dissociation. Transfection with Jbn-GFP or staining for endogenous Jbn revealed localization to the primary cilium and basal body in CGNs suggesting cilia localization is physiologically significant within the context of JS and cerbellar development. We additionally tested β-catenin colocalization since Jbn and β-catenin interact and β-catenin has recently been localized to primary cilia in fibroblasts. In CGNs, both β-catenin-GFP and endogenous β-catenin exhibited colocalization with Jbn at the base of the cilium supporting the association between Jbn and β-catenin and suggesting that this occurs at the basal body in neurons.

4.4 Discussion

Our findings represent the first description of a mouse model of Joubert syndrome and provide a mechanism for the resulting vermis hypoplasia. Loss of Ahi1 in the mouse leads to a smaller cerebellar vermis with a mild decrease in early proliferation which is not dependent on Shh. This midline size defect seems to be due to defective

midline fusion and an expanded roof plate. Wnt signaling at the site of midline fusion appears decreased in Ahi1-/- mice suggesting Wnt signaling within vermis precursors is required for midline fusion.

Previously, Wnt signaling mutant mice have been described to exhibit midline vermis defects. For example, the β-catenin conditional loss of function mouse exhibits a complete lack of cerebellar vermis(44) similar to the Wnt-1 swaying mutant mouse(42, 43). Additionally, the Wnt-1 swaying mutant mouse has previously been described to exhibit an expanded roof plate(45) similar to that seen in Ahi1-/- mice. Since the roof plate and cerebellar vermis are highly interdependent, our data would suggest the enlarged roof plate may result from decreased early vermis size, allowing for roof plate expansion into midline cerebellar territory. These findings implicate a mechanism for early Wnt signaling in vermis hemisphere fusion resulting in an expanded roof plate and later vermis defect.

Given the resulting vermis proliferation and size defects with loss of Ahi1 and early Wnt signaling, these results have implications not only for Joubert syndrome but also for cancers of the cerebellum known as medulloblastoma(51). Before its identification as mutated in Joubert syndrome, Ahi1 was first identified as an oncogene in certain forms of mouse and human leukemias(52, 53). Overexpressed Ahi1 is present in hyperproliferative cancer cells(53) supporting its role as a positive regulator of proliferation. Medulloblastoma occurs most often in the developing cerebellar vermis(54) suggesting overproliferation of vermal precursor cells is to blame. Our findings suggest Wnt signaling is involved in this process and Ahi1 is a regulator at the primary cilium which may represent an interesting candidate for investigation in medulloblastoma. In fact, a recent study identified a unique copy number variation in one particular patient derived medulloblastoma cell line which included Ahi1(55). This amplicon contained five

genes which included Ahi1 and was amplified 34-fold higher than normal. In addition, examination of mRNA levels in a mouse model of medulloblastoma revealed increased Ahi1 transcript levels in preneoplastic cells as well as tumor cells (GEO Profiles, NCBI). These findings suggest that Ahi1 may be upregulated in medulloblastoma, similar to that seen in leukemia, and that dysregulated Wnt signaling may be the mechanism of increased proliferation. This implication is supported by the fact that approximately 15% of sporadic medulloblastomas exhibit Wnt component mutations which lead to increased Wnt signaling(51). Thus, whereas loss of Ahi1 leads to decreased Wnt signaling and a smaller vermis, Ahi1 overexpression would be expected to lead to increased Wnt signaling and an overproliferative vermis, leading to medulloblastoma.

Although defects in Wnt signaling have previously been described in medulloblastoma(51), the mechanism of cancer development is not known since a role for Wnt signaling in cerebellar proliferation had not previously been described. Our findings are the first to provide a role for canonical Wnt signaling in early vermis fusion and proliferation. Thus, medulloblastoma likely arises from dysregulation of this process through overactivation of the pathway. Overall, our results are the first to describe a mechanism of Wnt signaling within the developing vermis which regulates subsequent proliferation and overall vermis size.

4.5 Methods

Plasmid constructs and materials

Ahi1-/- mice were used and heterozygotes were crossed to Batgal+ mice (kindly provided by S. Piccolo) as previously described(37). Patient mutation constructs were generated using the QuikChange Site-Directed Mutagenesis Kit (Stratagene). β-catenin GFP construct was obtained from K. Willert.

Histology and immunohistochemistry

We obtained brain sections by perfusion fixation followed by embedding in 10%/7.5% gelatin/sucrose and cryosectioning at 20 μm thickness. Sections were then stained for cresyl-violet and imaged for morphology. Size measurements were performed using ImageJ to quantify vermis area from three midline sections of each of three mice for each genotype, control or Ahi1-/-. X-gal staining was performed as previously described(37) for 1-3 hours on whole mount or sections. Littermates were stained in parallel in the same X-gal solution.

Immunostaining of sections or isolated cells was performed by blocking in 4% donkey serum in 0.1% TritonX, followed by staining with the following primary antibodies: anti-acetylated tubulin (Zymed 32-2700, 1:500 dilution), rabbit anti-Jbn(37) (Quality Controlled Biochemicals), rabbit anti-β-catenin (Cell Signaling, 95825, 1:200) rat anti-Brdu (Abcam, ab6326, 1:200), anti-n-myc (Cell Signaling, 9405, 1:200), and rabbit anti-PH3 (Upstate, 06-570, 1:200). For Jbn staining, we performed antigen retrieval by heating samples in 100 mM Tris, 5% urea, pH9.5 at 95 ºC for 10 min. Samples were then washed in PBS and stained with the following secondary antibodies: AlexaFluor donkey anti-mouse 594, donkey anti-rat 488, donkey anti-rabbit 488, goat anti-rabbit 350, (Molecular Probes, 1:500). Hoechst was used as the nuclear stain. We acquired and quantified images using a DeltaVision Spectris deconvolution or a FV1000 Spectral Deconvolution Confocal microscope (UCSD Neuroscience Microscopy Core). CGNs were isolated according to a previously published protocol(56) and fixed in 4% PFA 5 hrs after plating onto poly-D-lysine coated slides followed by washing, blocking, and staining.

Western blotting and luciferase

Western blotting was performed on lysates prepared in modified RIPA buffer using the following antibodies: anti N-myc (Cell Signaling, 9405), mouse anti-β-catenin (BD Transduction Labs, 610153), goat anti-GAPDH (Santa Cruz Biotech, SC-20357), mouse anti-GFP (Covance, B34), rabbit anti-TFIIH (Santa Cruz Biotech., SC-293), and mouse anti-α-tubulin (Sigma, T-6074). All antibodies were used at 1:1000 dilution. Rabbit anti-GFP (Genetex, Gtx26556, 1µg) was used for immunoprecipitations from modified RIPA lysates using protein A sepharose beads. For transient transfections of fibroblasts or IMCDs, Lipofectamine 2000 (Invitrogen) was used according to manufacturer's protocol. Transfection of CGNs was performed using Amaxa nucleofector primary neuron kit according to manufacturer's protocol. For luciferase assay, fibroblasts were grown in 12-well plates and transfected with 600ng Topflash, 120ng βGal, and 650ng of Jbn-GFP expression plasmid or empty vector (GFP was mutated at Y66G to disrupt fluorescence using QuikChange mutagenesis). Twenty-four hrs following transfection, cells were serum starved for 8hrs then treated overnight with WCM diluted 3:1 in serum free media. The luciferase assay was performed according to a previously published protocol(57) and β-galactosidase activity was measured using the Tropix Galacto-light Plus kit (Applied Biosystems, T1007).

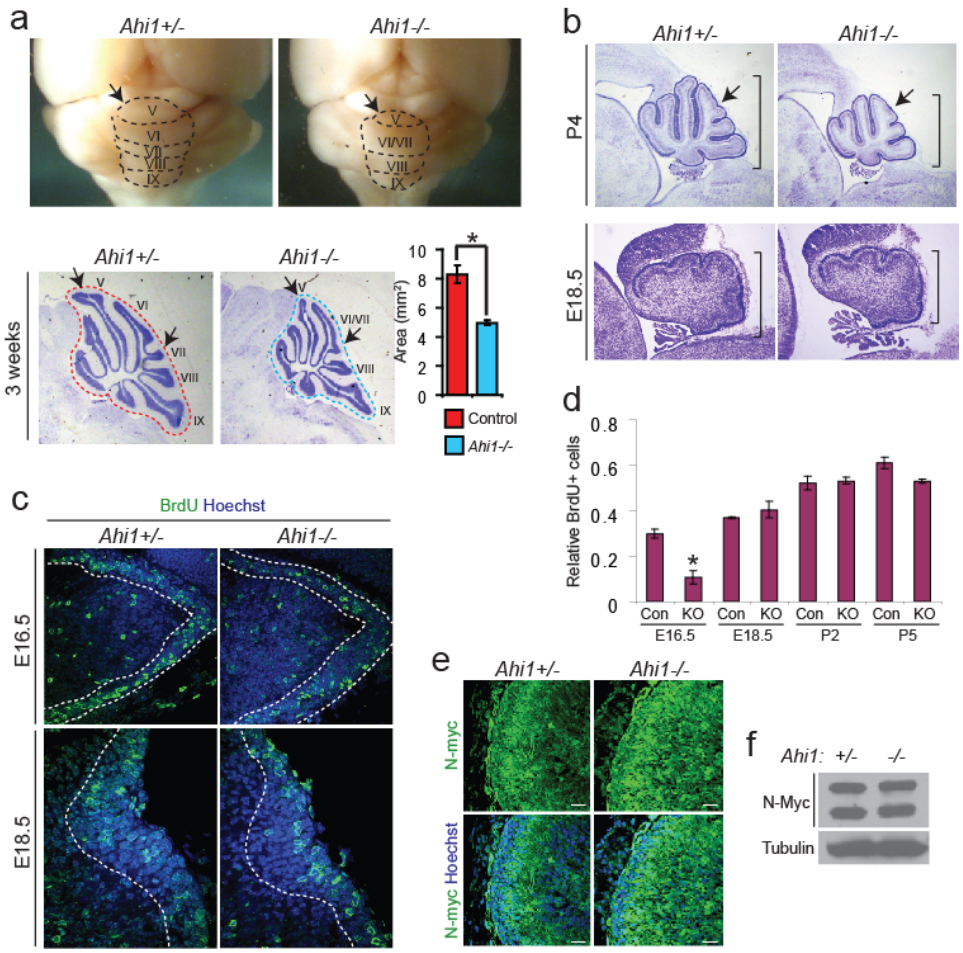

Figure 4.1 Reduced cerebellum size and foliation defects in Ahi1-/- mice. **a**. Top, whole mount images of representative mutant and littermate control brains. The vermal folia are outlined with a dashed line and folia V-IX are labeled. Bottom, midline sagittal cresyl-violet stained sections from representative littermates. Folia are labeled and arrows indicate foliation defects: decreased size of V and fusion of VI and VII. Quantification of vermis size is depicted in a histogram at the right generated from average area measurements of midline sections outlined in corresponding blue and red lines. **b**. Sagittal midline C-V stained sections from representative littermates aged P4 and E18.5 revealing the presence of a mild size defect (bars) and foliation defects (arrows). **c**. BrdU stained (green) sections from representative littermates aged E16.5 and E18.5. External granule layer is demarcated by dahed lines and Hoechst labels nuclei. **d**. Quantification of BrdU labeling EGL neurons indicated as average number of BrdU positive cells per total EGL cells. E16.5 reveals a significant decrease in relative BrdU stained cells. **e**. N-myc staining (green) in midline sagittal sections from P5 littermates. Hoechst labels nuclei. **f**. Western blot on whole cerebellum lysates from P5 littermates. N-myc antibody recognizes two bands as previously described. Tubulin is the loading control.

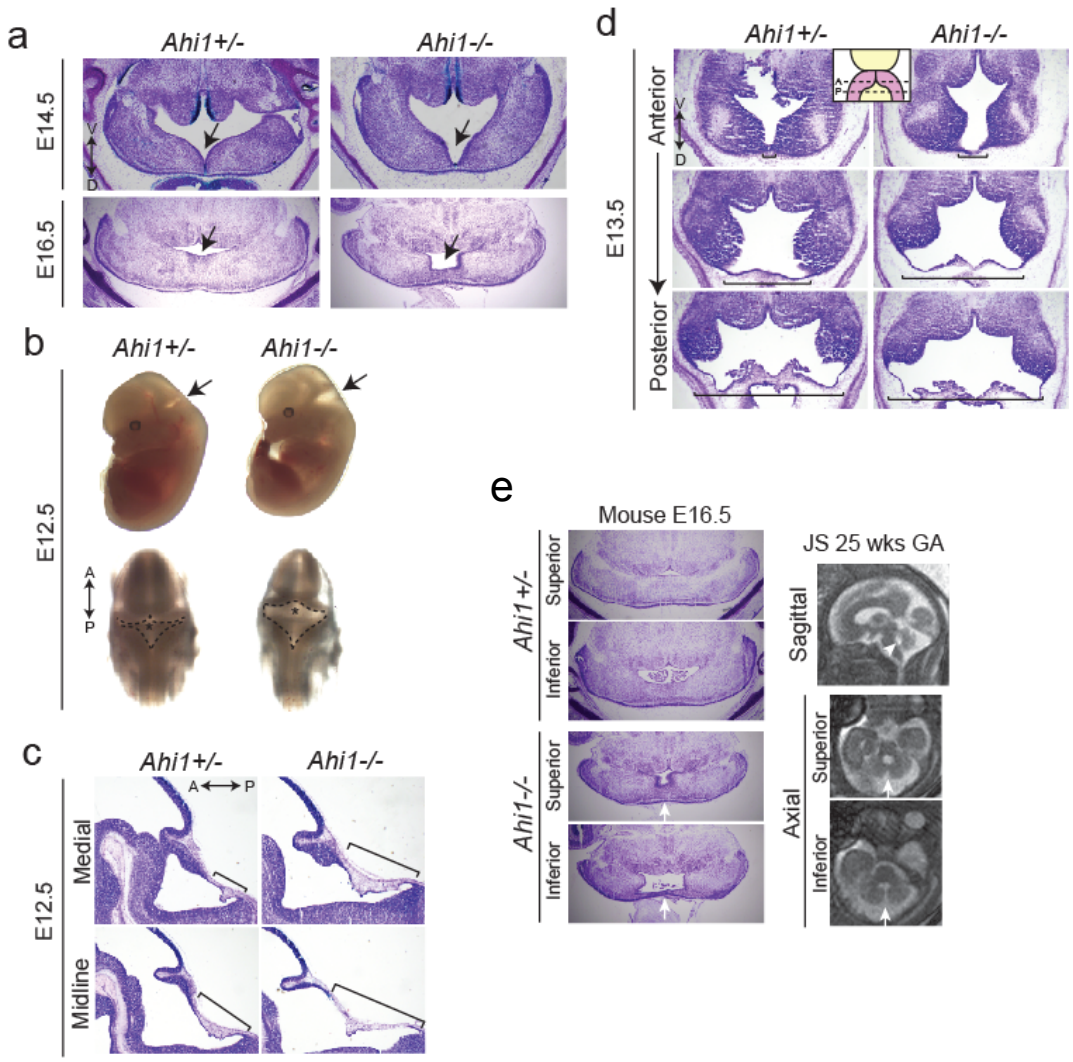

Figure 4.2 Midline fusion defect in Ahi1 null mice. **a**. Transverse C-V stained sections from littermates at E16.5 and E14.5 revealing midline fusion defect (arrows). **b**. Whole mount images of littermate embryos at E12.5 imaged from the side (top) and on the dorsal surface (bottom). Arrows point to the expanded roof plate and fourth ventricle. Dashed lines demarcate roof plate while asterisks point to cerebellar vermis anlage. Anterior (A) and posterior (P) directionality is depicted by a double arrow. **c**. Midline and medial sagittal C-V stained sections from E12.5 littermates revealing elongated roof plate (bars). **d**. Matched transverse C-V stained sections from littermates arranged in a series from anterior to posterior revealing the progressive posterior widening of the roof plate in Ahi1 mutant (bars). Diagram inset depicts approximate locations of anterior and posterior sections. **e**. Right, axial C-V stained sections from Ahi1 mutant and littermate control shown in series from superior to inferior. Left, fetal MRIs from a JS patient at 25 weeks gestational age (GA). Sagittal image reveal superiorly tilted and expanded fourth ventricle roof, while axial series reveals a gap between cerebellar hemispheres reflecting midline fusion defect (arrows) which is more severe on inferior sections similar to Ahi1 mutant mice.

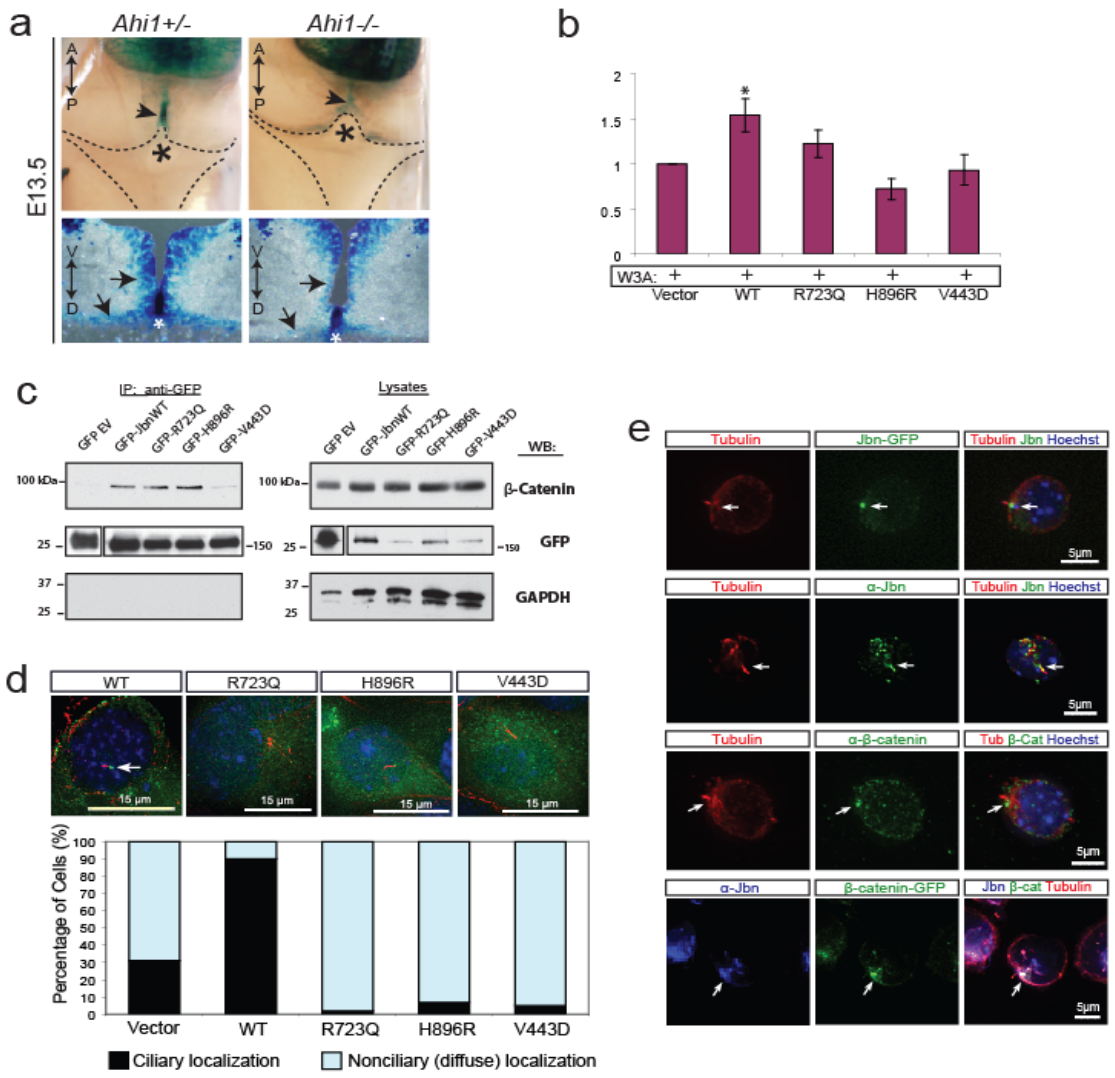

Figure 4.3 Wnt defect in JS models. **a**. Top, X-gal stained whole mount dorsal view of E13.5 Batgal+ littermates revealing Wnt activity at the site of hemisphere fusion (arrowheads). Bottom, anterior X-gal stained transverse sections from Batgal+ littermates. Asterisks depict roof plate directly abutting the site of midline fusion. Arrows point to cerebellar hemisphere cells surrounding the developing midline which exhibit Wnt activity in control but decreased activity in Ahi1 null sections which also exhibit defective fusion of surrounding cells. **b**. Luciferase activity in fibroblasts transfected with wild-type Jbn or patient mutation constructs and treated with Wnt3A (W3A) conditioned media. *P<0.05, Student's t-test, n=3. **c**. Co-immunoprecipitation of Jbn GFP constructs pulled down with GFP antibody and western blot for endogenous β-catenin which reveals interaction between β-catenin and wild-type Jbn as well R723Q and H896R but not with V443D. GFP western blot reveals efficiency of immunoprecipitation, while GAPDH is a negative control. **d**. Localization of Jbn patient mutations constructs (green) in IMCD cells stained for cilia (acetylated tubulin, red). Hoechst labels nuclei. Below, quantification of cilia localization in 100 cells for each construct.

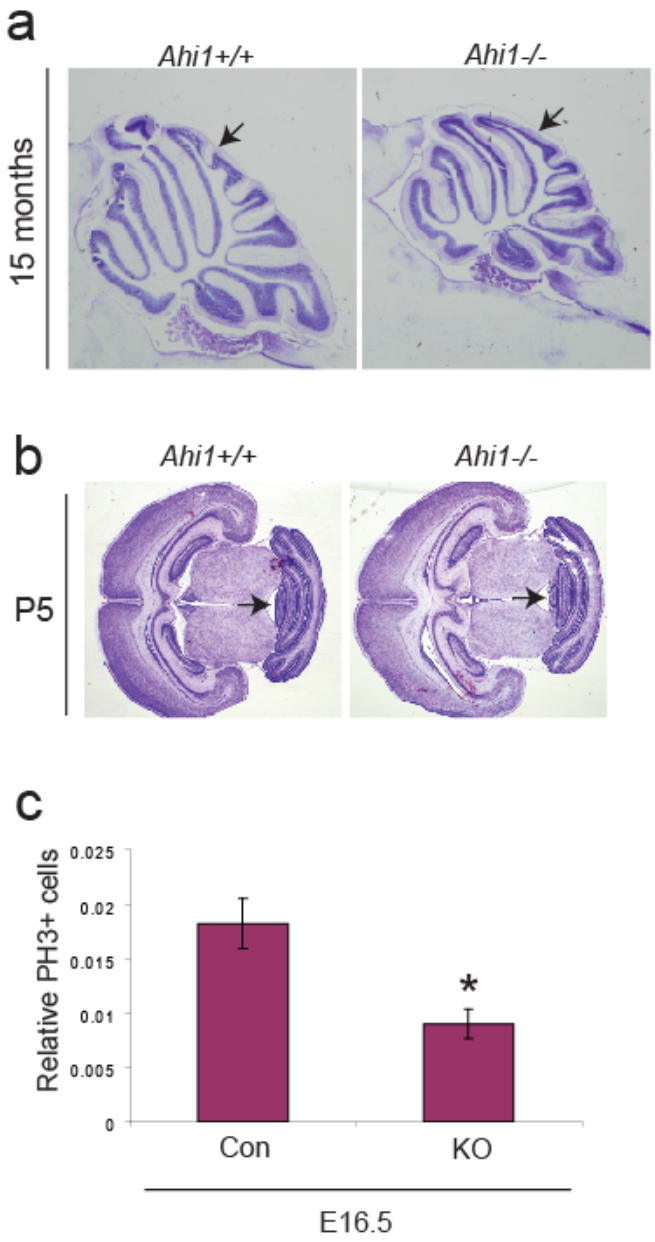

Supplementary Figure 4.1 Cerebellum phenotype of Ahi1 null mice. **a**. Representative 15 month old littermate sagittal C-V stained sections revealing persistent size and foliation defects (arrows). **b**. Transverse C-V stained sections from P5 littermates revealing specific vermis folia size defect particularly in folia V (arrows). **c**. Average number of phospho-histone H3 (PH3) stained EGL neurons at E16.5 relative to total cells in EGL. *P<0.05, Student's t-test, n=3.

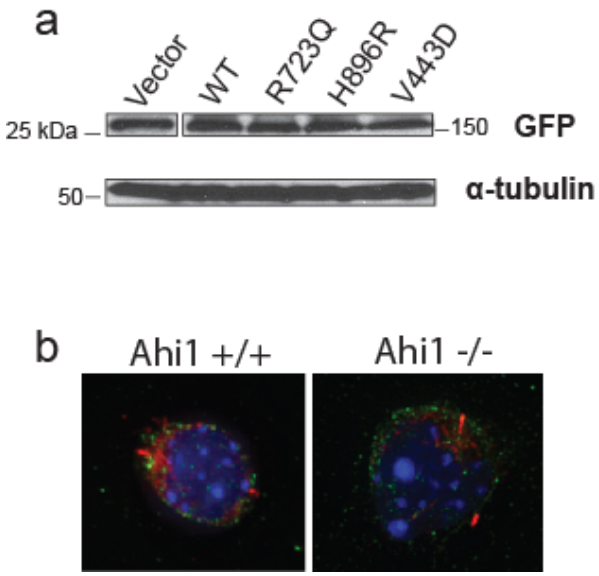

Supplementary Figure 4.2 Patient Mutations Exhibit Normal Expression **a**. Western blot from 293T cells transfected with patient mutations constructs and assayed for GFP levels. Tubulin represents the loading control. **b**. Cilia staining (acetylated tubulin, red) in isolated CGNs from P5 littermates. Hoechst labels nuclei (blue).

References

1. Badano JL, Mitsuma N, Beales PL, & Katsanis N (2006) *Annu Rev Genomics Hum Genet* **7,** 125-148.

2. Fliegauf M, Benzing T, & Omran H (2007) *Nat Rev Mol Cell Biol* **8,** 880-893.

3. Marshall WF (2008) *J Cell Biol* **180,** 17-21.

4. Lancaster MA & Gleeson JG (2009) *Curr Opin Genet Dev* **19,** 220-229.

5. Adams M, Smith UM, Logan CV, & Johnson CA (2008) *J Med Genet* **45,** 257-267.

6. Guay-Woodford LM (2006) *Pediatr Nephrol* **21,** 1369-1376.

7. Hildebrandt F & Zhou W (2007) *J Am Soc Nephrol* **18,** 1855-1871.

8. Joubert M, Eisenring JJ, Robb JP, & Andermann F (1969) *Neurology* **19,** 813-825.

9. Louie CM & Gleeson JG (2005) *Hum Mol Genet* **14 Spec No. 2,** R235-242.

10. Harris PC (2007) *Kidney Int* **72,** 1421-1423.

11. Ivarsson SA, Bjerre I, Brun A, Ljungberg O, Maly E, & Taylor I (1993) *Am J Med Genet* **45,** 542-547.

12. Marszalek JR, Ruiz-Lozano P, Roberts E, Chien KR, & Goldstein LS (1999) *Proc Natl Acad Sci U S A* **96,** 5043-5048.

13. Nonaka S, Tanaka Y, Okada Y, Takeda S, Harada A, Kanai Y, Kido M, & Hirokawa N (1998) *Cell* **95,** 829-837.

14. Morillas HN, Zariwala M, & Knowles MR (2007) *Respiration* **74,** 252-263.

15. Pazour GJ & Witman GB (2003) *Curr Opin Cell Biol* **15,** 105-110.

16. Singla V & Reiter JF (2006) *Science* **313,** 629-633.

17. Delmas P (2005) *Pflugers Arch* **451,** 264-276.

18. Nauli SM, Alenghat FJ, Luo Y, Williams E, Vassilev P, Li X, Elia AE, Lu W, Brown EM, Quinn SJ, Ingber DE, & Zhou J (2003) *Nat Genet* **33,** 129-137.

19. Schneider L, Clement CA, Teilmann SC, Pazour GJ, Hoffmann EK, Satir P, & Christensen ST (2005) *Curr Biol* **15,** 1861-1866.

20. Germino GG (2005) *Nat Genet* **37,** 455-457.

21. He X (2008) *Nat Cell Biol* **10,** 11-13.

22. Simons M, Gloy J, Ganner A, Bullerkotte A, Bashkurov M, Kronig C, Schermer B, Benzing T, Cabello OA, Jenny A, Mlodzik M, Polok B, Driever W, Obara T, & Walz G (2005) *Nat Genet* **37,** 537-543.

23. Wallingford JB (2006) *Hum Mol Genet* **15 Spec No 2,** R227-234.

24. Eggenschwiler JT & Anderson KV (2007) *Annu Rev Cell Dev Biol* **23,** 345-373.

25. Corbit KC, Aanstad P, Singla V, Norman AR, Stainier DY, & Reiter JF (2005) *Nature* **437,** 1018-1021.

26. Haycraft CJ, Banizs B, Aydin-Son Y, Zhang Q, Michaud EJ, & Yoder BK (2005) *PLoS Genet* **1,** e53.

27. May SR, Ashique AM, Karlen M, Wang B, Shen Y, Zarbalis K, Reiter J, Ericson J, & Peterson AS (2005) *Dev Biol* **287,** 378-389.

28. Gerdes JM, Liu Y, Zaghloul NA, Leitch CC, Lawson SS, Kato M, Beachy PA, Beales PL, DeMartino GN, Fisher S, Badano JL, & Katsanis N (2007) *Nat Genet* **39,** 1350-1360.

29. Corbit KC, Shyer AE, Dowdle WE, Gaulden J, Singla V, Chen MH, Chuang PT, & Reiter JF (2008) *Nat Cell Biol* **10,** 70-76.

30. Benzing T, Simons M, & Walz G (2007) *J Am Soc Nephrol* **18,** 1389-1398.

31. Blacque OE & Leroux MR (2006) *Cell Mol Life Sci* **63,** 2145-2161.

32. Ross AJ, May-Simera H, Eichers ER, Kai M, Hill J, Jagger DJ, Leitch CC, Chapple JP, Munro PM, Fisher S, Tan PL, Phillips HM, Leroux MR, Henderson DJ, Murdoch JN, Copp AJ, Eliot MM, Lupski JR, Kemp DT, Dollfus H, Tada M, Katsanis N, Forge A, & Beales PL (2005) *Nat Genet* **37,** 1135-1140.

33. Tobin JL & Beales PL (2007) *Pediatr Nephrol* **22,** 926-936.

34. Ferrante MI, Zullo A, Barra A, Bimonte S, Messaddeq N, Studer M, Dolle P, & Franco B (2006) *Nat Genet* **38,** 112-117.

35. Ming JE, Roessler E, & Muenke M (1998) *Mol Med Today* **4,** 343-349.

36. Torres VE & Harris PC (2006) *Nat Clin Pract Nephrol* **2,** 40-55; quiz 55.

37. Lancaster MA, Louie CM, Silhavy JL, Sintasath L, Decambre M, Nigam SK, Willert K, & Gleeson JG (2009) *Nat Med* **15,** 1046-1054.

38. Chizhikov VV, Davenport J, Zhang Q, Shih EK, Cabello OA, Fuchs JL, Yoder BK, & Millen KJ (2007) *J Neurosci* **27,** 9780-9789.

39. Spassky N, Han YG, Aguilar A, Strehl L, Besse L, Laclef C, Ros MR, Garcia-Verdugo JM, & Alvarez-Buylla A (2008) *Dev Biol* **317,** 246-259.

40. Dixon-Salazar T, Silhavy JL, Marsh SE, Louie CM, Scott LC, Gururaj A, Al-Gazali L, Al-Tawari AA, Kayserili H, Sztriha L, & Gleeson JG (2004) *Am J Hum Genet* **75,** 979-987.

41. Ferland RJ, Eyaid W, Collura RV, Tully LD, Hill RS, Al-Nouri D, Al-Rumayyan A, Topcu M, Gascon G, Bodell A, Shugart YY, Ruvolo M, & Walsh CA (2004) *Nat Genet* **36,** 1008-1013.

42. Thomas KR, Musci TS, Neumann PE, & Capecchi MR (1991) *Cell* **67,** 969-976.

43. McMahon AP & Bradley A (1990) *Cell* **62,** 1073-1085.

44. Schuller U & Rowitch DH (2007) *Brain Res* **1140,** 161-169.

45. Louvi A, Alexandre P, Metin C, Wurst W, & Wassef M (2003) *Development* **130,** 5319-5330.

46. Maretto S, Cordenonsi M, Dupont S, Braghetta P, Broccoli V, Hassan AB, Volpin D, Bressan GM, & Piccolo S (2003) *Proc Natl Acad Sci U S A* **100,** 3299-3304.

47. Millen KJ, Wurst W, Herrup K, & Joyner AL (1994) *Development* **120,** 695-706.

48. Cheng LE, Zhang J, & Reed RR (2007) *Dev Biol* **307,** 43-52.

49. Parisi MA, Doherty D, Eckert ML, Shaw DW, Ozyurek H, Aysun S, Giray O, Al Swaid A, Al Shahwan S, Dohayan N, Bakhsh E, Indridason OS, Dobyns WB, Bennett CL, Chance PF, & Glass IA (2006) *J Med Genet* **43,** 334-339.

50. Valente EM, Brancati F, Silhavy JL, Castori M, Marsh SE, Barrano G, Bertini E, Boltshauser E, Zaki MS, Abdel-Aleem A, Abdel-Salam GM, Bellacchio E, Battini R, Cruse RP, Dobyns WB, Krishnamoorthy KS, Lagier-Tourenne C, Magee A, Pascual-Castroviejo I, Salpietro CD, Sarco D, Dallapiccola B, & Gleeson JG (2006) *Ann Neurol* **59,** 527-534.

51. Marino S (2005) *Trends Mol Med* **11,** 17-22.

52. Jiang X, Hanna Z, Kaouass M, Girard L, & Jolicoeur P (2002) *J Virol* **76,** 9046-9059.

53. Jiang X, Zhao Y, Chan WY, Vercauteren S, Pang E, Kennedy S, Nicolini F, Eaves A, & Eaves C (2004) *Blood* **103,** 3897-3904.

54. de Haas TG & Kool M (2007) *Clin Neuropathol* **26,** 93-110.

55. McCabe MG, Ichimura K, Liu L, Plant K, Backlund LM, Pearson DM, & Collins VP (2006) *J Neuropathol Exp Neurol* **65,** 549-561.

56. Hatten ME (1985) *J Cell Biol* **100,** 384-396.

57. Nelson SB, Lawson MA, Kelley CG, & Mellon PL (2000) *Mol Endocrinol* **14,** 1509-1522.

The text of Chapter 4 in full is being prepared for submission, 2009, Lancaster MA, Gopal DJ, Silhavy JL, Kim J, Louie CM, and Gleeson, JG. The dissertation author is the primary researcher and author and the co-authors performed experiments and supervised the research which forms the basis of this chapter.

Chapter 5 Conclusion

5.1 The Cilium as a Signaling Hub

Although primary cilia have only recently received significant attention, our findings and others suggest this unique organelle may act as a general signaling hub which spatially regulates various signaling components. The primary cilium is derived from the primordial motile cilium and flagellum which exist on numerous eukaryotic single celled organisms(1). Motile cilia can be found on practically all multi-cellular organisms but the primary cilium seems to have been repurposed through evolution. Instead of allowing for motility of the cell or brushing fluid around the cell, the nonmotile primary cilium seems to act as an antenna(2).

These results have led to new insight into how a cell responds so quickly to extracellular signals like Wnt or Shh ligands. The resulting hypothesis is quite intuitive actually. One could imagine that a signaling pathway would transmit much more quickly intracellularly if all the necessary components were maintained in one discreet location. A vertebrate cell is extremely large relative to the protein components of a signaling pathway, and the nature of the intracellular environment prohibits very much diffusion of these components(3). Therefore, active transport within the cell, particularly from the membrane to the nucleus would need to be involved. Additionally, this transport and to some extent initial diffusion of components would be much facilitated if the components were concentrated within a subcellular compartment. Thus, the primary cilium seems to act as a signaling concentrator to allow for timely transmission of an extracellular signal.

This particularly seems to be the case for Shh signaling in which the Gli transcription factors are processed within the cilium, thus concentrating all the necessary downstream components in one location. These components function both to transmit

the signal and to regulate the cascade. In canonical Wnt signaling, the primary cilium again seems to concentrate regulatory components, but unlike the Shh pathway, this concentration leads to negative regulation of the pathway, through sequestration. Our findings are the first to describe this type of spatial regulation of the canonical Wnt pathway within a subcellular organelle.

Since the Wnt pathway is vital for a multitude of developmental and homeostatic functions throughout the vertebrate body(4), proper regulation of this pathway is key. A variety of defects can arise with abnormal regulation of this pathway including developmental abnormalities leading to fetal lethality or a variety of childhood diseases(5). Additionally, multiple forms of cancer have been linked to dysregulation of the pathway(6, 7) leading to hyperproliferation of cancer cells. Although the primary cilium has not specifically been examined in most of these Wnt dependent diseases, there is some data suggesting cilia may themselves be abnormally regulated within certain cancers(8). Future studies to examine the underlying regulation of cilia will be important in determining its effect on Wnt dependent transformation of cancer stem cells and development of cancer.

5.2 Canonical Wnt Signaling in Kidney Homeostasis

Cystic kidney disorders encompass a variety of renal diseases which can lead to end-stage renal failure due to progressive cyst development within the tubules of the kidney(9). We have examined the ciliopathy nephronophthisis (NPHP)(10) within a mouse model of loss of Jouberin. Since patients do not usually exhibit symptoms of renal disease until cysts have already formed, the mechanisms of cyst development were not previously known. We therefore examined mice at multiple stages of disease development in an effort to identify the causative events in NPHP pathogenesis. Overall,

our results were quite surprising. We found an unexpected decrease in canonical Wnt signaling as the cause of NPHP in these mice. Since Jbn is a cilia protein, and given that cilia are inhibitory to canonical Wnt signaling(11, 12), we were surprised to find that Jbn is required for adult Wnt signaling. Even more surprising perhaps was the discovery that canonical Wnt signaling appears active even in the healthy adult kidney, which had not previously been described. Our findings, therefore, not only provide the first glimpse of the causative events leading to cyst formation in NPHP, but also implicate a novel role for canonical Wnt signaling in adult renal homeostasis.

The finding that canonical Wnt signaling is necessary for homeostasis and that its loss can lead to cyst formation suggests that NPHP and perhaps related cystic kidney disorders may be treatable and perhaps preventable in at risk patients through reactivation of the pathway. Since there are already several Wnt activating drugs(13), this might be a route worth examining for possible therapies. Although not done in replicate, I have performed preliminary treatments in Ahi1-/- mice with either NaCl or with the Wnt pathway agonist lithium (LiCl) at therapeutic concentrations and examined subsequent kidney pathology. When a pair of aged Ahi1-/- mice were treated either with NaCl or with LiCl, I found that the LiCl treated mouse exhibited overall better kidney histopathology than the NaCl Ahi1-/- mice suggesting that activation of canonical Wnt signaling may have alleviated cyst formation in this mouse and perhaps even reversed some of it since these mice were quite aged (1.5 yrs of age). Additionally, I found that lithium treatment had no effect in a control Ahi1+/- mouse suggesting that activation of the pathway by itself does not lead to NPHP. This result, along with our previous findings, suggests that Wnt activation may represent an important option for development of therapeutic strategies in combating cystic kidney disorders.

Finally, the discovery that canonical Wnt signaling is active and necessary during healthy adult homeostasis is quite exciting. These results suggest that Wnt signaling may be active in a variety of other adult tissues and perhaps Wnt activation represents a common response to injury. Thus, even kidney cells, and probably other cell types as well, can undergo regeneration through Wnt dependent mechanisms. Since canonical Wnt signaling in adult tissues has primarily been thought of in the context of cancer formation, these findings switch the paradigm and support additional roles for this pathway in adult homeostasis. Thus, cancer progression may represent a dysregulation of normal homeostatic Wnt signaling. Future studies will need to examine regulation of the homeostatic Wnt signaling in an effort to reestablish pathway control within cancer cells. This will quite probably involve cilia regulation of the pathway, so targeted therapy development would benefit from investigating cilia targets in addition to Wnt pathway components.

5.3 Cilia Regulation of Wnt Signaling in the Developing Cerebellum

Since AHI1 was first identified as mutated in Joubert syndrome(14, 15), we initially generated the Ahi1 mutant mouse as a model of JS. The most striking defects in this mouse however were its kidney and eye (described by Carrie Louie, in press) phenotypes. Overall, the brain appeared only mildly affected so it was unclear whether this could be considered a good model of JS. Certainly it is a genetic model of the disease, but in contrast to JS, the cerebellum was only mildly affected. However, when we examined the brain at earlier stages, it became clear that this mouse exhibited defective vermis formation which mimics that seen in JS patients, particularly on fetal MRI. Therefore, we conclude that this mouse is in fact a good model of the disease and can provide insight into the mechanisms of JS pathogenesis.

Interestingly, not only has this mouse provided clues into the mechanisms of JS pathogenesis, but it has also proved insightful in terms of normal development of the cerebellum and potentially other disease states like medulloblastoma. In fact, whereas JS appears to be a defect of underproliferation of cerebellar precursor neurons, medulloblastoma is due to hyperproliferation of cerebellar granule neurons. Thus, we can potentially learn quite a lot from the pathogenic mechanisms of JS.

To underline the potential implications of our findings in cerebellar neuronal proliferation in general and as it pertains to medulloblastoma, recently, a study examining copy number variation in several patient derived medulloblastoma cell lines revealed one clone in particular which harbored an amplicon containing AHI1(16). AHI1 was one of five genes in the region which were amplified 34-fold higher than normal cerebellar granule neurons. Although whether AHI1 is indeed the responsible oncogene in this amplicon cannot be determined from this data alone, it suggests at least that AHI1 may represent an interesting candidate for future studies. Additionally, whole genome mRNA expression analysis in a mouse model of medulloblastoma (NCBI GEO Profiles) has revealed increased Ahi1 transcript levels in preneoplastic cells as well as in medulloblastoma tumor cells compared with normal cerebellar granule neurons. Overall this data, along with our findings, hint at the possibility that AHI1 is an oncogene not only in the context of leukemia and lymphoma as has previously been reported(17, 18), but also in the cerebellum.

In fact, Jouberin may represent an interesting potential therapeutic target in medulloblastoma, particularly that subset which contains mutations in the Wnt pathway(6). Until now, a role for Wnt signaling in proliferation of cerebellar precursors had not been described and its only clear role was in patterning at earlier timepoints such as E9.5. Our findings implicate not only a new mechanism for the Wnt pathway in

development of the cerebellum, but also potential insight into how mutations in Wnt components can lead to medulloblastoma. Most Wnt mutations in medulloblastoma occur in proteins involved in degradation of β-catenin or in β-catenin itself which prevents its cytoplasmic targeting to the proteasome. Since Jbn functions downstream of these perturbations in the pathway, it may represent a particularly unique potential therapeutic target. In fact, we may be able to use knowledge from JS patient mutations to intelligently design drugs targeting Jbn. For example, the V443D mutation(14) is located immediately adjacent to a putative phosphorylation site and this patient construct fails to interact with β-catenin and is defective in Wnt activity. Additionally, since the majority of patients with AHI1 mutations exhibit mainly cerebellar defects, perhaps targeting Jbn in medulloblastoma would represent a cerebellum specific effect on the Wnt pathway, potentially limiting future side effects. Thus, our findings both within the cerebellum as a whole, and mechanistically within the cerebellar neuron, provide insight into proliferation of precursors and the defects associated with disruption of this process.

Of course, these studies provide the most direct evidence into the role of Wnt signaling and the primary cilium within the JS afflicted cerebellum. The implications for cilium-based signaling are broad and suggest that the neuronal cilium in particular can be thought of as a concentrating signaling hub. The primary cilium overall seems to be a developmental organelle, and even when it is present in adult tissue, as in the kidney, it seems to play a role in developmental signaling within the context of regenerating tubules. Although there will certainly be exceptions to this, our results suggest a vital role for the cilium as a central hub and somewhat of a gateway to the nucleus in the case of Wnt signaling. It seems to act as a regulatory “turnpike” of sorts for Jbn and β-catenin which seems to fine-tune the pathway. Thus, the cilium maintains tight regulation of the pathway keeping it in perfect balance. If the pathway tilts to one side, a variety of

disorders may occur, from renal cyst development and JS in the case of decreased Wnt activity, to certain types of cancer when the pathway is increased. Overall, the primary cilium is an elegant signaling machine with enormous capabilities.

References

1. Snell WJ, Pan J, & Wang Q (2004) *Cell* **117,** 693-697.

2. Singla V & Reiter JF (2006) *Science* **313,** 629-633.

3. Batada NN, Shepp LA, & Siegmund DO (2004) *Proc Natl Acad Sci U S A* **101,** 6445-6449.

4. MacDonald BT, Tamai K, & He X (2009) *Developmental cell* **17,** 9-26.

5. Nusse R (2005) *Cell Res* **15,** 28-32.

6. Marino S (2005) *Trends Mol Med* **11,** 17-22.

7. Klaus A & Birchmeier W (2008) *Nature reviews* **8,** 387-398.

8. Plotnikova OV, Golemis EA, & Pugacheva EN (2008) *Cancer research* **68,** 2058-2061.

9. Torres VE & Harris PC (2006) *Nat Clin Pract Nephrol* **2,** 40-55; quiz 55.

10. Hildebrandt F & Zhou W (2007) *J Am Soc Nephrol* **18,** 1855-1871.

11. Gerdes JM, Liu Y, Zaghloul NA, Leitch CC, Lawson SS, Kato M, Beachy PA, Beales PL, DeMartino GN, Fisher S, Badano JL, & Katsanis N (2007) *Nat Genet* **39,** 1350-1360.

12. Corbit KC, Shyer AE, Dowdle WE, Gaulden J, Singla V, Chen MH, Chuang PT, & Reiter JF (2008) *Nat Cell Biol* **10,** 70-76.

13. Caricasole A, Copani A, Caruso A, Caraci F, Iacovelli L, Sortino MA, Terstappen GC, & Nicoletti F (2003) *Trends in pharmacological sciences* **24,** 233-238.

14. Dixon-Salazar T, Silhavy JL, Marsh SE, Louie CM, Scott LC, Gururaj A, Al-Gazali L, Al-Tawari AA, Kayserili H, Sztriha L, & Gleeson JG (2004) *Am J Hum Genet* **75,** 979-987.

15. Ferland RJ, Eyaid W, Collura RV, Tully LD, Hill RS, Al-Nouri D, Al-Rumayyan A, Topcu M, Gascon G, Bodell A, Shugart YY, Ruvolo M, & Walsh CA (2004) *Nat Genet* **36,** 1008-1013.

16. McCabe MG, Ichimura K, Liu L, Plant K, Backlund LM, Pearson DM, & Collins VP (2006) *Journal of neuropathology and experimental neurology* **65,** 549-561.

17. Jiang X, Hanna Z, Kaouass M, Girard L, & Jolicoeur P (2002) *Journal of virology* **76,** 9046-9059.

18. Ringrose A, Zhou Y, Pang E, Zhou L, Lin AE, Sheng G, Li XJ, Weng A, Su MW, Pittelkow MR, & Jiang X (2006) *Leukemia* **20,** 1593-1601.